Ribosomal Accuracy in Higher Eukaryotes – Mistranslation and Unfolded Protein Response

Dissertation

zur

Erlangung der naturwissenschaftlichen Doktorwürde

(Dr. sc. nat.)

vorgelegt der

Mathematisch-naturwissenschaftlichen Fakultät

der

Universität Zürich

von

Martin Dominique Meyer

von

Eschenbach / LU

Promotionskomitee

Prof. Dr. Erik C. Böttger (Vorsitz)

Prof. Dr. Leo Eberl

Prof. Dr. Vikram Panse

Prof. Dr. Peter Sander

Zürich, 10.09.2015

1 ACKNOWLEDGEMENTS

I would like to thank Prof. Dr. Erik C. Böttger for giving me the opportunity to work as a PhD student in his lab. You always had an open door- and ear policy for scientific questions and were very supportive in the cases of preparing scientific presentations and reports. Thanks to your critical reviews of my work I learned a great deal. I wish you many more successful years with interesting projects to come.

I am very grateful to Dr. Dimitri Sherbakov and Dr. Rashid Akbergenov, postdocs in the Böttger group; they were always interested in my work and gave me useful advice on many occasions. I very much appreciate the fact that Prof. Dr. Leo Eberl, Prof. Dr. Vikram Panse and Prof. Dr. Peter Sander agreed to act as members of my thesis committee in the PhD program in Molecular Life Sciences and took the time to monitor my progress.

A big thank you goes to the current and former members of the Böttger group; Stefan, Pietro, Heithem, Youjin, Pietro, Tanja J., and Thomas. All of you never hesitated to help me and offered me plenty of advice over the years. Also I would like to thank Susanna Salas for all of her help – for administrative objects and the many small but also important other things. In particular, special gratitude is reserved for Tanja Matt. Your friendship and love alone is already worth the years as PhD student! No matter what, I will always love you!

My dear friends, I love you all and I am very happy to have you! Biggest shouts go especially to Dario, Felix and Sam! You had always an open ear for my stories straight from the lab bench, even when most of the time I was speaking about stuff you didn't quite understand. Bringing me back down to earth or lifting me back up onto my feet when necessary, you always have been and always will

be there for me. I am tremendously thankful for having such reliable and loyal friends, you guys rock!

Most importantly, I want to thank my family! Mom, Dad, you were always supportive on all issues and matters. Without you I wouldn't be where I am today. I'd also like to thank my sister Danielle. I admire you for everything you do or did and I hope you stay the way you are! To my brother Roger; I deeply regret that I don't know what you're doing or where you are right now, but I won't give up hope that we'll see each other again soon.

2 SUMMARY

The ribosome is a large macromolecular complex which mediates protein synthesis using messenger RNA (mRNA) as a template and aminoacyl-transfer RNA (tRNA) as a substrate. High accuracy of translation is essential for all living cells. Aminoglycoside antibiotics are used in clinical medicine to treat life-threatening infections with gram-negative bacteria. Aminoglycosides target the highly conserved core structure of the ribosome, in particular the A-site, where they inhibit protein synthesis and prevent proper mRNA decoding.

The objective of this thesis was to analyze how aminoglycosides affect the human ribosome, i.e. to study aminoglycoside-induced translation inhibition and misreading. As a possible consequence of ribosomal misreading we investigated cellular unfolded protein responses, in particular in mitochondria (UPR^{mt}) and the endoplasmatic reticulum (UPR^{ER}).

The first part of the thesis examines how different aminoglycosides affect translation. Towards this end we established a gain-of-function assay to measure the efficacy of translational and ribosomal accuracy. This we did *in-vitro* using Rabbit Reticulocyte Lysate and *in-vivo* using HEK293 cells. We observed a significant correlation when comparing *in-vitro vs. in-vivo* data between translation inhibition or misreading induction. Geneticin was identified as the most potent misreading inducer and translation inhibitor of the cytoribosome. However, no direct correlation was found between translation inhibition and misreading, i.e. these two mechanisms are not directly connected. For example, gentamicin and apramycin inhibit the cytoribosome to a similar extent *in-vivo* but in contrast to the high misreading induction of gentamicin no induction was observed with apramycin. In the second part of the thesis we wanted to study the influence of misreading and translation inhibition on UPR^{mt}. As more than 99% of the mitochondrial proteins are produced in the cytosol but folded in the mitochondrium, misfolding of these imported proteins would be sensed inside the mitochondrium. The effect of aminoglycosides on UPR^{mt} was analyzed by monitoring the induction of reporter genes driven by the mito-chaperone Hsp60

promoter and the mito-protease ClpP promoter. We found that there is a strong correlation between translation inhibition and levels of induction of the UPR^{mt}. Finally, we studied the possible consequences of ribosomal misreading at the organism level. In murine cochlear explants, the aminoglycoside gentamicin induced CHOP, a prominent UPR^{ER} marker. *In vivo*, local aminoglycoside treatment caused high-frequency hearing loss in mice with a compromised UPR^{ER}, i.e. haplo-insufficient XBP1 ($XBP1^{+/-}$) mice. This was accompanied by reduced densities of spiral ganglion cells and synaptic ribbons.

3 ZUSAMMENFASSUNG

Das Ribosom ist ein grosser, makromolekularer Komplex, welcher Proteine herstellt unter Verwendung von messenger RNA (mRNA) als Vorlage und aminoacyl-transfer RNA (tRNA) als Substrat. Mit Aminoglykosiden werden Infektionen Gram-negativen Bakterien behandelt. Aminoglykoside binden an eine hochkonservierte Struktur des Ribosoms, die A-site, wodurch die Übersetzung von mRNA in Polypeptidketten ungenau, genannt Mistranslation, oder inhibiert wird.

Ziel dieser Arbeit war die Untersuchung des Einflusses von Aminoglykosiden auf das menschliche Ribosom, das heisst die Inhibierung der Translation sowie Induktion von Mistranslation. Weiter untersuchten wir die Konsequenzen von misgefalteten Proteinen oder inhibierter Translation auf zellulärer Ebene.

Im ersten Teil der Arbeit wird der Einfluss von verschiedenen Aminoglykosiden auf die Inhibition der Translation sowie die Induktion von Mistranslation untersucht. Wir haben dies mittels eines *gain-of-function* Assays getan, mit welchem wir die Genauigkeit des Ribosoms messen konnten. Durchgeführt wurden die Experimente mit Rabbit Reticulocyte Lysate, *in-vitro,* und HEK293 Zellen, *in-vivo.* Wir konnten eine signifikante Korrelation zwischen *in-vivo* und *in-vitro* Experimenten feststellen. Dabei wurde Geneticin als der stärkste Inhibitor als auch als der stärkste Induktor von Mistranslation identifiziert. Eine Korrelation zwischen Inhibition und Mistranslation konnte allerdings weder *in-vivo* noch *in-vitro* festgestellt werden. So sind zum Beispiel die Aminoglykoside Gentamicin und Apramycin *in-vivo* vergleichbar bezüglich der Inhibition, doch während Gentamicin in hohem Masse eine Mistranslation induziert ist eine solche bei Apramycin nicht zu sehen. Im zweiten Teil dieser Arbeit untersuchten wir die mitochondrielle *Unfolded Protein Response* (UPR^{mt}). Mehr als 99% der mitochondriellen Proteine werden im zytosol synthetisiert und erst danach im Mitochondrium gefaltet. Dort wird registriert falls ein Protein falsch gefaltet ist und eine UPR^{mt} wird induziert. Der Effekt von Aminoglykosiden auf die UPR^{mt} wurde mittels Reportergenen welche einen Hsp60 oder ClpP Promotor besitzen

gemessen. Die Inhibition der Translation und die Induktion der UPR^{mt} hatten in hohem Masse korreliert. Im dritten Teil dieser Arbeit analysierten wir den Einfluss von Aminoglykosiden in lebendem Gewebe. In murinen chochlea Explantaten induzierte das Aminoglykosid Gentamicin CHOP, ein prominenter Marker für die *Unfolded Protein Response* des endoplasmatischen Retikulums (UPR^{ER}). *In-vivo* verursachten lokal angewendete Aminoglykoside den Verlust des Hörvermögens im hoch-frequenten Bereich bei Mäusen mit gestörter UPR^{ER}, d.h. XBP1 haplo-insuffizient ($XBP1^{+/-}$). Weiter wurden geringere Dichten der Spiralganglionen und synaptischen Bänder festgestellt.

4 INTRODUCTION

4.1 The Ribosome

4.1.1 Architecture of the Ribosome

One of the most fundamental processes in life is protein synthesis. This basic process is carried out by the ribosome (from *ribo*nucleic acid; *soma* – Greek for body), a large ribonucleoprotein complex found in all living cells. This complex has a high molecular weight, ranging from 2.5 MDa in prokaryotes to more than 4 MDa in higher eukaryotes (Ben-Shem, Garreau de Loubresse et al. 2011, Lee and Gutell 2012). It is composed of a large and a small subunit, each containing ribosomal ribonucleic acids (rRNA) and ribosomal proteins (r-Proteins) (see Table 1). Despite large differences in size and compositional ratios of rRNA and r-Proteins, ribosomes from prokaryotes, eukaryotes and mitochondria share a highly conserved core structure. (see Figure 1 and Table 1).

Tab. 1: Overview of the composition of the ribosome across the three kingdoms of life.

Characteristics	**Bacteria**	**Archaea**	**Mitochondria**	**Eukaryota**
Ribosome Size	70S	70S	55S	80S
Small Subunit				
Sedimentation coefficient	30S	30S	28S	40S
Mass (MDa)	0.8	0.8	1.2	1.4
rRNA	16S	16S	12S	18S
Number of r-proteins	20	28	33	32
Large Subunit				
Sedimentation coefficient	50S	50S	39S	60S
Mass (MDa)	1.6	1.6	2.4	2.6
rRNA	23S, 5S	23S, 5S	16S	28S, 5.8S, 5S
Number of r-proteins	34	40	52	46

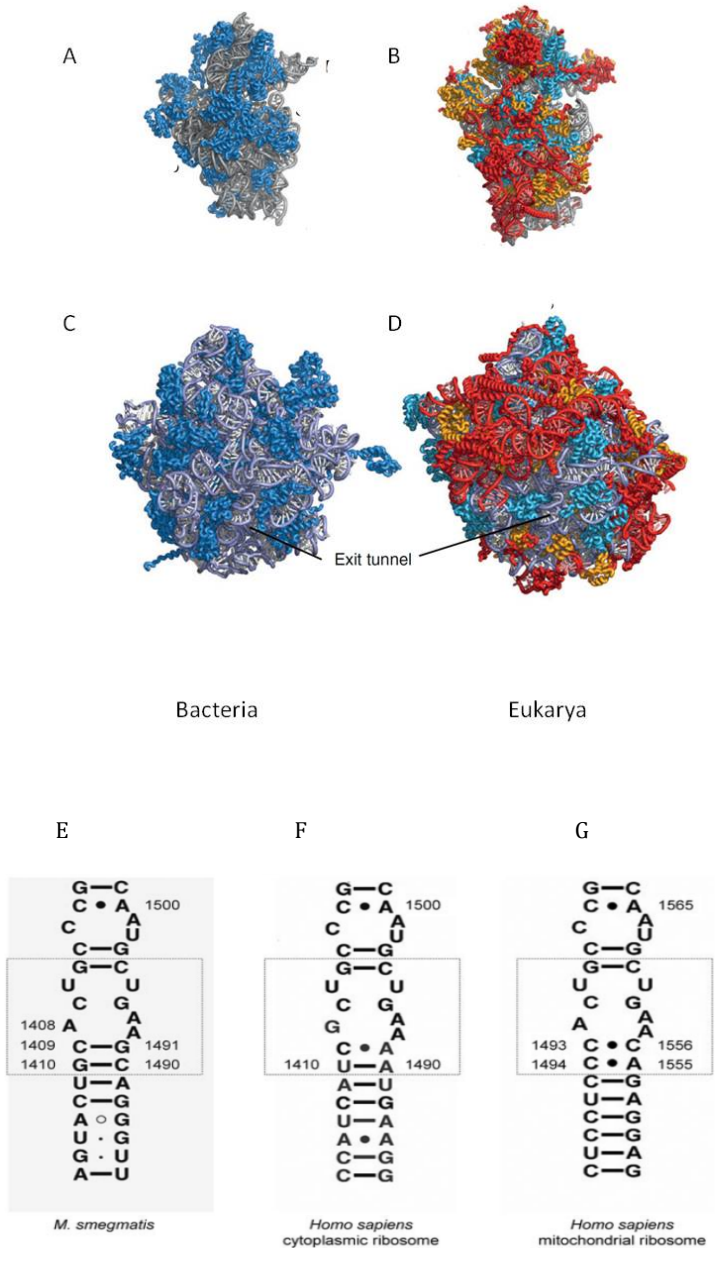

Fig. 1: Comparison of the bacterial and the eukaryotic ribosome. A) 30S subunit of the bacterial ribosome. B) 40S subunit of the eukaryotic ribosome. C) 50S subunit of the bacterial ribosome. D) 60S subunit of the eukaryotic ribosome. Shown is in all pictures the solvent-exposed side of the subunits. Eukaryotic ribosomes are color-coded as follows: universally conserved proteins are shown in light blue, proteins present in archaea and eukarya are shown in gold and proteins and RNA elements exlusively present in eukarya in red. E-G) Comparison of the secondary structures of the (E) bacterial, (F) human cytosolic, and (G) mitochondrial A-site rRNA(boxed). Nucleotides of *M. smegmatis* and human cytosolic rRNA are numbered according to *E.coli* rRNA numbering. Pictures A – C adapted from (Ramakrishnan, Davies et al. 1995), E – F from (Matt et al. 2010)

4.1.2 Mechanisms of Translation

Genetically encoded information on messenger ribonucleic acids (mRNA) is decoded by amino acylated transfer ribonucleic acids (aa-tRNA) to produce amino acid chains. The two ribosomal subunits perform the core function of the ribosome: the tasks of tRNA recognition and polypeptide chain elongation (see Figure 2). The small subunit contains the aa-tRNA decoding site (A-site) where the codon-anticodon interaction takes place, i.e. the mRNA sequence is translated into an amino acid sequence. Each amino acid is specified by three bases (one codon) according to the genetic code (Ochoa 1967). In this code each amino acid is defined by one or more distinct codons and is delivered by a specific tRNA to the A-site. The large ribosomal subunit contains the peptidyl transferase center (P-site) where peptidyl transfer and hydrolysis reactions occur.

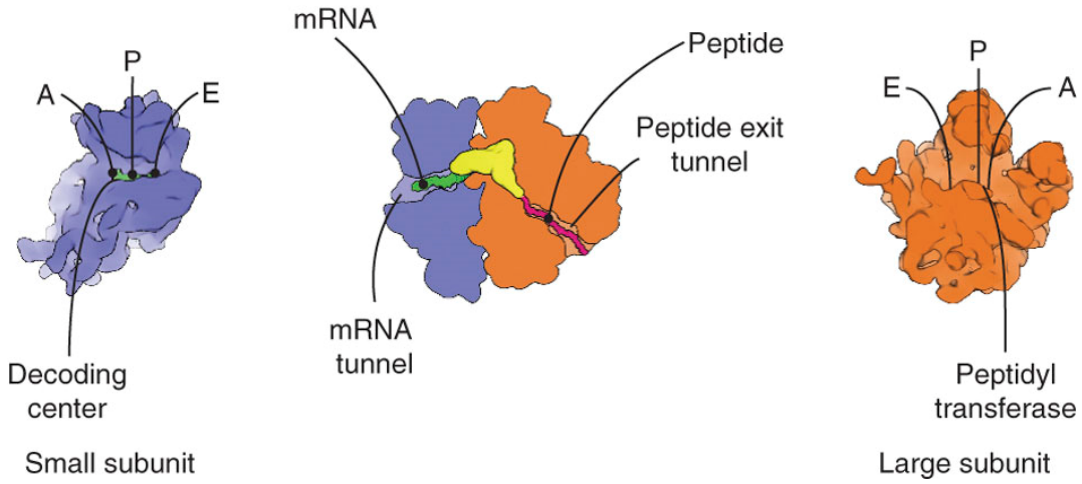

Fig. 2: The ribosomal core functions. The small and the large ribosomal subunits are shown in blue and ochre, respectively. The mRNA is shown in green, the tRNA bound to the ribosome in yellow and the emerging nascent polypeptide in pink. Picture from (Melnikov, Ben-Shem et al. 2012)

Translation proceeds in three phases: initiation, elongation, and termination. In the initiation process of translation the small subunit of the ribosome binds a ternary complex consisting of initiation factors, Met-tRNA and GTP. During

initiation, most eukaryotic mRNAs are translated by a cap-dependent mechanism, which requires recognition of the cap structure at the 5' end of the mRNA by eIF4E complexed with eIF4G and eIF4A – the so-called eIF4F complex (Pestova, Kolupaeva et al. 2001). A pre-initiation complex consisting of a 40S ribosomal subunit loaded with eIF3, eIF1 and eIF1A, initiator fMet-tRNA^{Met}, eIF2 and GTP binds the eIF4F-mRNA complex and scans along the 5'-UTR of the mRNA to reach the start codon, AUG. A free 60S ribosomal subunit, stabilized by eIF6 and eIF3, binds to the small subunit and subsequently the elongation cycle is launched (Hinnebusch 2014). This reaction requires an additional initiation factor, eIF-5, which hydrolyses the eIF-2-bound GTP, thereby releasing the initiation factors from the ribosome (see Figure 3).

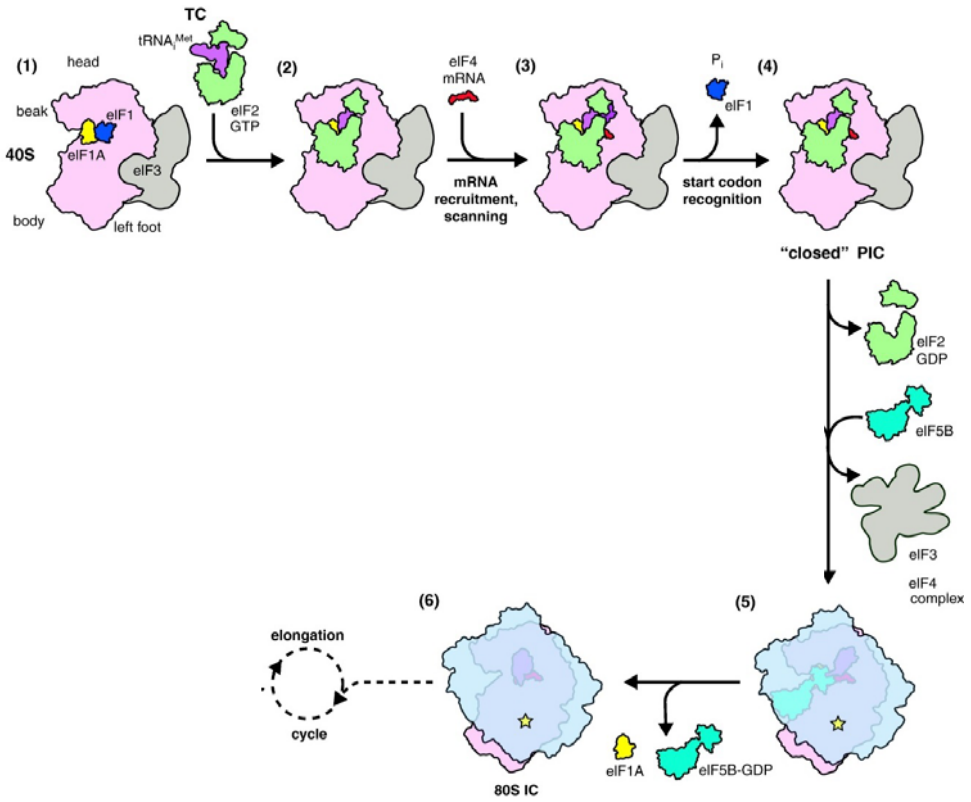

Fig. 3: Translation initiation in eukaryotic cells. Picture from (Voigts-Hoffmann, Klinge et al. 2012).

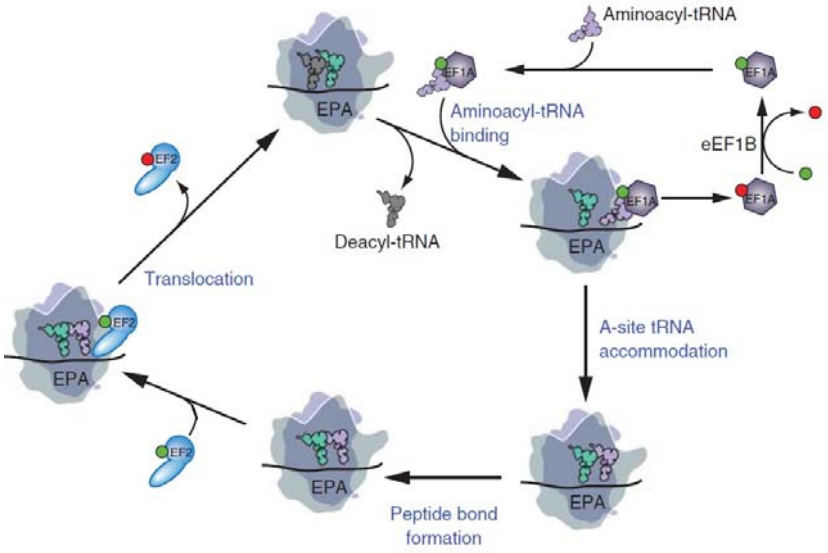

Fig. 4: Translation elongation in eukaryotic cells. Picture from (Dever and Green 2012)

Elongation is assisted by elongation factors eEF1A and eEF2. The ribosome selects cognate tRNAs based on Watson-Crick complementarity between the mRNA and the tRNA anticodon. During elongation a ternary complex comprised of GTP, elongation factors, and aa-tRNA is delivered to the ribosomal A-site where it reacts with the peptidyl-tRNA in the ribosomal P-site. Forming a peptide bond the peptidyl-tRNA becomes bound to the aa-tRNA. The ribosome translocates to the next triplet, using the energy from elongation factor and GTP hydrolysis, i.e. the peptide-carrying tRNA is moved to the P-site and the deacetylated tRNA is shifted into the E-site remaining the A-site empty for the next cycle (see Figure 4).

Elongation continues until the ribosome recognizes a stop codon in the A-site, UAA, UAG, or UGA, resulting in hydrolysis of the peptidyl tRNA mediated by the ternary complex consisting of the release factors eRF1 and eRF3, and GTP. Upon hydrolysis of GTP, eRF3 is released. The release of the completed polypeptide and dissociation of the ribosomal subunits is accompanied by binding of the ATPase ABCE1/Rli1 which supports accommodation of eRF1. During recycling, which is required to allow further rounds of translation, both

ribosomal subunits dissociate from the mRNA (Jackson, Hellen et al. 2012) (see Figure 5).

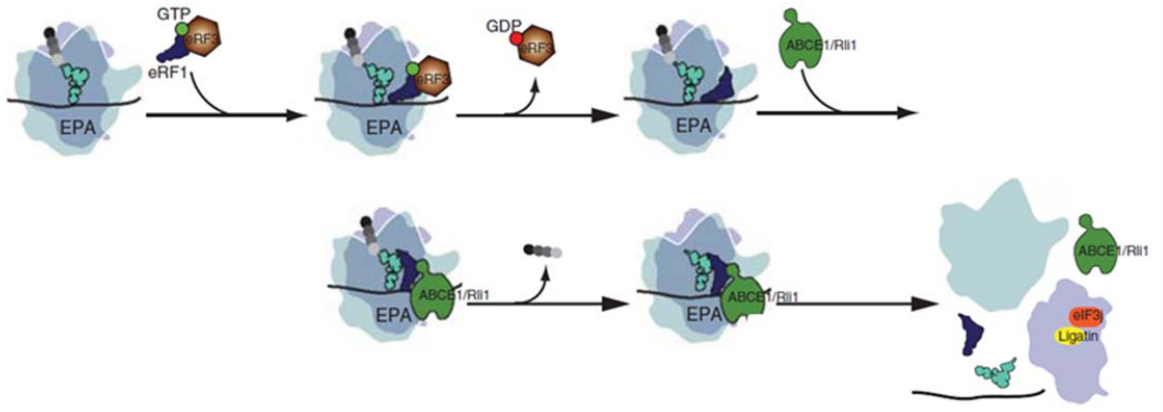

Fig. 5: Translation termination in eukaryotic cells. The big ribosomal subunit is shown in light grey, the small subunit in dark grey. eRF1 is shown in blue, eRF3 is shown in brown, GTP is shown as a green circle and GDP is shown as red circle. Figure from (Weddle, Tu et al. 1995).

4.1.3 Ribosomal Accuracy

High accuracy of translation is critical as erroneous protein synthesis may result in protein misfolding or decreased protein functionality. However, high speed of protein synthesis is required to react appropriately to intra- and extra-cellular changes. Thus, translation should occur in a well-balanced manner addressing the requirements for both, speed and fidelity. During decoding the ribosome recognizes the geometry of codon-anticodon base pairing at the first two positions of the codon but monitors the third codon less stringently (Balasubramaian and Seetharamulu 1983). Codon-anticodon pairs with only one mismatch are referred to as near-cognate. Pairs with more than one mismatch are referred to as non-cognate. Binding of the ternary complex to the ribosomal A-site is reversible, and non-cognate ternary complexes usually dissociate at this stage (Gast, Peters et al. 1987). The specificity results from molecular interactions which take advantage of differences in the free energy (ΔΔG) of

binding between cognate, near-cognate, and non-cognate substrates. Once the binding takes place in the A-site, rRNA nucleotides (G530, A1492, and A1493; *E. coli* numbering) interact with the mRNA-tRNA codon-anticodon minihelix. The rRNA nucleotide G530 moves from a *syn*- to an *anti*-conformation upon cognate tRNA binding. The rRNA nucleotides A1492 and A1493 are constantly moving, thus steadily opening and closing the A-site. The closed form of the A-site is stabilized by cognate tRNAs but not by near-cognate tRNA (see Figure 6). This stabilization of the flip-out of the nucleotides A1492 and A1493 operates as mechanism to ensure binding of a cognate tRNA. Upon tRNA binding, EF-Tu hydrolyses GTP while bound to the ribosome. This represents a branch point where either the aminoacyl end of the tRNA becomes available for peptidyl transfer (cognate tRNA), or the tRNA dissociates from the ribosome (near-cognate tRNA). Overall, the error rates of translation *in vivo* have been estimated to be in the order of 10^{-3} to10^{-4} per codon (Ogle and Ramakrishnan 2005, Salas-Marco and Bedwell 2005, Konstantinidis, Patsoukis et al. 2006, Fan-Minogue and Bedwell 2008, Vallabhaneni and Farabaugh 2009, Zaher and Green 2009, Keeling, Wang et al. 2012, Qin, Liu et al. 2012).

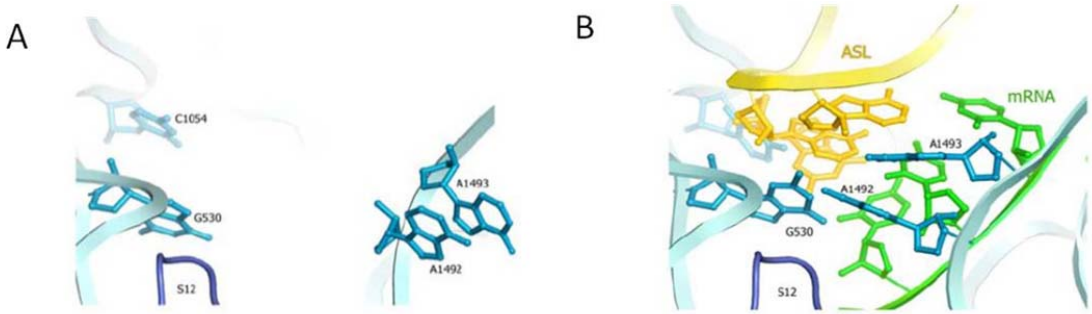

Fig. 6: Structure of the bacterial ribosomal decoding A-site of the small subunit. A) Open/empty A-site with nucleotides A1492 and A1493 flipped into the minihelix 44 of the 16S rRNA. B) Closed A-site by binding of a cognate tRNA (yellow) to the mRNA (green). This interaction stabilizes the flip out of the nucleotides A1492 and A1493 (blue) and the flip from *syn*- to *anti*-conformation of G530 (blue). Picture adapted from (Laurberg, Asahara et al. 2008).

4.1.4 Aminoglycosides

As protein synthesis is an indispensable process for all living cells, it makes a formidable target for antimicrobial substances. Many antibiotics target the ribosome, mainly by binding to the rRNA of either the small or the large ribosomal subunit. These classes of antibiotics include aminoglycosides, spectinamides, macrolides, lincosamides, tetracyclines and oxazolidinones.

Aminoglycosides are bactericidal antimicrobials, water-soluble and relatively stable at different temperatures and pHs (Lynch and Puglisi 2001, Dandliker, Pratt et al. 2003, Szychowski, Kondo et al. 2011, Matt, Ng et al. 2012). The term “aminoglycoside” is derived from the chemical structure of these compounds, which are made up of amino groups attached to glycosides. These antibiotics occur naturally and are isolated from *Micromonospora* (suffix –micin) or *Streptomyces* (suffix –mycin). Aminoglycosides share a common neamine core consisting of a glucopyranosyl (ring I) glycosidally linked to position C4 of the hexose 2-deoxystreptamine (ring II). Ring II is substituted with additional aminosugars on either C5 (4,5-Aminoglycosides, ring III and IV) or C6 (4,6-Aminoglycosides, ring III). There are also unusual aminoglycoside-structures, e.g. apramycin with a monosubstituted 2-deoxystreptamine and a bicyclic sugar moiety or hygromycin B with its ring III resulting from a dual ether linkage between ring II and ring IV (see Figure 7).

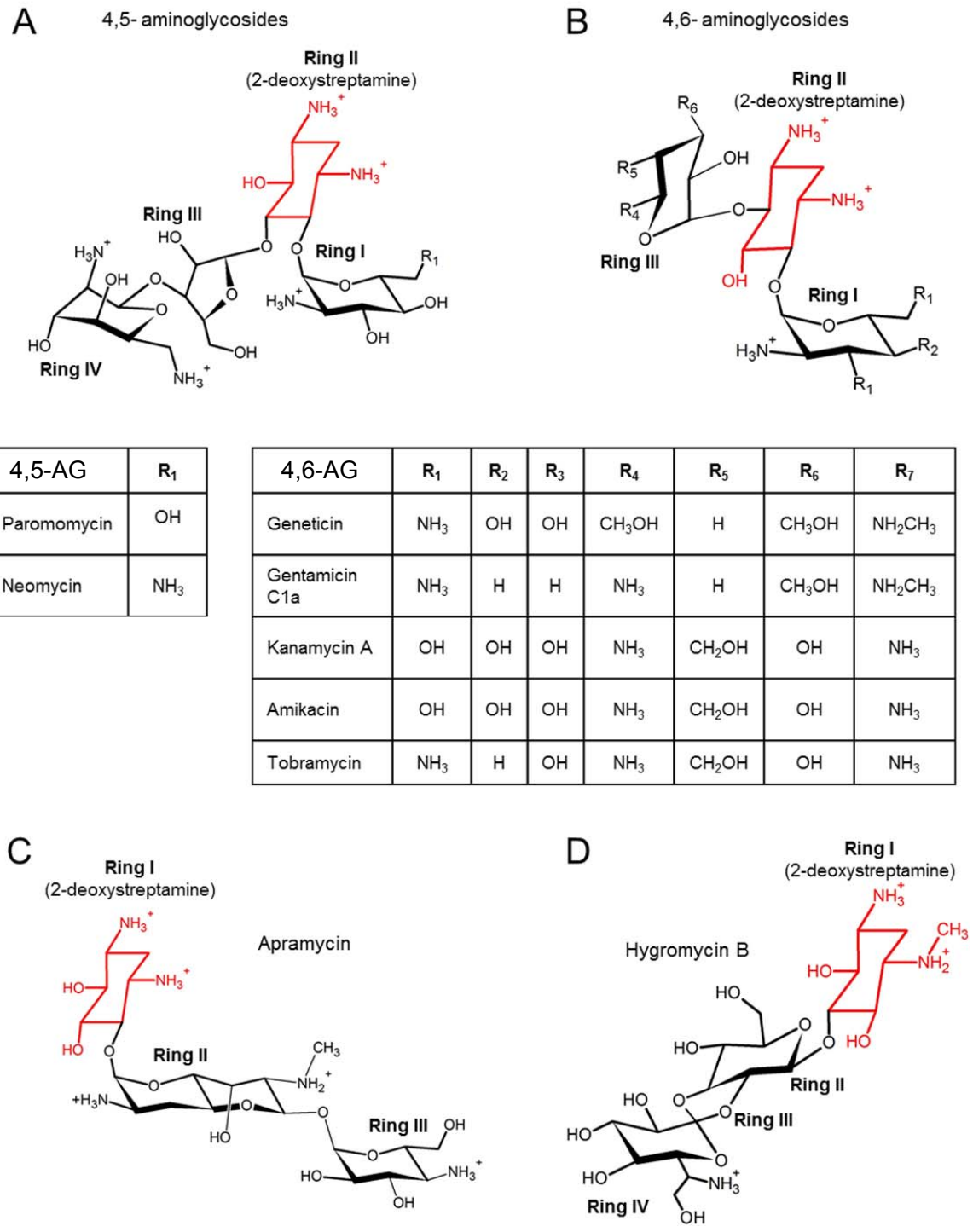

4,5-AG	R_1
Paromomycin	OH
Neomycin	NH_3

4,6-AG	R_1	R_2	R_3	R_4	R_5	R_6	R_7
Geneticin	NH_3	OH	OH	CH_3OH	H	CH_3OH	NH_2CH_3
Gentamicin C1a	NH_3	H	H	NH_3	H	CH_3OH	NH_2CH_3
Kanamycin A	OH	OH	OH	NH_3	CH_2OH	OH	NH_3
Amikacin	OH	OH	OH	NH_3	CH_2OH	OH	NH_3
Tobramycin	NH_3	H	OH	NH_3	CH_2OH	OH	NH_3

Fig. 7: Chemical structure of 2-deoxystreptamine aminoglycosides used in this study. Ring I (2-deoxystreptamine, red) and ring II build the backbone of this class of antibiotics, a common neamine core. A) 4,5-aminoglycosides paromomycin and neomycin. B) 4,6-aminoglycosides with various substituents. Note that amikacin contains an additional (l)-α-hydroxy-γ-aminobutyric amide (L-HABA chain)at the aminogroup

of C1 of ring II (Kondo, Francois et al. 2006). C) Apramycin, and D) Hygromycin B, compounds with a unique structure within the class of aminoglycosides.

4.1.5 Aminoglycosides and Misreading

Aminoglycosides bind reversibly to the A-site of bacterial ribosomes where they make extensive interactions with the rRNA of the small ribosomal subunit internal loop containing A1492 and A1493 (see Figures 3C) (Carriere, Vijayabaskar et al. 2002, Borovinskaya, Shoji et al. 2008, Fan-Minogue and Bedwell 2008, Szaflarski, Vesper et al. 2008, Tselika, Konstantinidis et al. 2008, Kramer, Vallabhaneni et al. 2010, Fernandez, Malchiodi et al. 2011, Matt, Ng et al. 2012, Demirci, Murphy et al. 2013). Ring I of aminoglycosides is located in the internal loop of the rRNA formed by nucleotides A1408, A1492, A1493 and the C1409-G1491 base pair. Two hydrogen bonds are formed by ring I to A1408, mimicking a pseudo base-pair. Further, ring I participates in a stacking interaction with G1491. The hydroxyl groups at position O3' and O4' of ring I form additional hydrogen bonds to the phosphates of A1492 and A1493 (see Figure 8A). Ring II of the aminoglycosides is located between nucleotides A1493, G1494, and U1495. The 1-aminogroup of ring II interacts with the O4 of U1495 and the 3-aminogroup interacts with N7 of G1494. (Blanchard, Fourmy et al. 1998, Slezak, Persky et al. 1998, Pfister, Hobbie et al. 2003, Francois, Russell et al. 2005). The positioning of aminoglycosides ring I and II is virtually universal at this position. The rings III and IV of 4,5-aminoglycosides or ring III of 4,6-aminoglycosides make additional interactions with the helix 44 of the A-site (Hobbie, Bruell et al. 2006, Hobbie, Pfister et al. 2006, Hobbie, Kalapala et al. 2007, Matt, Ng et al. 2012, Dudek, Romanowska et al. 2014, Perez-Fernandez, Shcherbakov et al. 2014)**.** For 4,5-aminoglycosides ring III and IV reach down the drug binding pocket towards G1491 whilst for 4,6-aminoglycosides ring III reaches up the drug binding pocket towards U1406 (see Figure 8B). Crystal structures of ribosomes with aminoglycosides show a flip-out of A1492 and A1493. Thus, aminoglycosides stabilize the local conformational changes in the decoding site as if a cognate tRNA is present (Laurberg, Asahara et al. 2008). Mimicking the

binding of a cognate tRNA, this stabilized conformational alteration would allow the incorporation of a near-cognate tRNA and result in misreading. As aminoglycosides bind to the evolutionary conserved core structure of the ribosome, these chemicals may not only exert an antimicrobial effect but may also bind to the eukaryotic cytosolic ribosomes (Duff 1992).

4.1.6 Protein Quality Control and Cellular Stress Response in Eukaryotes

Newly synthesized proteins are usually folded directly after translation either in the cytosol (cellular proteins) or in the endoplasmatic reticulum (ER) (membrane and secreted proteins) (Pfanner, Rassow et al. 1990, Hendrick and Hartl 1995, Trombetta and Parodi 2003). Folding is supported by molecular chaperones; proteins that interact, stabilize or help a non-native protein to reach its native conformation but are not present in the final functional protein. Eukaryotic cells survey the proper protein folding and eliminate misfolded proteins to restore protein homeostasis. In general there are three different response types known: i) cytosolic heat shock response (HSR), ii) ER unfolded protein response (UPR^{ER}) and, iii) mitochondrial unfolded protein response (UPR^{mt}) (Vujanac, Fenaroli et al. 2005, Voellmy and Boellmann 2007, Lee, Liu et al. 2009, Jacobs and Marnett 2010, Chakrabarti, Chen et al. 2011). The latter will be discussed in more detail in section 4.2.4.

The cytosolic heat shock response induces four different heat shock factors (HSF1-4) in higher eukaryotes with HSF1, a transcriptional regulator, as the major player. Under normal conditions, HSF1 is mostly bound to the chaperones heat shock protein 70 (HSP70) and HSP90 to build an inert monomeric complex. Under stress conditions, e.g. increased load of denatured cytosolic proteins, HSF1 is displaced from chaperones HSP70 and HSP90 which are recruited to exert their chaperone function. Additionally, HSF1 is posttranslationally modified including phosphorylation/dephosphorylation, acetylation/deacetylation, sumoylation and the inactive monomeric form of HSF1 is shifted into an active trimeric form and translocated to the nucleus. This trimeric form is competent for

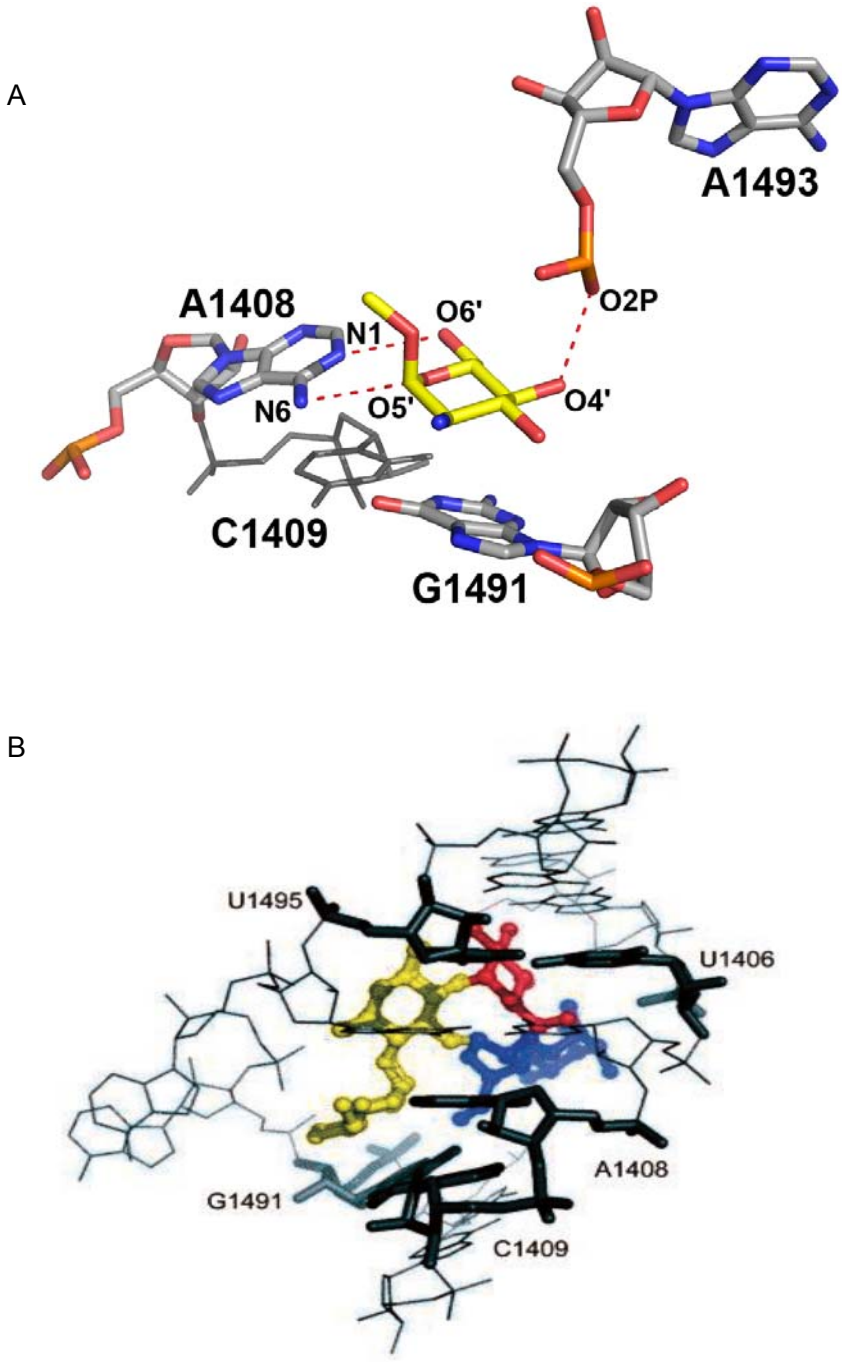

Fig. 8: Tertiary structure of the A-site in complex with aminoglycosides. A) Ring I of paromomycin (yellow) builds hydrogen bonds (red dashed) with the A-site nucleotides A1408 and A1493. There is also a stacking interaction between ring I and G1491. Interactions of O3' and A1492 are not shown. Adapted from (Perez-Fernandez, Shcherbakov et al. 2014) B) Tobramycin (ring III in red) and paromomycin (ring III and IV in blue), the common neamine core is shown in yellow. Picture adapted from (Akbergenov 2011).

DNA binding at the promoter sequences of the 5' region of *hsp* genes. These conserved sequences are known as heat shock elements (HSE). When proteostasis is restored excessive HSPs inactivate HSF1 and transcription of HSPs is stopped (see Figure 9) (Adachi, Liu et al. 2009, Lee, Liu et al. 2009).

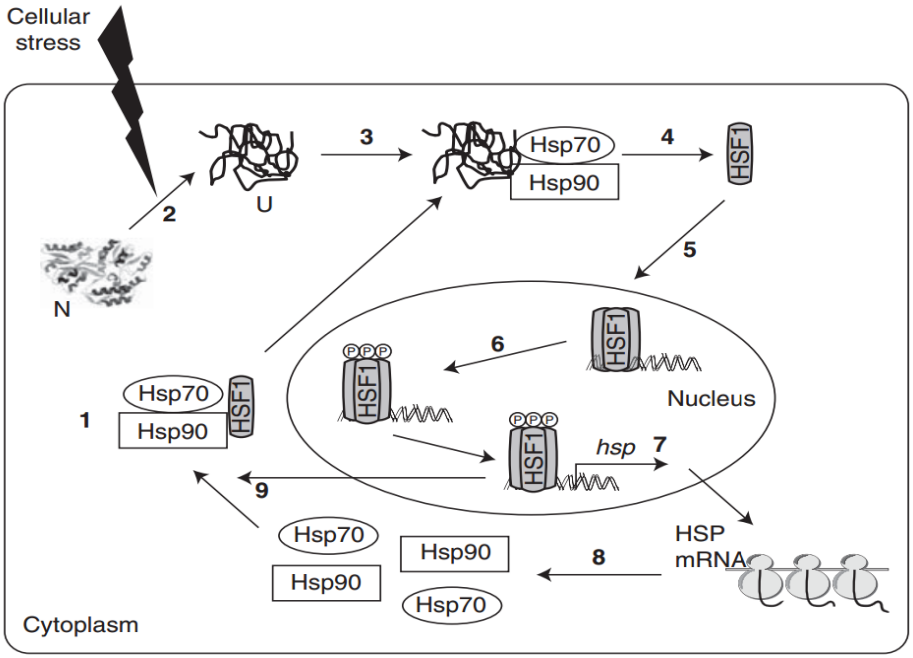

Fig. 9: Schematic overview of the transcriptional regulation of the cytosolic heat shock response. (1) Inert monomeric complex of Hsp70, Hsp90 and HSF1. (2) Cellular stress increasing the load of un- or misfolded proteins. (3 and 4) Misfolded proteins bind to Hsp70 and Hsp90, resulting in the displacement of HSF1. (5 and 6) Trimerized HSF1 translocates to the nucleus, undergoing posttranslational modifications. (7 and 8) Induction of transcription of numerous *hsp* genes, including Hsp70 and Hsp90, by binding of the activated HSF1 to the HSE resulting in translation of HSPs. (9) After the load of non-native proteins decreases HSF1 shifts back into its inert monomeric form. N = native protein, U = unfolded protein. Figure adapted from (Vabulas, Raychaudhuri et al. 2010).

In the UPR^{ER}, three distinct transmembrane sensor systems are known which all use the chaperone BiP as a regulator. In proteostasis, the transmembrane domains of the three sensors are associated with BiP. Upon accumulation of

unfolded proteins in the ER-lumen BiP dissociates to exert its chaperone activity and kicks of UPR^{ER} (see Figure 10).

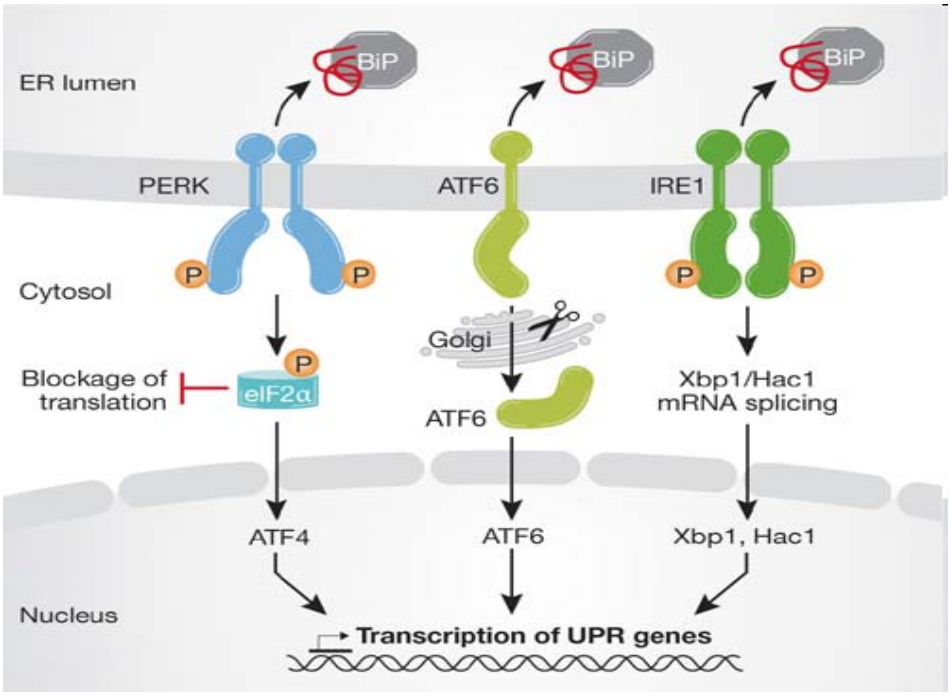

Fig. 10: Schematic overview of the three distinct sensor systems of the unfolded protein response in the ER. Figure from (Cyr and Hebert 2009).

The first sensor system is PERK (Protein kinase RNA (PKR)-like ER Kinase), a type I transmembrane protein with kinase activity. PERK is composed of an ER luminal stress sensor and a cytosolic protein kinase domain. Dissociation of BiP from the N-terminus of PERK initiates dimerization and autophosphorylation of the kinase domain. Activated PERK phosphorylates eIF2α which leads to three downstream effects, i) a generally attenuated translation initiation to decrease the protein folding load, ii) expression of pro-survival genes, e.g. cellular inhibitor of apopotosis (cIAP) and iii) an increased clearance of the accumulated proteins from the ER, e.g. by ER-associated degradation. In this case, ER α-mannosidase I removes the terminal mannose residue from oligosaccharides attached to proteins. Subsequently, misfolded proteins are transported out of the ER back into the cytosol. However, the retro-translocon responsible for this process is

unclear (Tsai, Ye et al. 2002). Once the unfolded or misfolded proteins are in the cytosol they are degraded by the ubiquitin proteasome system (Hershko, Ciechanover et al. 2000). Decreased protein translation is not universal; genes with internal ribosomal entry site (IRES) sequences in the 5' untranslated regions can bypass the eIF2α translational block and induce the expression of pro-survival functions such as amino acid transport or protein secretion by ATF4 (Verfaillie, Rubio et al. 2012). The second sensor system is ATF6, (Activating Transcription Factor 6), a type II transmembrane domain protein with a basic leucin zipper (bZIP) transcription factor in its cytoplasmic domain. This transcription factor induces transcription of specific UPR genes (Chakrabarti, Chen et al. 2011, Smith, Granell et al. 2011). ATF6 is activated by undergoing intramembrane proteolysis. The cleavage at a juxtamembrane site allows the 50 kDa transcriptional domain of ATF6 to be translocated to the nucleus. There, it regulates expression of genes containing ATF/cAMP response elements or ER stress response elements. Cleaved ATF6 induces a gene expression program together with other transcription factors and regulators, e.g. nuclear factor Y (NF-Y). Like this, chaperone activity and degradation of unfolded proteins can be increased. For example, ATF6 upregulates the expression of BiP or the ER-degradation-enhancing alpha-mannosidase-like protein (EDEM1). Additionally, ATF6 induces the expression of the X-box-binding protein 1 (XBP1) which regulates the expression of chaperones (Chakrabarti, Chen et al. 2011). The third sensor system is IRE1 (Inositol-Requiring Protein-1), a 100 kDa type I transmembrane protein with splicing activity. The N-terminus of IRE1, located in the ER-lumen, senses unfolded or misfolded proteins. BiP dissociates and IRE1 proteins form a complex which acts specifically as an RNase which cleaves a 26-nucleotide intron from the XBP1-mRNA to generate a 41 kDa frameshift variant (sXBP1) that acts as a potent transcription factor for UPR genes with pro-survival and pro-apoptotic effects (Paschen 2003, Gupta, Deepti et al. 2010, Shao, Shan et al. 2014).

4.2 Mitochondria

4.2.1 Organization and Function

Mitochondria are double-membrane bound organelles which range in size from 0.5 to 2 µm in diameter. The number of mitochondria per cell is highly variable, depending on the organism or tissue – up to several thousand mitochondria per cell have been observed. Mitochondria are often referred to as cellular power plant reflecting their high metabolic activity for the generation of adenosine triphosphate (ATP) by oxidative phosphorylation (OXPHOS). Further important roles are the involvement in cell cycle control, calcium (Ca^{2+}) homeostasis, generation of FeS clusters as essential cofactors for mitochondrial and cytosolic proteins, and fatty acid oxidation (Gray, Burger et al. 1999, Lang, Gray et al. 1999, Lang, Seif et al. 1999). It is well established that mitochondria evolved from a single endosymbiotic event around two billion years ago where an α-proteobacterium was engulfed by a precursor of the modern eukaryotic cell [9]. In other words a prokaryotic organism with highly efficient energy production machinery was taken up by a eukaryotic cell and kept as an organelle. Thus, mitochondria possess their own genome, which is often circular and present in one to many copies (Lohse, Drechsel et al. 2007, Preuten, Cincu et al. 2010, Copeland and Longley 2014, St John 2014). During evolution, most of the genomic material of the α-proteobacterium progenitor was rapidly lost or transferred to the nuclear genome of the host, e.g. all of the complex II protein subunits from OXPHOS. This event is known as endosymbiotic gene transfer (EGT) and reduced the mitochondrial genome content from several thousand protein coding genes, depending on the organism, down to 3 to 67 protein coding genes in present day mitochondria (Chevallet, Lescuyer et al. 2006). In humans, over 95% of the mitochondrial proteome is nuclear encoded and has to be translated in the cytosol and subsequently imported into the mitochondrion. The mitochondrial genome consists of a multicopy, circular, double-stranded DNA molecule of 16.6 kb. It encodes 13 essential polypeptides of the OXPHOS system, i.e. components of complex I, III, IV and the ATP synthase (see figure

11) (Lang, Gray et al. 1999). In addition to the proteins, mitochondria encode 22 tRNAs and the two rRNAs used for the mitoribosomal subunits. The remainder of the mitochondrial proteome is encoded by the nuclear genome, translated in the cytosol and imported into each mitochondrion. At present the total proteome of mitochondria is suggested to be 1100 - 1400 distinct gene loci encoding mitochondrial proteins (Taylor, Fahy et al. 2003, Meisinger, Sickmann et al. 2008, Meyer, Taylor et al. 2008, Pagliarini, Calvo et al. 2008, Lotz, Lin et al. 2014).

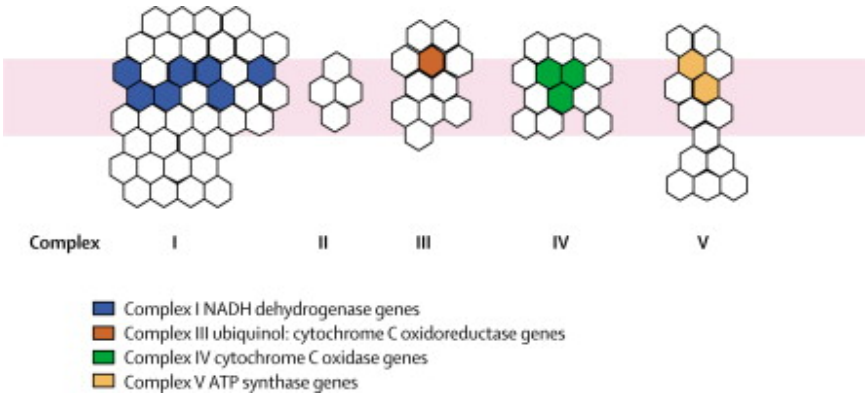

Fig. 11: Mitochondrial respiratory chain and oxidative phosphorylation system. Each colored hexagon represents a polypeptide product of a single mitochondrial gene. Picture from (Ramakrishnan 1997)

Mitochondria are composed of four compartments: the outer and inner membranes, the intermembrane space (IMS), and the matrix, each of which has its special tasks and specificities. The outer mitochondrial membrane (OMM) serves as a first barrier of the compartmentalized organelle and resembles other eukaryotic membranes. The presence of voltage-dependent anion channels (VDAC) and the protein import machinery make it permeable to metabolites and proteins (Kay, Li et al. 1997, Ghosh, Pandey et al. 2007, Ahmed, Muhammed et al. 2010). (Hajek and Bedwell 1994, Raja and Greenberg 2014). The inner mitochondrial membrane (IMM) itself is highly structured and differentiated into compositionally and functionally distinct regions. Lipid trafficking, mitochondrial

protein import and respiratory chain complex assembly take place within the inner boundary region while the cristae, invaginations that penetrate the matrix, house assembled respiratory complexes where ATP synthesis via OXPHOS takes place. Within the IMS mainly exchange of lipids, ions and various metabolites is taking place but most importantly it is the site where the electrochemical gradient is being built up by pumping protons across the proton-impermeable IMM into the IMS. The innermost compartment is completely enclosed by the IMM and called the matrix. It harbors the mitochondrial DNA, is the place of the tricarboxylic acid cycle (TCA cycle), production of reactive oxygen species (ROS) and control of autophagy and apoptosis (Glick, Beasley et al. 1992, Kaldi and Neupert 1998, Gordon, Dancis et al. 2000, Hoogenraad and Ryan 2001).

The main task of mitochondria, ATP generation, is mainly done by oxidation of the products from cytosolic glycolysis, pyruvate and NADH. Each pyruvate molecule is actively transported from the cytosol into the matrix of the mitochondria. There, combined with acetyl-CoA, it serves as substrate in the TCA cycle to produce the reduced cofactors NADH and $FADH_2$, and in addition one ATP. The reduced cofactors are then used as source of energy for oxidative phosphorylation by the electron transport chain (ETC). There, protons from the cofactors are pumped over the IMM into the IMS to generate a membrane potential. When returning into the matrix the protons pass the ATP synthase and per three protons one ATP is generated. Overall, eukaryotic cells are able to produce ~30 molecules of ATP per molecule of glucose (Yonally and Capaldi 2006) (see Figure 12).

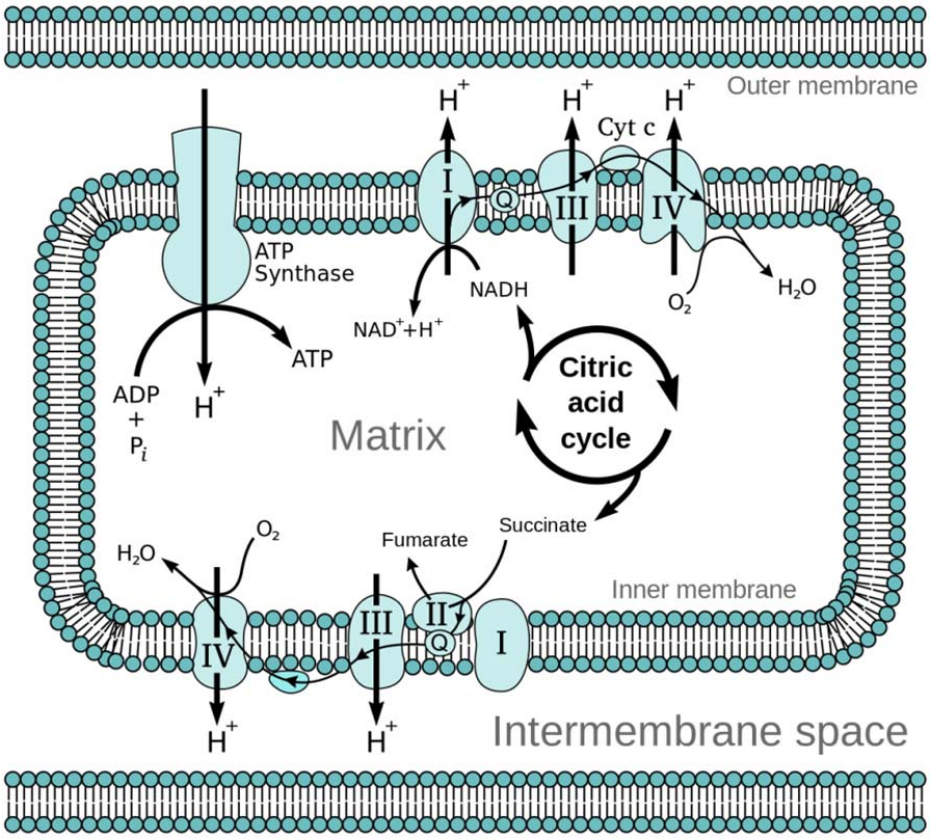

Fig. 12: Overview of ATP production in mitochondria (Wikipedia 2007).

4.2.2 Diseases Related to Mitochondrial Malfunction

Along with the importance of these organelles are risks for diseases or disorders caused by malfunctional mitochondria (see Table 3). The vast majority of mitochondria associated diseases are maternally inherited. Mitochondria and therefore mitochondrial DNA (DNA^{mt}) are derived from the ovum, as the sperm's mitochondria enter the egg but are immediately ubiquitinated and destructed inside the embryo (Raurell, Southern et al. 1997). Diseases and malfunctions can either occur because of large-scale DNA^{mt} rearrangements or point mutations. An example for a disease associated with a point mutation of DNA^{mt} is sensorineural deafness. Single nucleotide alterations of the 12S rRNA, A1555G or C1494T, were identified as a source of nonsyndromic deafness (Tuggle, Birket et al. 2014). These mutations both locate to a highly conserved part of the 12S

rRNA and form a similar RNA base-pair (compare secondary structures in Figure 1G). This region is essential for the decoding function of the A-site of the small subunit of the mitochondrial ribosome (Milon and Rodnina 2012). The clinical phenotype produced by these mutations range from normal hearing to severe congenital deafness, most probably depending on the nuclear background (Aeffner, Abdulrahman et al. 2013). In addition, patients carrying these mutations are particularly susceptible to aminoglycoside-mediated ototoxicity (Kramer and Hopper 2013). Sequence analyses of the mitochondrial genome in patients with aminoglycoside induced ototoxicity have shown that the two mutations A1555G and C1494U of the 12S rRNA account for up to 33% of the cases (Dutnall, Tafrov et al. 1998).

Tab. 3: Frequent diseases associated with mitochondria. Adapted from (Andre Mattman 2011)

Syndrome and features	**Genetics**
Leigh syndrome Neonatal subacute encephalopathy with bilateral symmetric midbrain and basal ganglia necrosis on MRI	Autosomal recessive, mitochondrial DNA, X-linked (SURF1)
MERRF Myoclonic epilepsy with ragged-red fibres on muscle biopsy	Mitochondrial DNA, mito-tRNAs
MELAS Mitochondrial encephalopathy with lactic acidosis and stroke-like episodes	Mitochondrial DNA, mito-tRNAs
MIDD Maternally inherited diabetes and deafness	Mitochondrial DNA, mito-tRNAs
Kearns-Sayre syndrome External ophtalmoplegia, pigmentary retinopathy, elevated CSF protein, cerebellar ataxia, and cardiac conduction defects	Mitochondrial DNA, 5kb deletion (12 genes)

Nonsyndromic Deafness Mild to severe permanent hearing loss caused by damage to structures in the inner ear	Mitochondrial DNA (MT-RNR1)

4.2.3 Mitochondrial Protein Import

As much as 10% to 15% of the nuclear genes of eukaryotic organisms encode for mitochondrial proteins which are translated on cytosolic ribosomes and subsequently imported into the mitochondrion (Kaldi and Neupert 1998, Gray, Burger et al. 1999, Cameron, Hurd et al. 2005, Copeland and Longley 2014). Thus, highly specific and efficient import machineries are essential to guide these proteins into the mitochondrion and sort them to the diverse compartments. To do so, mitochondrial proteins have precursor-recognizing receptors, membrane spanning pores and proteolytic enzymes that mediate import of precursor proteins. The mitochondrial precursor proteins contain various targeting sequences, depending on their final destination in the mitochondria (see Figure 13).

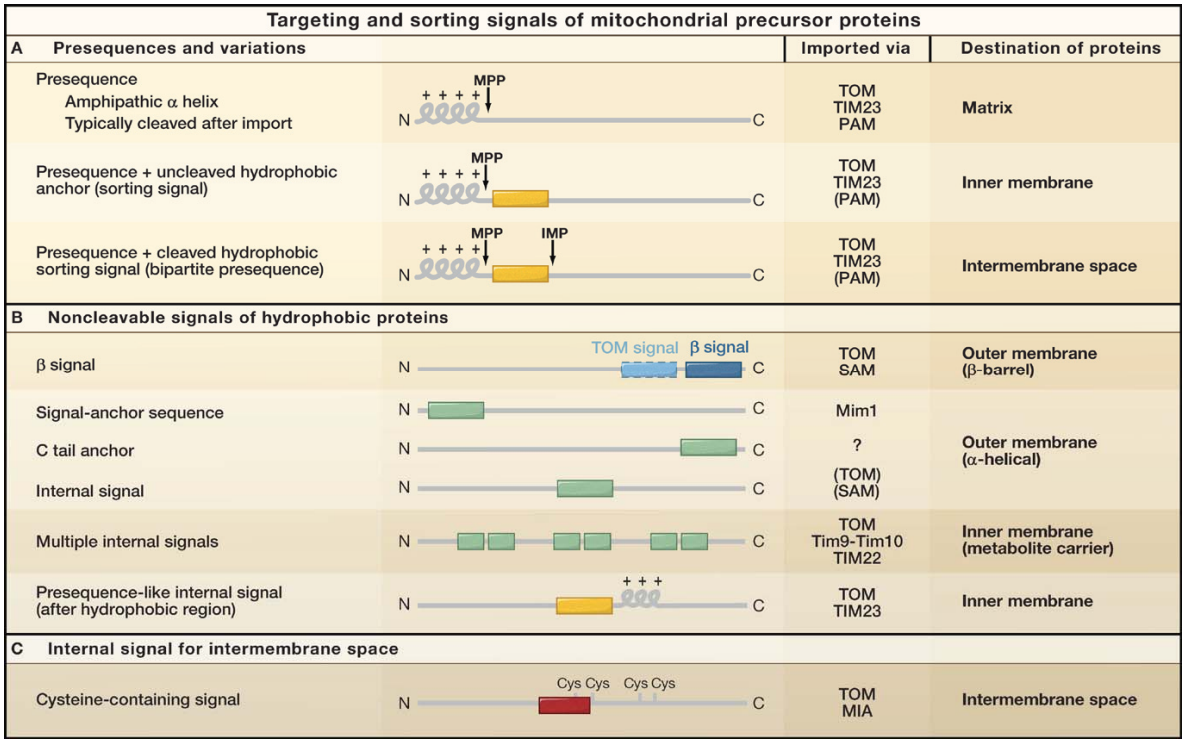

Fig. 13: Targeting and Sorting Signals of Mitochondrial Precursor Proteins. Three main classes of signals are shown: A) Presequences which are usually cleaved off by MPP and IMP, B) Noncleavable signals of hydrophobic proteins, and C) Internal signals for IMS.Picture from (Ramakrishnan, Southern et al. 1998).

Matrix proteins usually have an N-terminal presequence termed matrix-targeting sequence (MTS) consisting of 10 to 80 amino acids. They often form amphipathic α-helices which are positively charged and have a hydrophobic surface. After import the MTS is cleaved off by a mitochondrial processing peptidase (MPP) (Gordon, Dancis et al. 2000, Ozawa, Sako et al. 2003). IMM proteins contain either hydrophobic internal targeting signals or presequences followed by a hydrophobic membrane anchor sequence that retains the protein in the IMM. Typically these signals remain part of the mature protein (Doonan, Marra et al. 1984, Pfaller, Steger et al. 1988, Glick, Beasley et al. 1992). IMS proteins were also shown to have presequences followed by a hydrophobic membrane anchor (Doonan, Marra et al. 1984, Pfaller, Steger et al. 1988, Glick, Beasley et al. 1992, Kaldi and Neupert 1998). In contrast to IMM proteins, these presequences are cleaved off by MPPs and an inner membrane protease to release them into the

IMS. Most OMM proteins contain a non-cleavable targeting sequence followed by a long hydrophobic stretch. The presequence guides the protein to the mitochondria and the hydrophobic stretch is responsible for the insertion to the OMM (Glick, Beasley et al. 1992, Kaldi and Neupert 1998, Gordon, Dancis et al. 2000, Hoogenraad and Ryan 2001).

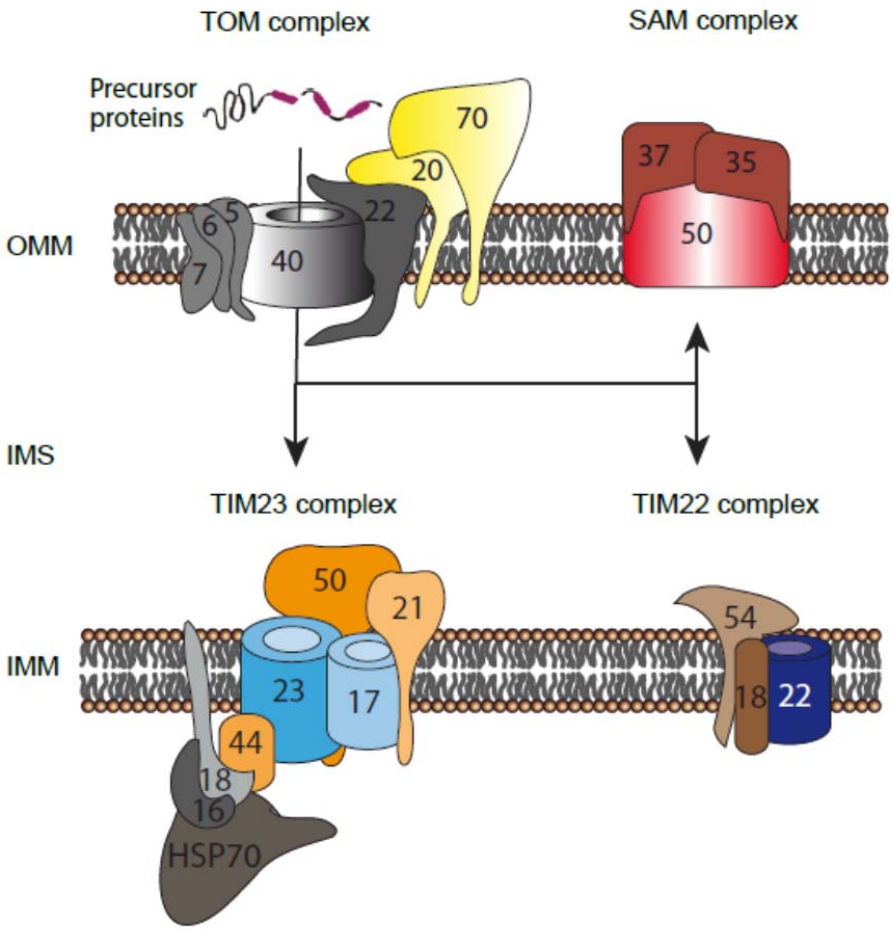

Fig. 14: The four main complexes of the mitochondrial protein import machinery. Figure adapted from (Rettig 2011).

In most eukaryotes four distinct high molecular weight protein complexes exist within the OMM and the IMM to mediate protein translocation (see Figure 14). The translocase of the outer mitochondrial membrane (TOM) is the main entry

gate for essentially all proteins that have to be imported. It is built out of 7 proteins around a pore-forming β-barrel protein (Ryan, Wagner et al. 2000, Kato and Mihara 2008). A second OMM translocase complex, also carrying a β-barrel protein as core component, is a sorting and assembly machinery (SAM). The SAM complex inserts proteins into the OMM, after import of proteins into the IMS (Doonan, Marra et al. 1984, Glick, Beasley et al. 1992, Kaldi and Neupert 1998). Within the IMM two translocases of the inner mitochondrial membrane (TIM) exist, TIM22 and TIM23. The first one, TIM22, is thought to insert hydrophobic carrier proteins into the IMM. The core of the second complex, TIM23, is built of the translocase channel Tim23, the precursor recognition and channel gating subunit Tim50, and Tim17 which is involved in motor recruitment and lateral preprotein sorting (Doonan, Marra et al. 1984, Glick, Beasley et al. 1992, Kaldi and Neupert 1998, Davis, Sepuri et al. 2000). Through coupling respiratory chain complexes III and IV with the TIM23 complex the membrane potential around TIM23 is increased, giving the driving force for protein translocation by exerting an electrophoretic effect on positively charged MTS. For complete translocation over the IMM into the matrix an additional driving force next to the electrophoretic effect is necessary. This is provided by the ATP-driven mitochondrial heat shock protein mtHsp70. Once the proteins are imported into the matrix their presequences are cleaved off by MPPs and the proteins are folded into their native form by matrix localized chaperones (Sirrenberg, Bauer et al. 1996, Gordon, Dancis et al. 2000, Yoneda, Benedetti et al. 2004).

4.2.4 Mitochondrial Quality Control and Unfolded Protein Response

Several factors challenge the homeostasis of the mitochondrial protein-folding environment including complexities in mitochondrial biogenesis, e.g. reactive oxygen species (ROS) that are generated within mitochondria, environmental factors such as changes in temperature, or exposure to toxins (Haynes and Ron 2010). In addition, protein synthesis in the cytosol and the mitochondria have to

be synchronized as ETC complexes I, III, IV and the ATP synthase contain subunits encoded and produced in different parts of the cell, i.e. mitochondria or nucleus and cytosol (Haynes and Ron 2010). To promote efficient mitochondrial protein folding and complex assembly, mitochondria have a dedicated repertoire of molecular chaperones located in both the IMS and matrix. For example, the nuclear encoded Hsp60 chaperonin is located in the matrix, and consists of both Hsp60 and Hsp10 subunits which form a barrel-shaped complex. The Hsp60 chaperonin primarily facilitates the folding of relatively small, soluble monomeric proteins (Baena-Lopez, Alonso et al. 2008, Felk, Ohrt et al. 2010, Rocha, Ferreira et al. 2011). In addition to molecular chaperones, mitochondria house several quality control proteases, e.g. ClpXP or Lon, that recognize and degrade those proteins that fail to fold or assemble correctly (Missiakas, Schwager et al. 1996, Smakowska, Czarna et al. 2014). The importance of maintaining the mitochondrial protein-folding environment can be emphasized by diseases associated with a compromised balance of the mitochondrial proteome. For example, mutations of Hsp60 or in the mitochondrial quality control protease Paraplegin cause spastic paraplegia, and the mitochondria-specific translation inhibitors paraquat and rotenone as well as an *Htra2*-deletion cause Parkinson's-like symptoms (Moisoi, Klupsch et al. 2009). In addition to a variety of diseases, loss of mitochondrial protein homeostasis has been associated with the aging process (Pan 2011, Gregersen, Hansen et al. 2012, Cuadrado-Tejedor, Cabodevilla et al. 2013, Kumar, Gibbs et al. 2013).

In response to the accumulation of unfolded or misfolded proteins, cells mount a mitochondrial unfolded protein response (UPR^{mt}). The UPR^{mt} is an organelle specific pathway with no direct connection to the UPR of the ER (Zhao, Wang et al. 2002, Yoneda, Benedetti et al. 2004, Horibe and Hoogenraad 2007). UPR^{mt} is a mitochondria-to-nuclear signal transduction pathway resulting in the induction of mitochondrial protective genes including mitochondrial molecular chaperones and proteases to re-establish protein homeostasis within the mitochondrial protein-folding environment. The signal transduction mechanism from mitochondria to the nucleus is still a topic of ongoing research. The transcription

factors CHOP and C/EBPβ are required for Hsp60 transcription (see Figure 15). The presence of an activator protein-1 (AP1) site was revealed by analysis of the promoters of CHOP and C/EBPβ and hence suggested the presence of the Jun transcription factor which makes the involvement of JNK2, a kinase upstream of Jun, likely. Jun becomes phosphorylated upon mitochondrial stress whilst a JNK2 inhibitor attenuates the response. However, it is unlikely that CHOP, C/EBPβ and Jun are the only transcription factors involved in the UPR^{mt} as the CHOP binding sites involved in mitochondrial stress response are flanked by two additional conserved sequences, the so-called mitochondrial UPR elements (MUREs) (Zhao, Wang et al. 2002).

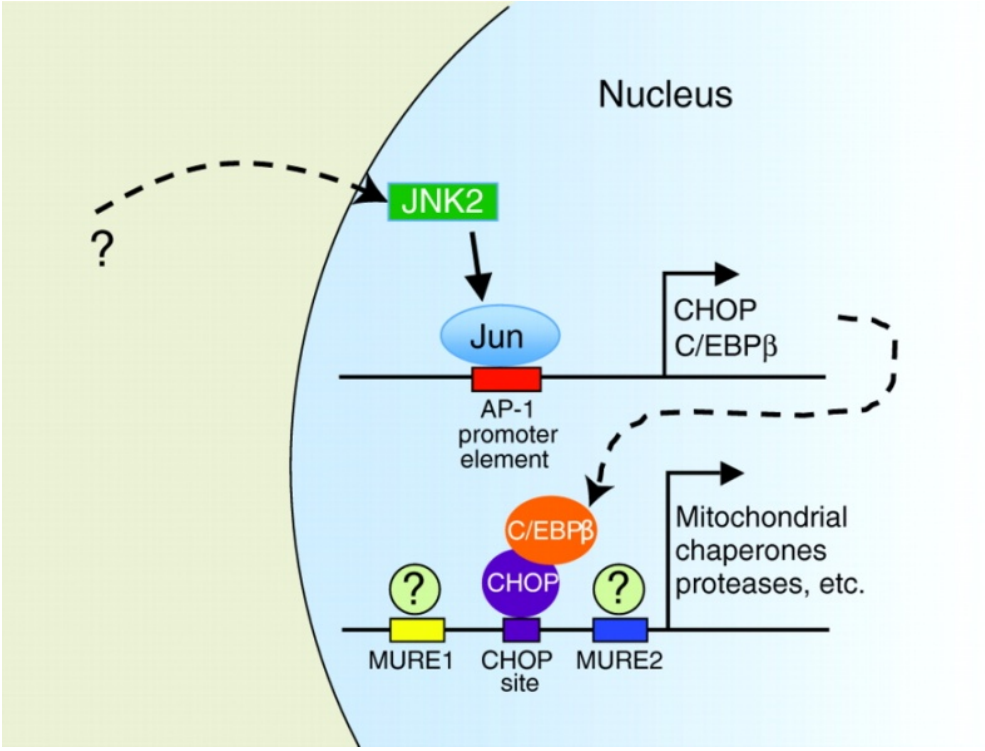

Fig. 15: Mitochondrial UPR signaling in mammalian cells. Figure taken from (Haynes and Ron 2010)

Much more is known about the signaling pathway of UPR^{mt} in *C. elegans* (Haynes, Petrova et al. 2007, Haynes and Ron 2010, Haynes, Yang et al. 2010, Baker, Nargund et al. 2012, Nargund, Pellegrino et al. 2012, Haynes, Fiorese et al. 2013, Pellegrino, Nargund et al. 2013). The protease ClpXP degrades

unfolded or unassembled proteins into peptides of approximately 8-20 residues which are pumped across the inner membrane by the ABC-transporter HAF-1 and then across the outer membrane to the cytosol. It was suggested that the peptide efflux weakens mitochondrial import (Nargund, Pellegrino et al. 2012). The main UPRmt regulator, the transcription factor ATFS1, contains both nuclear localization/export (NLS) and mitochondrial targeting sequences (MTS). Under protein homeostasis conditions ATFS1 is transported into the mitochondria and degraded (Nargund, Pellegrino et al. 2012). However, because of impaired protein import due to proteotoxic stress in mitochondria leads to translocation of ATFS1 to the nucleus. Further, the homeobox proteins DVE-1 and UBL-5 form a complex and bind to the *hsp-60* promoter to promote ATFS-1 binding to activate transcription. Transcriptional upregulation of mitochondrial chaperone genes leads to their subsequent import into mitochondria, thus relieving stress and re-establishing mitochondrial protein homeostasis (see Figure 16). ATFS1 also functions to increase the expression of proteins involved in mitochondrial import, ROS detoxification and protection against mitochondrial dysfunction (Nargund, Pellegrino et al. 2012).

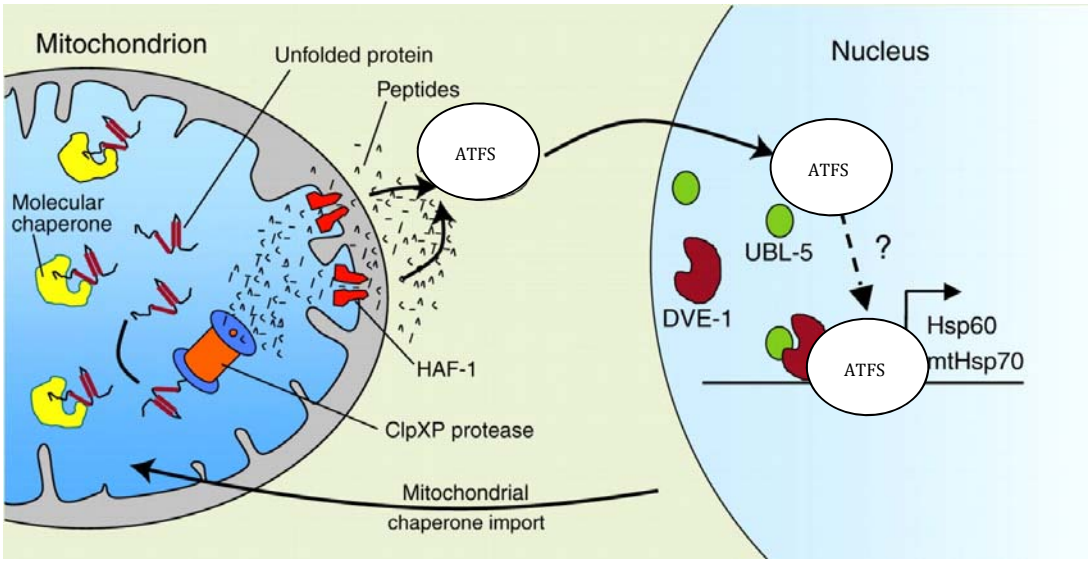

Fig 16: Model of the UPR^{mt} in *C. elegans.* Figure taken from (Haynes and Ron 2010).

5 RESULTS

5.1 Aminoglycoside-Induced Misreading

5.1.1 Codon Selection for Gain-of-Function Assay

Missense errors during protein synthesis result from incorrect codon recognition (Daviter, Gromadski et al. 2006). Not all codons are error prone and not all codons are equally sensitive to be misread on aminoglycoside treatment (Kramer and Farabaugh 2007). The ideal codon for the experimental analysis of aminoglycoside induced misreading is not error prone but is mistranslated when a misreading inducing drug is applied.

Several systems have been used to analyze the frequency of erroneous decoding, e.g. lysine incorporation, radiolabelling, 2D-gel electrophoresis, and restoring enzymatic activity of reporters (Edelmann and Gallant 1977, Edelmann and Gallant 1977, Parker 1989, Soslau and Parker 1989, Cornut and Willson 1991, Kramer and Farabaugh 2007, Ortego, Whittenton et al. 2007). For our purpose we decided to use the gain-of-function assay previously described by Kramer et al. (Kramer and Farabaugh 2007) (see Figure 17).

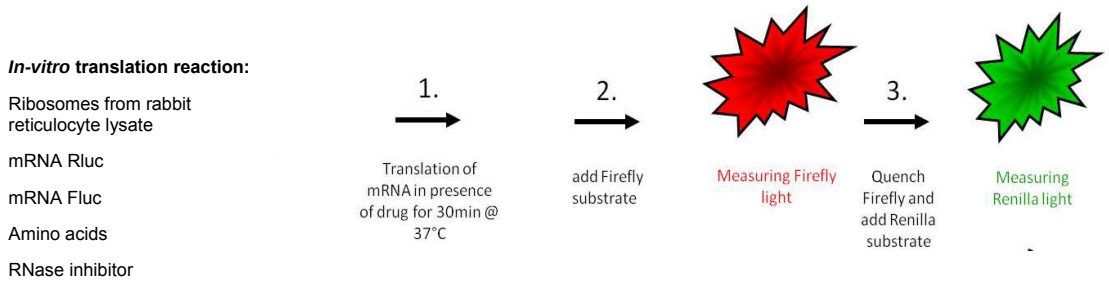

Fig. 17: Schematic procedure of the *in vitro* dual luciferase assay. *In vitro* translation, i.e. RRL ribosomes translating the mRNAs of Fluc and Rluc.

Measurements of relative luminescence units (RLU) of firefly luciferase serve as basis for this assay. To determine drug-mediated translation inhibition, the antibiotic was titrated and the reduction of RLUs was plotted. By preparing such

curves the IC25, IC50 and IC75 values can be elicited, i.e. the drug concentrations at which the inhibition of translation activity is 25%, 50%, or 75%, respectively.

Residues H245 or K529 in the catalytic center are the amino acids responsible for orientation of the substrates luciferin and ATP in the active site (Branchini, Magyar et al. 1998, Branchini, Murtiashaw et al. 2000). To determine misreading we used a mutated firefly luciferase. By mutating the cognate wild type codon $H245^{CAC}$ or $K529^{AAA}$ to a near-cognate codon the activity of the firefly luciferase is significantly reduced. Mutations were introduced in the active site, for a summary see Table 4. Misreading of these codons would restore firefly luciferase function; hence such mutations can be used to compare the rate of decoding errors. As a reference a wild type renilla luciferase was used in all reactions.

Near-cognate mutations at codon $K529^{AAA}$ decreased enzymatic activity up to 2500-fold compared to wildtype firefly luciferase (see Table 4 and Figure 18). To test which mutation best serves our purpose, we used the aminoglycoside paromomycin, which is known to induce misreading (Davies, Gorini et al. 1965, Palmer and Wilhelm 1978, Mironova, Provorov et al. 1982, Eustice and Wilhelm 1984, Tuite and McLaughlin 1984). When rabbit reticulocyte lysate (RRL) ribosomes were treated with 10 µM paromomycin near-cognate mutant luciferases showed a relative increase of signal intensity of 3.9-fold up to 9.1-fold as compared to luciferases produced from untreated ribosomes (see Table 4 and Figure 18).

Near-cognate mutations at codon $H245^{CAC}$ decreased the enzymatic intensity up to 3200-fold compared to the wildtype firefly luciferase (see Table 4 and Figure 18). Treatment of ribosomes with paromomycin resulted in a relative increase of the firefly luciferase activity of 4.2-fold and 25.1-fold for near-cognate codons $H245^{GAC}$ and $H245^{CGC}$, respectively. Near-cognate codons $H245^{CAG}$ and $H245^{UAC}$ showed no increase of relative signal intensity (see Table 4 and Figure 18) as they are naturally error prone, i.e. these codons are highly misread without

any antibiotic treatmet of the ribosome. As a negative control the non-cognate mutant $H245^{AGA}$ was used.

Based on these results, further experiments to measure aminoglylcoside induced mistranslation were conducted with a reporter construct containing the near-cognate H245(CAC → CGC) nucleotide point mutation.

Tab. 4: List of the mutated codons and corresponding values of firefly activity (RLU) with the corresponding standard error of the mean (SEM) *in vitro*. Mistranslation was induced with 10μM paromomycin. Wildtype Firefly activity corresponds to 100'000 RLU and all measurements were done in triplicates.

	Untreated		**10 μM paromomycin**		**Fold induction**
Codon	**RLU**	*SEM*	**RLU**	*SEM*	
K529 AGA	38	*6*	151	*6*	**3.9**
K529 AGG	31	*5*	274	*61*	**8.9**
K529 AAU	22	*9*	100	*19*	**4.5**
K529 AAC	15	*4*	75	*2*	**4.8**
K529 UUU	129	*30*	76	*10*	0.6
H245 CAG	551	*55*	579	*4*	1.1
H245 GAC	31	*5*	130	*15*	**4.1**
H245 UAC	4376	*54*	3654	*162*	0.8
H245 CGC	153	*26*	3842	*448*	**25.1**
H245 AGA	28	*0*	29	*2*	1
WT	100'000	---	---	---	---

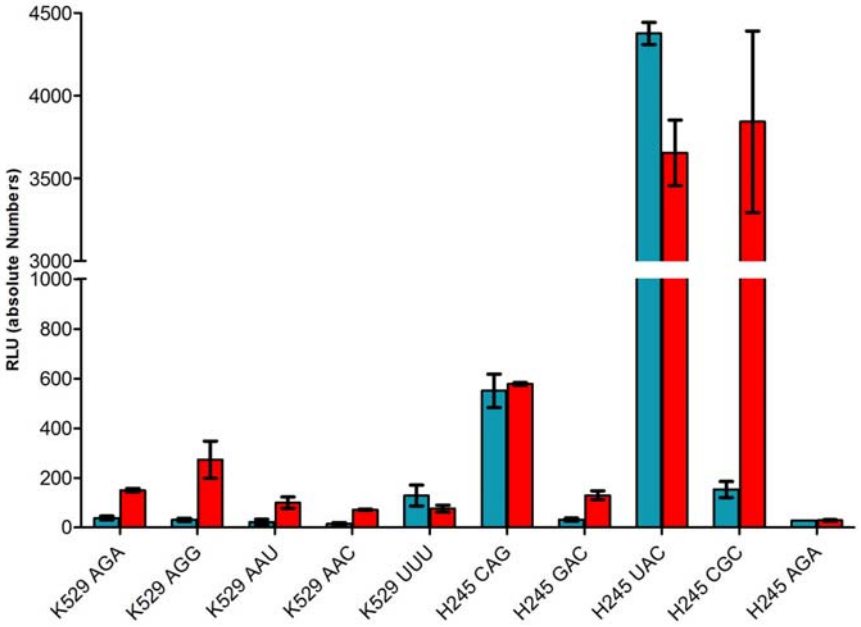

Fig. 18: *In vitro* measurements of firefly luciferase activity using different mRNA constructs. Blue bars represent reactions without drug and red bars represent reactions containing 10µM paromomycin. Error bars show SEM of triplicates and y-axis is disrupted for better view.

5.1.2 *In vitro* System: Translation Inhibition

One of the effects of aminoglycosides on translation is inhibition of protein synthesis. Aminoglycosides inhibit protein synthesis by blocking the translocation of the ribosome (Champney 2006, Borovinskaya, Shoji et al. 2008, Feldman, Terry et al. 2010).

A set of eight aminoglycosides was chosen for these studies and inhibition of protein synthesis was measured by determining the dose-responses *in vitro* in rabbit reticulocyte lysate (RRL). Geneticin and hygromycin B showed IC50 values of 0.3 µM and 0.1 µM, respectively. Further determined IC50 values were 11 µM for gentamicin, 25 µM for paromomycin, 44 µM for neomycin, and 60 µM for apramycin. The IC50 value of tobramycin was 95 µM, that of amikacin 141 µM, and that of kanamycin A 294 µM (see Figure 19). The modeled dose-response curves from the experimentally measured luminescence units (RLU) could be fitted accurately, with squared Pearson-product-moment (R-square) values from 0.96 to 0.99.

5.1.3 *In vitro* System: Misreading Induction

To study the effects of aminoglycosides on ribosomal accuracy we used the mutant H245^{CGC} Fluc mRNA and analyzed the activities at various doses of drugs (see Figure 20). For geneticin, gentamicin and paromomycin high misreading levels were observed. Little to no misreading was observed for kanamycin A and apramycin.

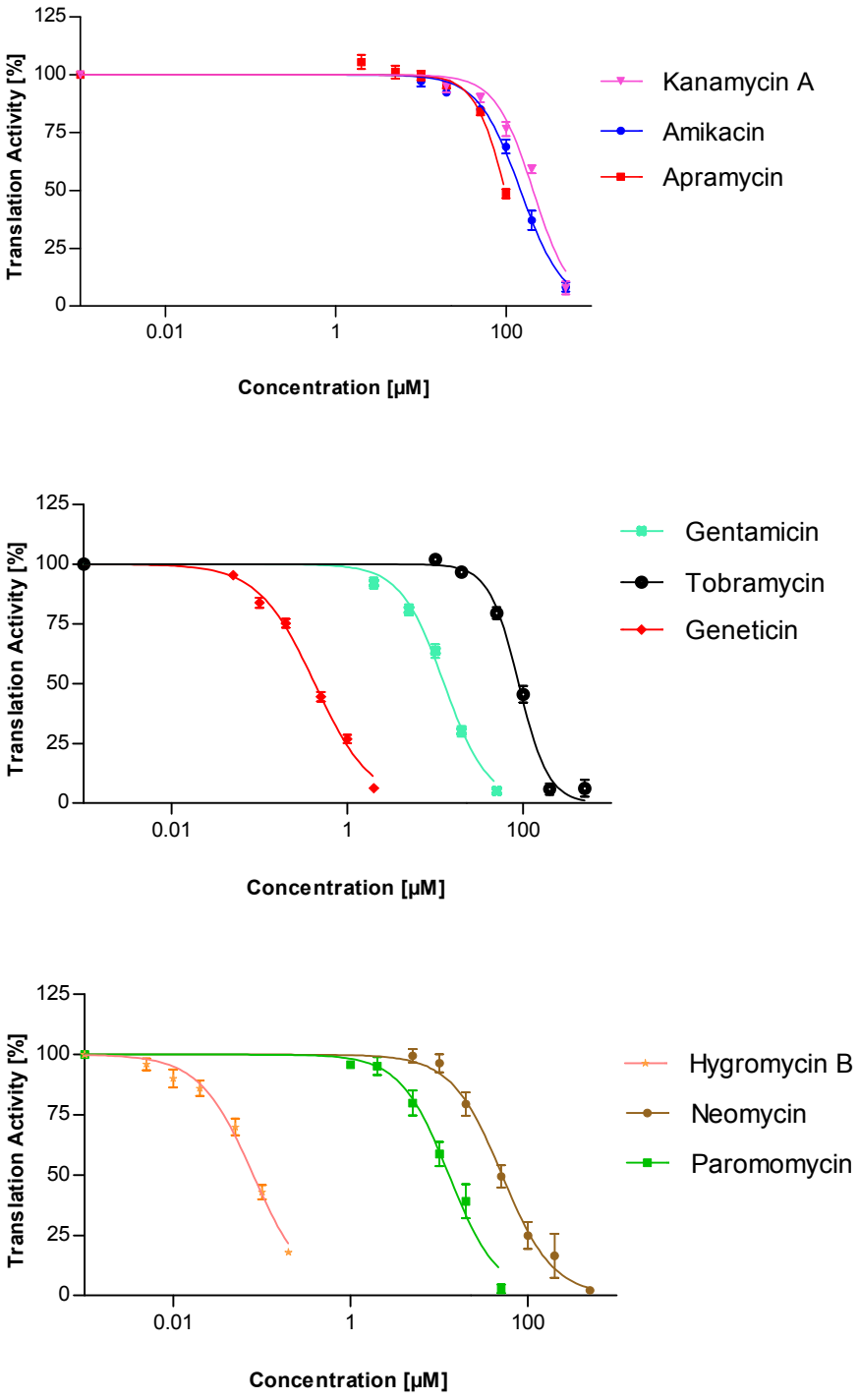

Fig. 19: Aminoglycoside induced inhibition of translation of Fluc mRNA by RRL ribosomes *in vitro*. Error bars represent the SEM of triplicates.

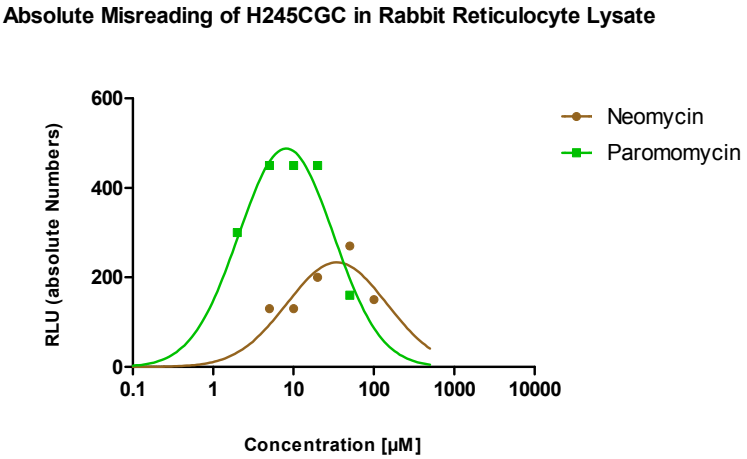

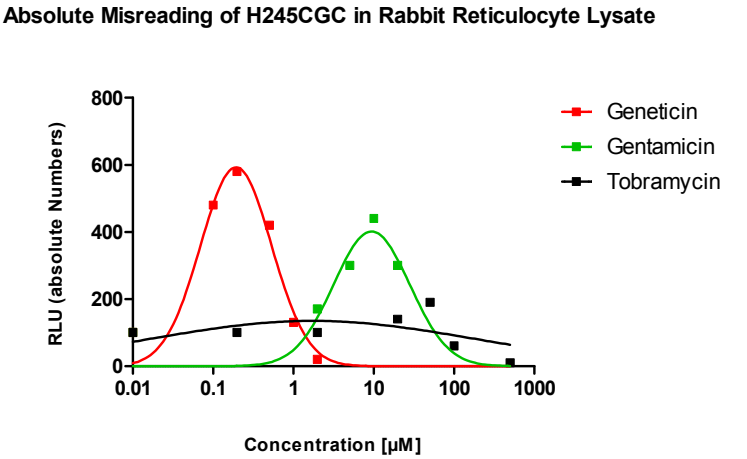

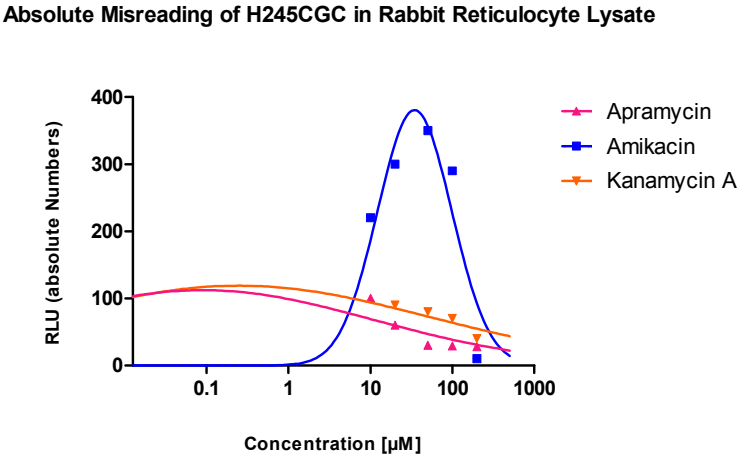

Fig. 20: Absolute Numbers of Firefly activity *in vitro*. Untreated reaction mixtures were set as reference at 100.

Mistranslation can be possibly masked by translation inhibition. Therefore, we related the experimentally measured Fluc values to translation inhibition:

i) Definitions

R_{WT} = Signal of hRluc WT from Reference construct

R_{Mut}= Signal of hRluc WT from Mistranslation construct

F_{WT} = Signal of hFluc WT from Reference construct

F_{Mut} = Signal of hFluc Mut from Mistranslation construct

ii) Quantity of proteins

➔ $hRluc_x = hFluc_x$

⇔ $hFluc_x / hRluc_x = 1$

⇔ $hFluc_{Mut} / hRluc_{Mut} = hFluc_{WT} / hRluc_{WT}$

⇔ $hFluc_{Mut}/hFluc_{WT} = hRluc_{Mut}/hRluc_{WT}$

➔ $hRluc_{Mut} / hRluc_{WT} = EQ$

$hFluc_{Mut} = hFluc_{WT} * EQ$

iii) Curves

Inhibition = F_{WT} *(at conc. x, with 100 = value measured with no aminoglycoside)*

Mistranslation = $(F_{Mut}/F_{WT})*(R_{WT}/R_{Mut})$ *(at conc. x, with 100 = value measured with no aminoglycoside)*

Fold Induction = Mistranslation (conc. x) / Mistranslation (conc. 0)

Following normalization all aminoglycosides except apramycin showed a dose-response of misreading induction (see Figure 21). At IC50, a 15.0-fold

misreading induction was observed for paromomycin, followed by geneticin with 11.4-fold at IC50. Gentamicin and amikacin showed an induction of 8.8- and 7.7-fold, respectively. With neomycin a 4.6-fold, tobramycin a 3.6-fold and kanamycin A a 3.0-fold misreading induction was found. No misreading induction was observed for apramycin. When these experiments were performed with Fluc mRNA containing the non-cognate mutation $H245^{AGA}$ no Fluc activity was observed for the tested aminoglycosides.

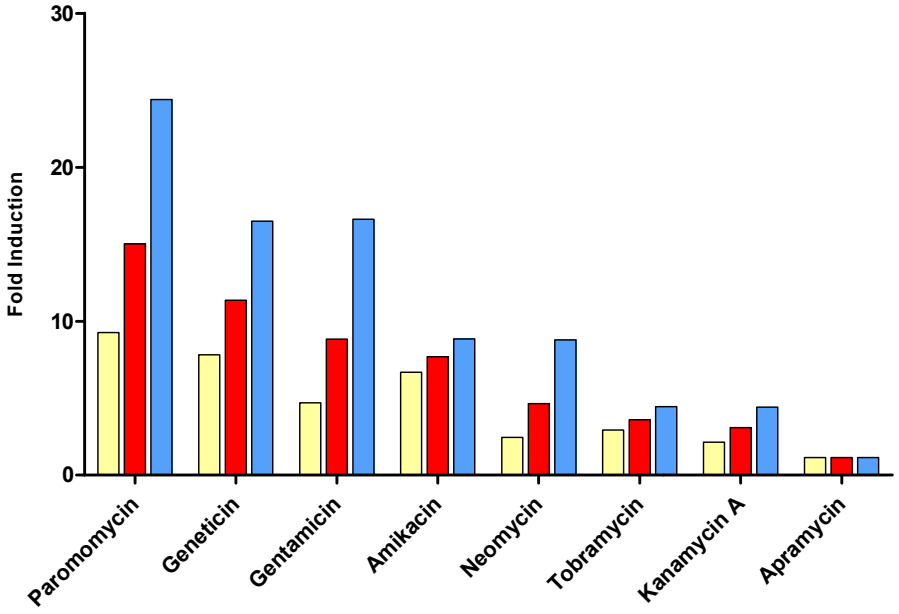

Fig. 21: Fold induction of misreading *in vitro* at IC25 (yellow), IC50 (red), and IC75 (blue). Values were calculated by comparing Fluc mut/Fluc wt.

5.1.4 *In vivo* System: Translation Inhibition

As a next step, we studied translation inhibition in an eukaryotic *in vivo* model system. HEK293 cells were transfected with a plasmid coding for two luciferases fused by a 27 nucleotide linker (see Figure 22).

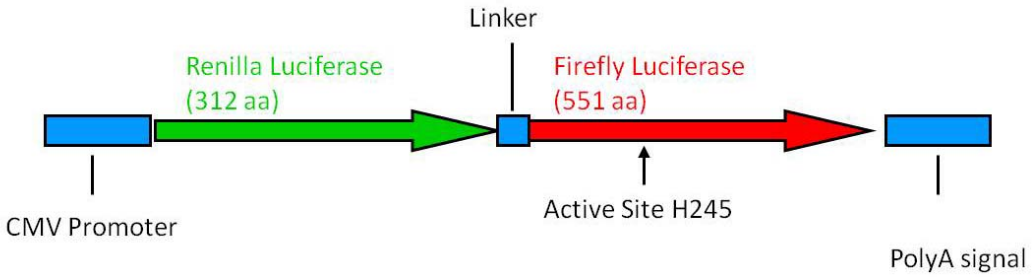

Fig. 22: Luciferase construct used for measurements of *in vivo* misreading experiments. The two luciferases renilla and firefly were fused with a 27 nucleotide linker sequence. Transcription is under control of a CMV promoter and the construct contains a standard poly-A signal at the 3' end.

The 5' luciferase, Rluc, was used to control for transfection efficiency and translation inhibition, whilst the 3' luciferase, Fluc containing the H245^{CGC} mutation, served to measure misreading. Cells were grown in DMEM and then transferred to a serum free growth medium containing 15µg/ml saponine, a mild non-ionic detergent to permeabilize cell membranes. After 24 hours of incubation, cells were lysed and luciferase activities were measured.

Dose-response curves were measured (see Figure 23). Geneticin and hygromycin B were the strongest translation inhibitors with IC50s of 4.6 µM and 2.6 µM, respectively. Paromomycin had an IC50 of 249 µM followed by gentamicin with an IC50 of 473 µM. IC50s were 552 µM for apramycin, 769 µM for neomycin, 841 µM for tobramycin, and 919 µM for amikacin. Fitted curves showed an R-square of 0.96 to 0.99.

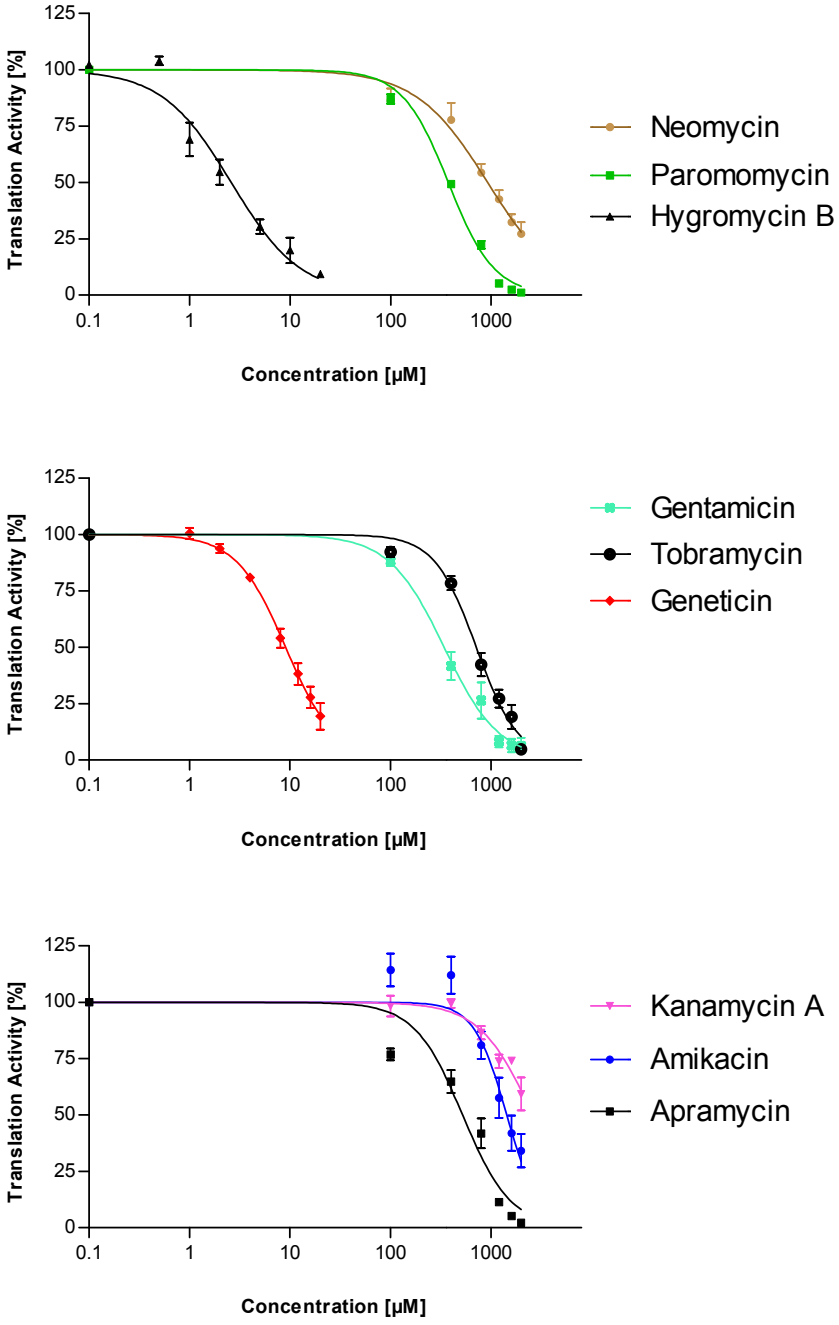

Fig. 23: Inhibition of translation *in vivo* by different aminoglycosides. Error bars represent the SEM of triplicates.

5.1.5 *In vivo* System: Misreading Induction

We analyzed misreading induction in HEK293 cells using Fluc H245^{CGC} constructs. Increasing amounts of drugs were applied and firefly activities were measured (see Figure 24). Geneticin showed the most pronounced absolute increase of misreading. As the effect on translation accuracy can be masked by the inhibitory effect of aminoglycosides, we normalized the measured mutant firefly luciferase values by relating them to the values of the renilla luciferase which is fused to the Fluc (see Figure 22).

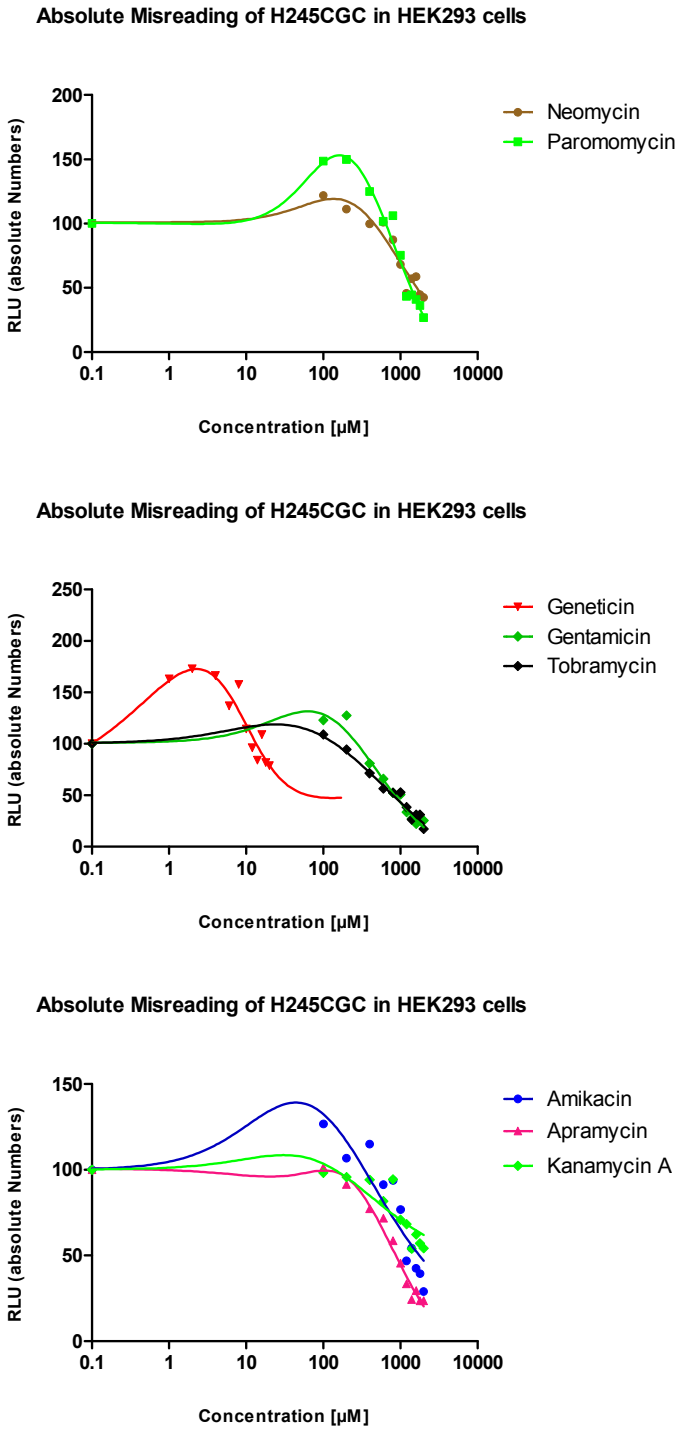

Fig. 24 Absolute numbers of firefly activity *in vivo*. A) 4,5-aminoglycosides and apramycin, B) 4,6-aminoglycosides. Untreated reaction mixtures were set as reference at 100. Error bars represent the SEM of triplicates.

When Fluc numbers were normalized to translation inhibition, four out of eight drugs showed an induction of misreading in vivo (see Figure 25). Geneticin was the most potent drug with a 4.0-fold induction of mistranslation at IC50. Other strong misreading inducers were amikacin (3.2 fold at IC50), paromomycin (2.8-fold at IC50) and gentamicin with 2.2-fold at IC50. No significant misreading induction at IC50 was observed for apramycin, neomycin, tobramycin and kanamycin A. No misreading was observed when experiments were performed with a $H245^{AGA}$ construct.

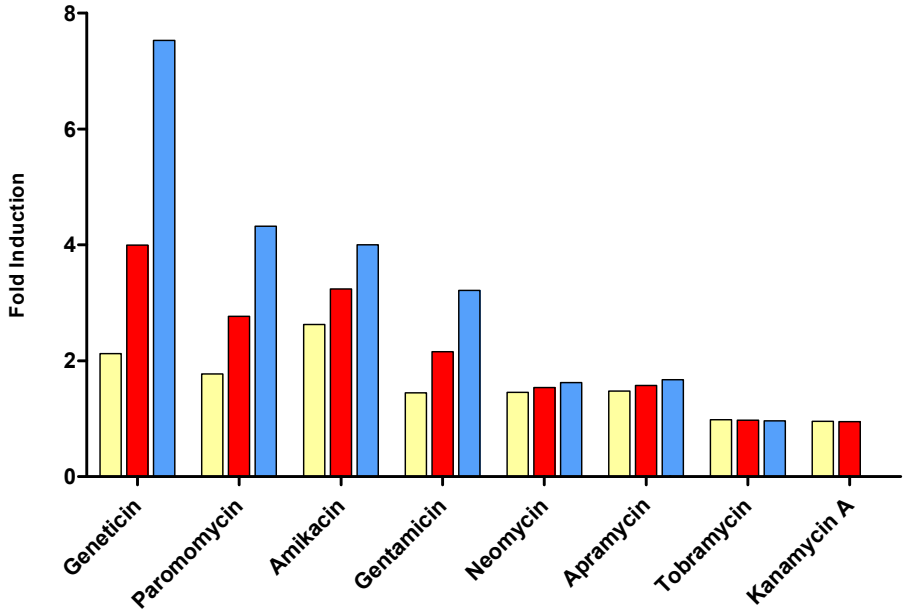

Fig. 25: Fold induction of misreading *in vivo* at IC25 (yellow), IC50 (red), and IC75 (blue). For kanamycin A the IC75 was not in a reasonable range and therefore calculation of the induction may lead to false conclusions.

5.1.6 Discussion

Aminoglycosides are potent antibiotics that target the ribosome. The interaction of aminoglycosides with the cytosolic ribosome results in translation inhibition and affects the fidelity of translation. In the subset of aminoglycosides analyzed

here, the potency to inhibit translation of the different compounds was found to cover a wide range of concentrations. Experiments demonstrated IC50 over three orders of magnitude with hygromycin B as the most potent compound tested *in vitro* and *in vivo*. In general, the concentrations needed to reach IC50 were around 10- to 20-fold lower *in vitro* than *in vivo* – reflecting the prescence of the cell membrane in the *in vivo* system. However, the results correlate well when comparing IC50 values of *in-vitro* and *in-vivo* experiments (see Figure 26). In both systems the most potent aminoglycoside tested was hygromycin B, closely followed by geneticin. The aminoglycosides amikacin and kanamycin A were in both systems the least effective compounds.

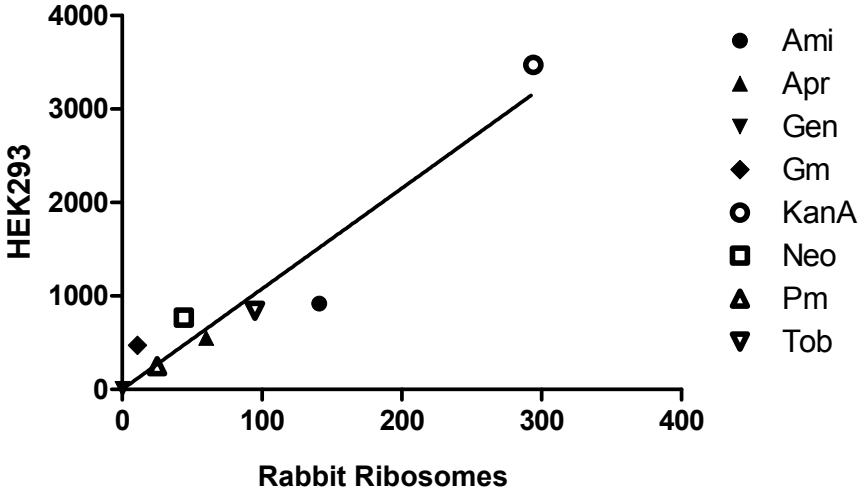

Fig. 26: Comparison of IC50 values in RRL versus IC50 values in HEK293 cells. Numbers on x- and y-axis represent the concentration of drug in µM. The accuracy of fit corresponds to an R-square (squared Pearson-product-moment) of 0.86 and is assumed to be significant with $p<0.01$.

Similar to translation inhibition the induction of misreading correlates also well between the *in vitro* and the *in vivo* measurements (see Figure 27). Geneticin and paromomycin were shown to be very potent inducers of misreading. On the opposite apramycin, tobramycin and kanamycin A showed little or no misreading at IC50.

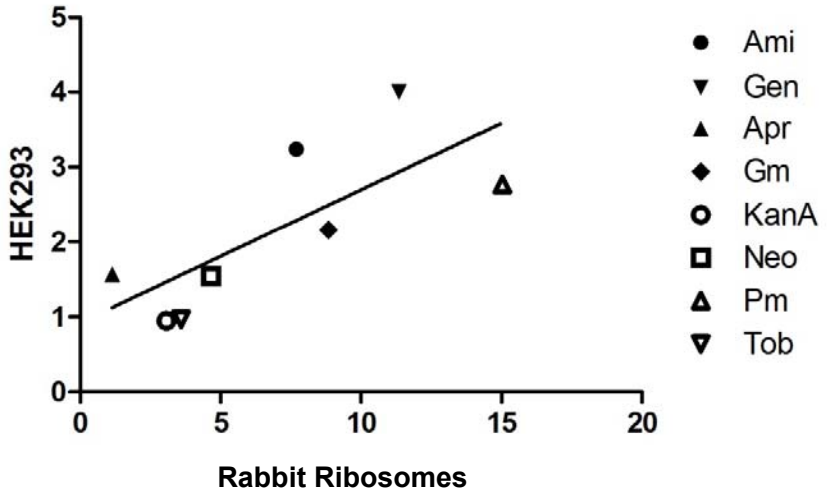

Fig. 27: Comparison of fold induction of misreading in RRL versus fold induction of misreading in HEK293 cells at IC50. The accuracy of fit corresponds to an R-square of 0.78 and is assumed to be significant with $p<0.05$.

We also assessed the correlation of misreading with readthrough – the latter data was kindly provided by Stefan Duscha. Readthrough was measured with a similar assay as used for misreading. Within the linker sequence of the 5' renilla luciferase and the 3' firefly luciferase a stop codon was introduced and the amount of readthrough was determined. The higher values for readthrough measurements most likely reflect the fact that for readthrough of a premature stop codon virtually any amino acid can be incorporated to result in a functional protein. In contrast, for functional proteins in the misreading assay only the correct near-cognate amino acid restores the active center of the protein. As shown in Fig. 28 aminoglycoside-induced misreading and aminoglycoside-induced readthrough correlate well.

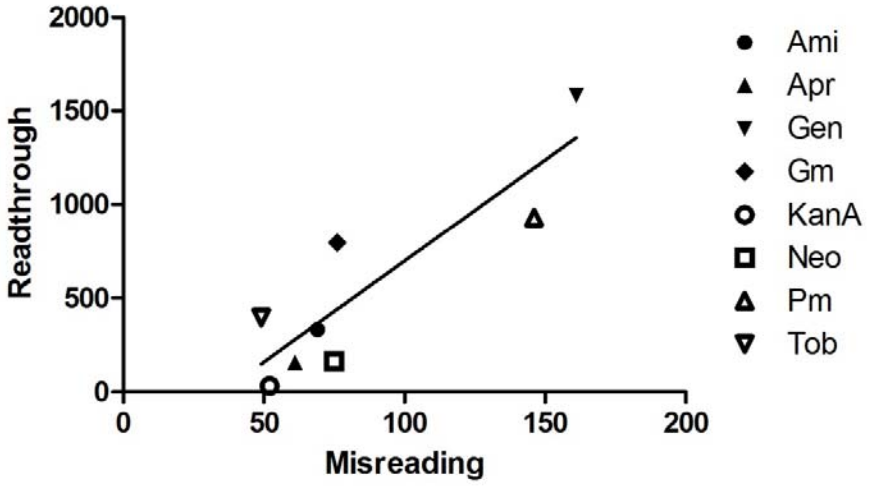

Fig. 28: Comparison of readthrough induction versus misreading induction in HEK293 cells at IC50. Numbers on x- and y-axis represent the measured luminescence. The accuracy of fit corresponds to an R-square of 0.78 and is assumed to be significant with $p<0.01$.

5.2 Drug-Induced Mitochondrial Unfolded Protein Response

5.2.1 Test System and Drugs used

Misfolded proteins may lead to an unfolded protein response (UPR). Over 99% of the mitochondrial proteins are produced by cytosolic ribosomes. Proteins produced in the cytosol usually fold inside the mitochondria and are therefore recognized if misfolded at their destination (Pfaller, Steger et al. 1988). Considering the misreading potential of aminoglycosides, we set out to study wether aminoglycosides which induce misreading on the cytosolic ribosome induce a mitochondrial UPR (UPR^{mt}). Induction of Hsp60 or ClpP can be used as marker of UPR^{mt} (Zhao, Wang et al. 2002). HEK293 cells were transfected with a reporter plasmid containing the promoter of either Hsp60 or ClpP fused to a firefly luciferase gene as reporter (see Figure 29). After 24 hours, medium was replaced and drug was added. Cells were then incubated for another 48 hours. Hsp60 and ClpP expression levels were detected by measuring firefly luciferase activity. As internal translation control, cells were co-transfected with a plasmid containing β-galactosidase under control of a CMV promoter (see Figure 29).

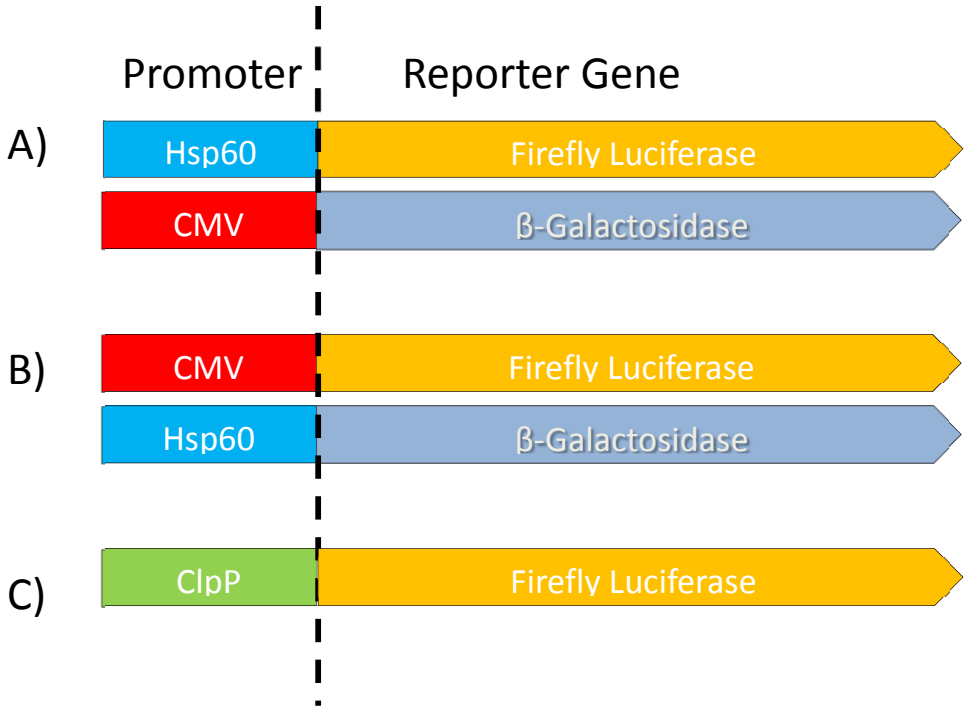

Fig 29: Schematic view of the constructs used to measure UPR^{mt} induction. A) Original constructs as supplied by Houtkooper et al. (Houtkooper, Mouchiroud et al. 2013) B) Constructs used to verify results obtained with original constructs. C) Construct to assess ClpP induction as supplied by Zhao et al. (Zhao, Wang et al. 2002).

In this study we used the 4,6-aminoglycosides geneticin and gentamicin, the unique aminoglycoside hygromycin B, the glutarimide antibiotic cycloheximide, the tetracycline doxycycline, and linezolid which belongs to the class of oxazolidinones.

When assessing the translation inhibition of the cytosolic ribosome, a dose-response curve was observed for hygromycin B, geneticin, cycloheximide and gentamicin. Doxycycline and linezolid, on the other hand, did not show any translation inhibition of the cytosolic ribosome (see Figure 30).

To analyze the effect of the used antibiotics on the mitochondrial ribosome, we performed *in organello* translation. With this method we monitored the productivity of the mito-ribosome, in particular COX1 translation. In brief, mitochondria from HEK293 cells were isolated and different concentrations of

drugs were added to reaction mixtures containing ^{35}S-methionine. After two hours, reactions were stopped and samples were resolved by SDS-PAGE. Hygromycin B and gentamicin showed a clear dose-response on inhibiting the mitochondrial ribosome. In contrast, geneticin showed only little inhibition of the mitochondrial ribosome even up to a concentration of 1000 µM. We found also significant translation inhibition of the mitochondrial ribosome when we applied doxycycline or linezolid. No inhibition was observed when using cycloheximide (see Figure 31).

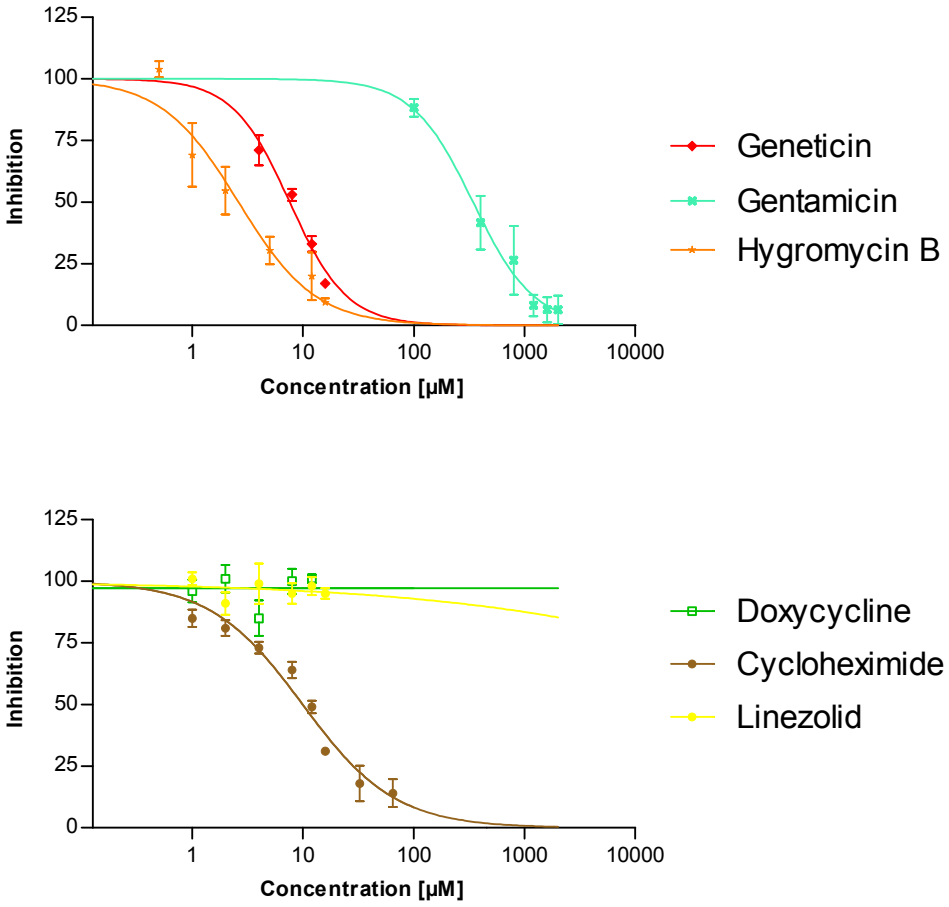

Fig. 30: Translation inhibition of the cytosolic ribosome *in vivo* by doxycycline, cycloheximide, linezolid, gentamicin, hygromycin B and geneticin.

A)

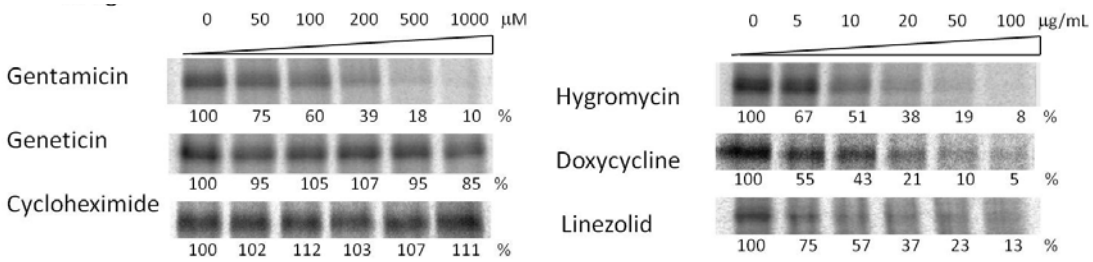

B)

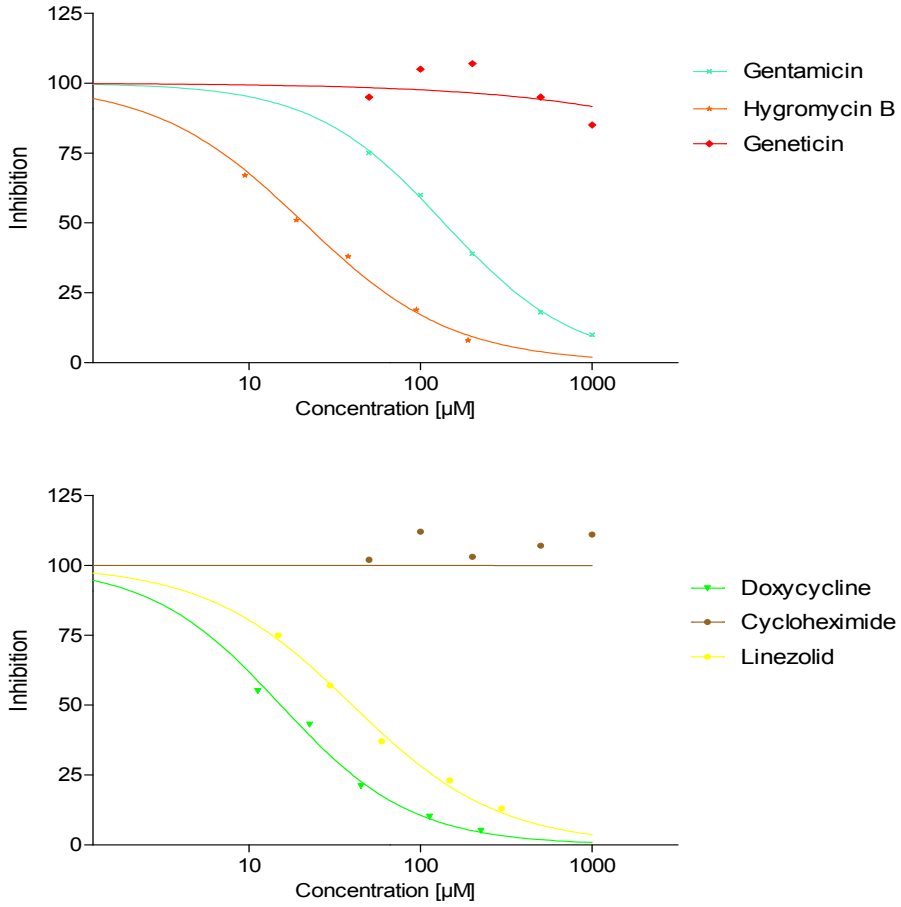

Fig. 31: *In organello* translation of COX1. A) SDS-PAGE gel of the mtDNA encoded protein COX1. Gentamicin, geneticin, and cycloheximide were titrated from 0 to 1000 µM. Hygromycin B, doxycycline and linezolid were titrated from 0 to 100 µg/ml. B) Inhibition curve prepared from data measured from gel of COX1 expression.

5.2.2 Mito-UPR: Validation of the system

We analyzed UPR^{mt} by measuring the activity of a reporter gene fused to the promoter of the genes Hsp60 and ClpP. As translation control, a reporter gene fused to the constitutively active CMV promoter was used. We initially wanted to exclude an artifact resulting from promoter-reporter gene combination. Therefore, we prepared different promoter-reporter gene constructs (compare Figure 29 A and B). We compared the results from HEK293 cells co-transfected with two plasmids containing Hsp60-Fluc and CMV-lacZ with the results from HEK293 cells co-transfected with two plasmids containing Hsp60-lacZ and CMV-Fluc. Cells were co-transfected for 24 hours under standard conditions and then medium was replaced with low-glucose DMEM containing the indicated concentrations of drug. After 48 hours of incubation, cells were lysed and Fluc and β-galactosidase activity was measured. Surprisingly, regardless of their target (cytosolic or mitochondrial ribosome) all ribosomal inhibitors were found to induce reporter activity. The resulting values for induction of UPR^{mt} were between 1.7 and 2.1 for cells treated with drugs and 0.9 to 1.1 for controls (see Figure 32). Statistical analysis showed that there is no significant difference between the two constructs used for measurements ($p = 0.8823$).

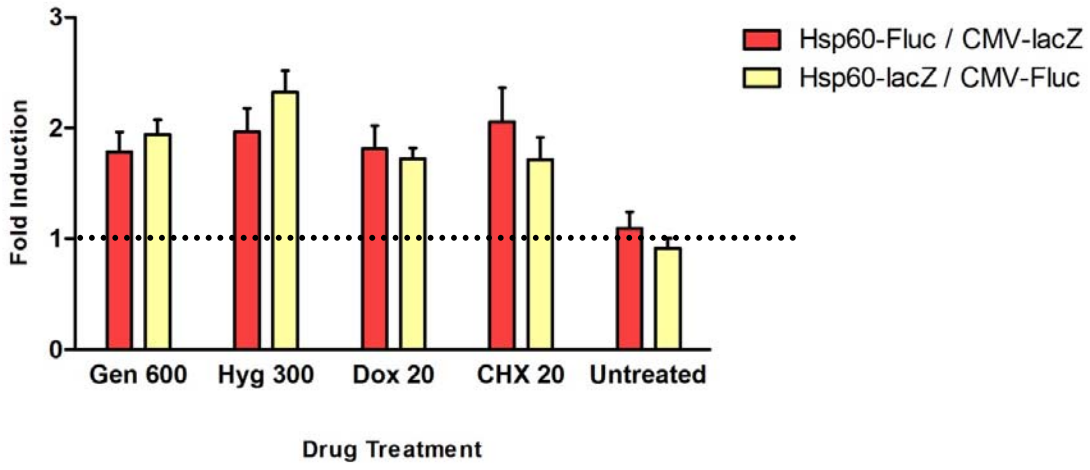

Fig. 32: Comparison of UPR^{mt} reporter systems. Cells were treated with geneticin (600 µM), hygromycin B (300 µM), doxycycline (20 µg/ml) or cycloheximide (20 µM). Error bars indicate SEM of triplicates.

5.2.3 Mito-UPR: Dose – Response

In a first hypothesis, we assumed that aminoglycoside induced mistranslation and as a consequence misfolded proteins should trigger a specific UPR^{mt}. A mutant version of the mitochondrial matrix protein ornithine transcarbamylase (OTC) was used as positive control as established by Zhao et al. (Zhao, Wang et al. 2002). The Hsp60 promoter activities in cells transfected with plasmids containing either the wild type or mutant version of OTC were compared. The mutant, OTCΔ, is characterized by a deletion of the phosphate binding domain (aminoacids 30-114) and is known to elicit UPR^{mt}. Using various drugs in different concentrations, we prepared a dose-response correlation using the Hsp60-Fluc reporter. Dose-dependent induction of UPR^{mt} was observed for doxycycline, cycloheximide, geneticin, hygromycin B and, gentamicin (see Figure 33). As a negative control we used tunicamycin which does not interfere with ribosomal translation activity and did not elicit any UPR^{mt}.

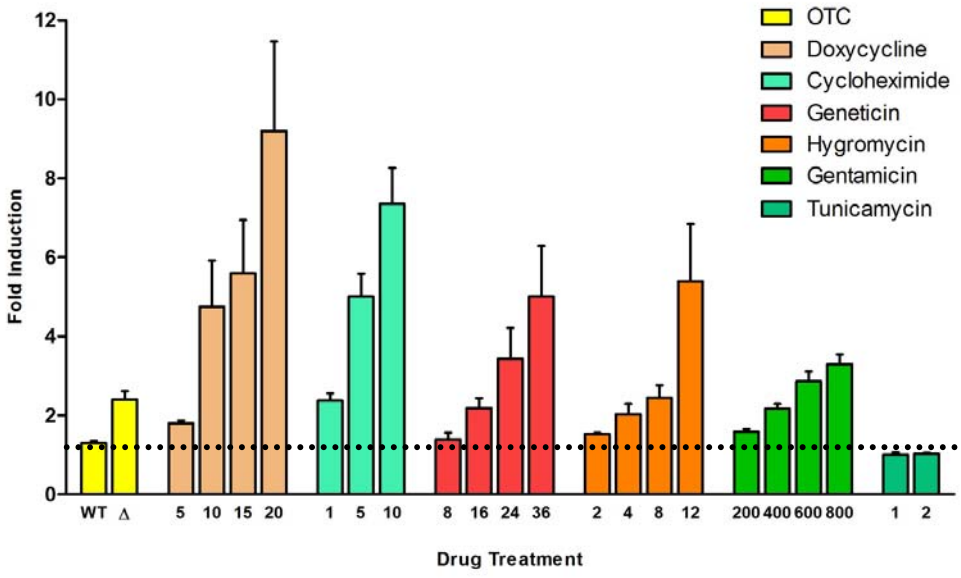

Fig. 33: Hsp60 Induction in HEK293 cells grown in F10 with 15 µg/ml saponin. Concentrations are in µM for cycloheximide, geneticin, hygromycin B, and gentamicin, in µg/ml for doxycycline and tunicamycin. OTC: Ornithinetranscarbamylase. Error bars indicate SEM of triplicates.

5.2.4 Mito-UPR: Induction of ClpP and Hsp60

Next to the mitochondrial chaperone Hsp60, ClpP, a subunit of the mitochondrial AAA+ protease ClpXP, was found to be regulated in a UPR^{mt} dependent manner (Aldridge, Horibe et al. 2007). Doxycycline targets the mitochondrial ribosome only and induced both reporter to a comparable level, i.e. 1.9-fold for Hsp60 and 1.8-fold for ClpP. A similar result was obtained with linezolid which also targets the mitochondrial ribosome only with 2.1-fold for Hsp60 and 1.8-fold for ClpP. Hygromycin B, which targets both the cytosolic and the mitochondrial ribosome, induces Hsp60 3.1-fold and ClpP 2.6-fold. The highest induction of Hsp60 showed geneticin with 4.0-fold where it induces ClpP 2.5-fold. Cycloheximide induced Hsp60 2.5-fold and ClpP 1.7-fold (see Figure 34). Interestingly, independent of the applied drug the induction of Hsp60 was always higher than the induction of ClpP.

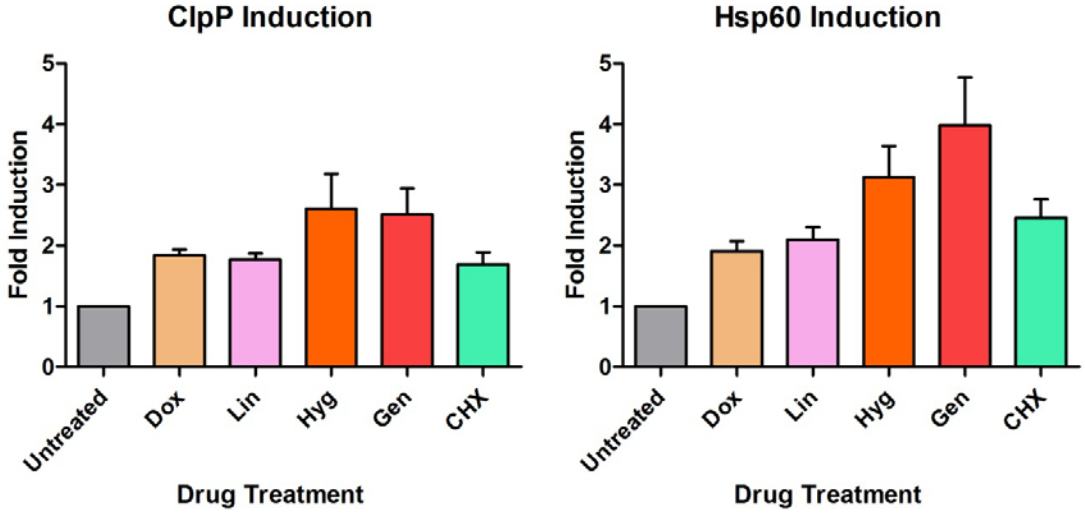

Fig. 34: A) Analysis of ClpP and Hsp60 induction by different drugs. Cells were grown in DMEM and incubated with drug for 48 hours. Concentrations of drugs were 20 µg/ml doxycycline (Dox), 20 µg/ml linezolid (Lin), 300 µM hygromycin B (Hyg), 600 µM geneticin (Gen), 20 µM cycloheximide (CHX). Error bars indicate SEM of triplicates.

5.2.5 Discussion

To maintain homeostasis in mitochondria, cells possess a well regulated system of chaperones and proteases (Zhao, Wang et al. 2002, Haynes and Ron 2010). Disturbance of homeostasis leads to a mitochondria-specific unfolded protein response (UPR^{mt}). This can be triggered by an imbalance of nuclear and mitochondrial encoded proteins, e.g. in the electron transport chain, or by an insufficient abundance of mitochondrial chaperones. To produce an imbalance we applied translation inhibitors to whole cell cultures and measured induction of specific UPRmt genes. In a first step we validated the inhibiting effect on the cytosolic ribosome. The inhibiton curves of hygromycin B and geneticin are nearly identical with those from the misreading experiments before (compare Figure 23 and Figure 30) and can therefore be used as a control to support the results of the inhibition of the cyto-ribosome by the other compounds. We also hypothesized that geneticin should elicit an UPR^{mt} because of its mistranslation inducing effect. However, induction of UPR^{mt} was observed not only for geneticin but for cycloheximide, which inhibits translation on a comparable level but does not induce any misreading. Cycloheximide should have served to estimate the amount of UPR^{mt} induction by translation inhibition only. Using this method it would have been possible to identify the amount of UPR^{mt} induction by misfolded proteins. Recent findings by Houtkooper et al. shed light on this unexpected result by revealing the importance of the mito-nuclear protein imbalance for induction of UPR^{mt} (Houtkooper, Mouchiroud et al. 2013). Our results demonstrate that UPR^{mt} is induced irrespective of where the mito-nuclear protein imbalance originates, i.e. UPR^{mt} is induced whether the mito-ribosome (linezolid and doxycycline), the cyto-ribosome (geneticin and cycloheximide), or both types of ribosomes (hygromycin B and gentamicin) are affected. Apparently, translation inhibition of either the cytosolic or the mitochondrial translation is sufficient to induce UPR^{mt}. Another finding was the clear correlation between the induction of Hsp60 and ClpP (see Figure 35). Both proteins are involved in UPRmt but differ significantly in their functional role. Hsp60 has chaperone activity while ClpP acts as a mitochondrial protease. A mito-nuclear protein imbalance most likely affects

respiratory chain formation as its subunits orginate from both, the cytosol and the mitochondrium (see Figure 11), e.g. incomplete and therefore non-functional respiratory chain complexes lead to increased reactive oxygen species (ROS) production (Baker, Tatsuta et al. 2011).

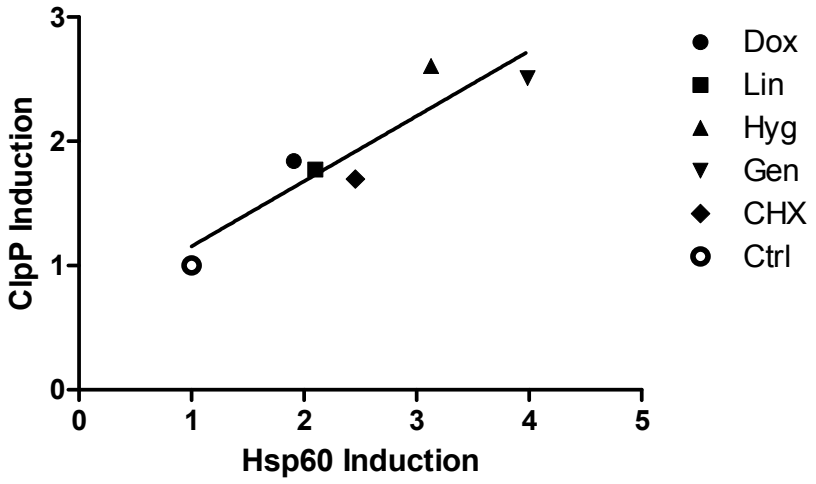

Fig. 35: Comparison of fold induction of Hsp60 versus fold induction of ClpP in HEK293 cells. The goodness of fit corresponds to an R-square of 0.84 and is assumed to be significant with $p<0.01$

6 MATERIAL AND METHODS

6.1 Cell Culture

Cell line HEK293 (Invitrogen) was used for *in vivo* experiments. Cells were grown in DMEM (Gibco) containing 10% FBS (v/v) and 4.5 g Glucose per liter in 10 cm petri-dishes at 37 °C and 5% CO_2. When reaching 90% confluency, cells were split by washing 2 times with 5 ml prewarmed PBS followed by detaching with 850 µl 0.05% Trypsin (Gibco) and resuspension in 2 ml DMEM. Cells were then seeded to new petri-dishes with an initial confluency of 5 – 10%.

6.2 Plasmids

6.2.1 Dual Luciferase Assay *in-vitro*

Name	Gene of Interest	Usage
pT7-Rluc	Renilla Luciferase	Internal Control
pT7-Fluc WT	Firefly Luciferase WT	Internal Control
pT7-Fluc K529AGA	Mutated firefly luciferase to produce mRNA for measuring misreading *in-vitro* in rabbit reticulocyte lysate	
pT7-Fluc K529AGG		
pT7-Fluc K529AAU		
pT7-Fluc K529AAC		
pT7-Fluc K529UUU		
pT7-Fluc H245CAG		
pT7-Fluc H245GAC		
pT7-Fluc H245UAC		
pT7-Fluc H245CGC		

pT7-Fluc H245AGA	

6.2.2 Dual Luciferase Assay *in-vivo*

Name	Gene of Interest	Usage
pRM-Rluc-Fluc	Fusion of renilla luciferase and firefly luciferase under CMV promoter	Wildtype control with internal standard
pRM-Rluc-Fluc H245CGC	Fusion of renilla luciferase and mutated firefly luciferase with mutation in the active center under CMV promoter	Construct with near-cognate mutation of H245 to measure misreading including internal standard
pRM-Rluc-Fluc H245AGA	Fusion of renilla luciferase and mutated firefly luciferase with mutation in the active center under CMV promoter	Construct with non-cognate mutation of H245 for usage as negative control

6.2.3 UPR^{mt}

Name	Gene of Interest	Usage
pRM-Hsp60-Fluc	Firefly luciferase under control of the Hsp60 promoter	Measurement of UPR^{mt} induction in eukaryotic cells *in-vivo* (Source: Houtkooper, Mouchiroud et al., 2013)
pRM-CMV-β-Gal	β-Galactosidase under control of the CMV promoter	Internal control / standard to normalize Hsp60 induction data (Source: Houtkooper, Mouchiroud et al., 2013)
pRM-Hsp60- β-Gal	β-Galactosidase under control	Measurement of UPR^{mt} induction in eukaryotic cells

	of the CMV promoter	*in-vivo*
pRM-CMV-Fluc	Firefly luciferase under control of the Hsp60 promoter	Internal control / standard to normalize Hsp60 induction data
pRM-ClpP-Fluc	Firefly luciferase under control of the ClpP promoter	Measurement of UPRmt induction in eukaryotic cells *in-vivo* (Source: Zhao, Wang et al., 2002)

6.3 Dual Luciferase Assay *in-vitro*

Rabbit reticulocyte lysate (RRL, Promega) was used for *in vitro* translation. Fluc mRNAs with different mutations were used in *in vitro* translation reactions; in addition Rluc mRNA was used as internal control (see 6.2.1). Firefly and renilla luciferase mRNAs were produced using T7 RNA polymerase (Fermentas) *in vitro* on templates of modified plasmids pGL4.14 (firefly luciferase) and pGL4.75 (renilla luciferase) (both Promega). In these plasmids the mammalian promoter driving transcription of luciferases was replaced by the T7 bacteriophage promoter. A standard 15 µl reaction contained 10 µl RRL, 2 µg of *in vitro* transcribed reporter mRNA, 200 µM amino acid mixture, 12 Units RNasin (Fermentas) and serially diluted aminoglycosides. The reaction mixture was incubated at 37º C for 35 min. Following incubation, luciferase assay substrate (Promega) was added (75 µl) and luciferase activities were determined using a luminescence microplate reader (Bio-Tek Instruments; FLx800).

6.4 Dual Luciferase Assay *in-vivo*

HEK293 cells were grown to 80% confluency at 37º C in DMEM supplemented with 10% FBS (v/v) (Invitrogen) and subsequently transfected using TurboFect transfection reagent (Fermentas) and pRM Rluc-Fluc according to the manufacturer's instructions. Following transfection cells were incubated for 24

hours. Medium was replaced by F10 (Invitrogen) w/o FBS. Serially diluted aminoglycoside antibiotics were added together with saponin (15 µg/ml) and cells were incubated for another 24 hours. Cells were lysed and luciferase activities were determined. Vector pRM Rluc-Fluc was constructed on the basis of vectors pGL4.14 and pGL4.75 (Promega). Following digestion of pGL4.14 with NheI/SalI, the resulting 3.6 kb fragment (Fluc with SV40 polyA signal) was inserted into vector pGL4.75 digested with XbaI/SalI (Rluc under control of the CMV promoter). The resulting 7.6 kb transitional construct pRep-00 carries two separate genes Rluc and Fluc. Rluc and Fluc were fused by a 27 nt linker, encoding the 9 amino acid polypeptide STCDQPFGF using overlap PCR mutagenesis resulting in vector pRM Rluc-Fluc. The Rluc activity was used as an internal standard.

6.5 β-Galactosidase Assay

To measure β-Galactosidase activity, an adapted version of the method developed by Nielsen et al. was used (Nielsen, Chou et al. 1983). Cells were lysed with lysis buffer from dual luciferase assay (Promega). 50 µl of cell lysate were mixed with 950 µl Z-Buffer (1mM $MgSO_4$, 10 mM KCl, 50 mM β-Mercaptoethanol, 60 mM Na_2HPO_4, 40 mM NaH_2PO_4, pH 7.5) and preincubated for 5 min at 37°C, followed by addition of 200 µl ONPG solution (4mg/ml o-nitrophenolgalactosid, 60 mM Na_2HPO_4, 40 mM NaH_2PO_4, pH 7.5). This mixture was incubated until a detectable yellow color formed at 37°C in the dark (approx. 2 hours). Then 300 µl 1 M Na_2CO_3 was added to terminate the reaction and absorption at 420 nm was measured in a photometer (Eppendorf).

6.6 Mitochondrial in-organello Translation

Mitochondria were isolated from HEK293 cells as described. HEK293 cells were collected from a 90% confluent 10-cm plate, washed with 1 X PBS and re-suspended in 1 ml of extraction buffer (20 mM Hepes-KOH pH 7.5, 0.25 M

sucrose, 10 mM KCl, 1.5 mM MgCl2, 1 mM EDTA, 1mM EGTA, 1mM DTT). Cells were broken by passing 5 times through a syringe needle 0.45x12 mm, centrifuged 5 min at 800g and the supernatant transferred to a new Eppendorf tube. The pellet was re-suspended in 1 ml of extraction buffer, passed through a syringe needle 0.45x12 mm, centrifuged for 5 min at 800g, the supernatant collected, combined with the previous supernatant and centrifuged 15 min at 10000g. The resulting pellet was used as mitochondria-enriched fraction. Mitochondrial in-organello translation was performed with slight modifications as described. The mitochondria-enriched pellet was re-suspended in 1ml of mitochondria reaction buffer containing 20 mM Tris-HCl pH 7.2, 90 mM KCl, 4 mM MgSO4, 1.5 mM KH2PO4, 20 mM glutamate, 0.5 mM malate, 14 mM sucrose, 44 mM sorbitol, 1 µM methionine, 2 mM ADP, 0.1 mM amino acids (-methionine), 1 mg/ml BSA (fatty acids free), 0.1 mg/ml cycloheximide. 15 µl of S35-methionine [370 MBq(10mCi)/ml, specific activity 37 TBq(1000Ci)/mmol, Hartmann Analytic KSM-01] were added, the suspension split into aliquots of 54 µl and drugs added to a final reaction volume of 60 µl (compounds were dissolved in H2O with pH adjusted to 7.5 using 5 M KOH). Reaction mixtures were incubated for 2 h at 30 °C with shaking. After incubation the reaction mixtures were centrifuged for 5 min at 15000g, the supernatants discarded and pellets washed with cold washing buffer containing 10 mM Tris-HCl pH 7.4, 320 mM sucrose, 1 mM EDTA, centrifuged 5 min at 15000g and pellets re-suspended in 10 µl of H2O. SDS loading buffer was added and the samples were resolved by 18% SDS polyacrylamide gelelectrophoresis. The gel was fixed, dried and exposed on a phosphoimager screen. Translation was quantified using Aida Image Analyzer v. 3.52 (Fuji) by scanning COX1 protein expression.

7 REFERENCES

Adachi, M., Y. Liu, K. Fujii, S. K. Calderwood, A. Nakai, K. Imai and Y. Shinomura (2009). "Oxidative stress impairs the heat stress response and delays unfolded protein recovery." PLoS One **4**(11): e7719.

Aeffner, F., B. Abdulrahman, J. M. Hickman-Davis, P. M. Janssen, A. Amer, D. M. Bedwell, E. J. Sorscher and I. C. Davis (2013). "Heterozygosity for the F508del mutation in the cystic fibrosis transmembrane conductance regulator anion channel attenuates influenza severity." J Infect Dis **208**(5): 780-789.

Ahmed, M., S. J. Muhammed, B. Kessler and A. Salehi (2010). "Mitochondrial proteome analysis reveals altered expression of voltage dependent anion channels in pancreatic beta-cells exposed to high glucose." Islets **2**(5): 283-292.

Akbergenov, R. e. a. (2011). Decoding and deafness: Two sides of a coin. Ribosomes. M. V. Rodnina, Wintermeyer, W., Green, R.**:** 249-261.

Aldridge, J. E., T. Horibe and N. J. Hoogenraad (2007). "Discovery of genes activated by the mitochondrial unfolded protein response (mtUPR) and cognate promoter elements." PLoS One **2**(9): e874.

Andre Mattman, S. S., Michelle M. Mezei, Ramona Salvarinova-Zivkovic, Majid Alfadhel, Yolanda Lillquist (2011). "Mitochondrial disease clinical manifestations: An overview." BCMJ **53**(4): 5.

Araki, K. and K. Nagata (2011). "Protein folding and quality control in the ER." Cold Spring Harb Perspect Biol **3**(11): a007526.

Baena-Lopez, L. A., J. Alonso, J. Rodriguez and J. F. Santaren (2008). "The expression of heat shock protein HSP60A reveals a dynamic mitochondrial pattern in Drosophila melanogaster embryos." J Proteome Res **7**(7): 2780-2788.

Baker, B. M., A. M. Nargund, T. Sun and C. M. Haynes (2012). "Protective coupling of mitochondrial function and protein synthesis via the eIF2alpha kinase GCN-2." PLoS Genet **8**(6): e1002760.

Baker, M. J., T. Tatsuta and T. Langer (2011). "Quality control of mitochondrial proteostasis." Cold Spring Harb Perspect Biol **3**(7).

Balasubramaian, R. and P. Seetharamulu (1983). "A conformational rationale for the wobble behaviour of the first base of the anticodon triplet in tRNA." J Theor Biol **101**(1): 77-86.

Ben-Shem, A., N. Garreau de Loubresse, S. Melnikov, L. Jenner, G. Yusupova and M. Yusupov (2011). "The structure of the eukaryotic ribosome at 3.0 A resolution." Science **334**(6062): 1524-1529.

Benham, A. M. (2012). "The protein disulfide isomerase family: key players in health and disease." Antioxid Redox Signal **16**(8): 781-789.

Bernasconi, R. and M. Molinari (2011). "ERAD and ERAD tuning: disposal of cargo and of ERAD regulators from the mammalian ER." Curr Opin Cell Biol **23**(2): 176-183.

Blanchard, S. C., D. Fourmy, R. G. Eason and J. D. Puglisi (1998). "rRNA chemical groups required for aminoglycoside binding." Biochemistry **37**(21): 7716-7724.

Borovinskaya, M. A., S. Shoji, K. Fredrick and J. H. Cate (2008). "Structural basis for hygromycin B inhibition of protein biosynthesis." RNA **14**(8): 1590-1599.

Branchini, B. R., R. A. Magyar, M. H. Murtiashaw, S. M. Anderson and M. Zimmer (1998). "Site-directed mutagenesis of histidine 245 in firefly luciferase: a proposed model of the active site." Biochemistry **37**(44): 15311-15319.

Branchini, B. R., M. H. Murtiashaw, R. A. Magyar and S. M. Anderson (2000). "The role of lysine 529, a conserved residue of the acyl-adenylate-forming enzyme superfamily, in firefly luciferase." Biochemistry **39**(18): 5433-5440.

Cameron, J. M., T. Hurd and B. H. Robinson (2005). "Computational identification of human mitochondrial proteins based on homology to yeast mitochondrially targeted proteins." Bioinformatics **21**(9): 1825-1830.

Carriere, M., V. Vijayabaskar, D. Applefield, I. Harvey, P. Garneau, J. Lorsch, A. Lapidot and J. Pelletier (2002). "Inhibition of protein synthesis by aminoglycoside-arginine conjugates." RNA **8**(10): 1267-1279.

Chakrabarti, A., A. W. Chen and J. D. Varner (2011). "A review of the mammalian unfolded protein response." Biotechnol Bioeng **108**(12): 2777-2793.

Champney, W. S. (2006). "The other target for ribosomal antibiotics: inhibition of bacterial ribosomal subunit formation." Infect Disord Drug Targets **6**(4): 377-390.

Chevallet, M., P. Lescuyer, H. Diemer, A. van Dorsselaer, E. Leize-Wagner and T. Rabilloud (2006). "Alterations of the mitochondrial proteome caused by the absence of mitochondrial DNA: A proteomic view." Electrophoresis **27**(8): 1574-1583.

Copeland, W. C. and M. J. Longley (2014). "Mitochondrial genome maintenance in health and disease." DNA Repair (Amst) **19**: 190-198.

Cornut, B. and R. C. Willson (1991). "Measurement of translational accuracy in vivo: missense reporting using inactive enzyme mutants." Biochimie **73**(12): 1567-1572.

Cuadrado-Tejedor, M., J. F. Cabodevilla, M. Zamarbide, T. Gomez-Isla, R. Franco and A. Perez-Mediavilla (2013). "Age-related mitochondrial alterations without neuronal loss in the hippocampus of a transgenic model of Alzheimer's disease." Curr Alzheimer Res **10**(4): 390-405.

Cyr, D. M. and D. N. Hebert (2009). "Protein quality control--linking the unfolded protein response to disease. Conference on 'From Unfolded Proteins in the Endoplasmic Reticulum to Disease'." EMBO Rep **10**(11): 1206-1210.

Dandliker, P. J., S. D. Pratt, A. M. Nilius, C. Black-Schaefer, X. Ruan, D. L. Towne, R. F. Clark, E. E. Englund, R. Wagner, M. Weitzberg, L. E. Chovan, R. K. Hickman, M. M. Daly, S. Kakavas, P. Zhong, Z. Cao, C. A. David, X. Xuei, C. G. Lerner, N. B. Soni, M. Bui, L. L. Shen, Y. Cai, P. J. Merta, A. Y. Saiki and B. A. Beutel (2003). "Novel antibacterial class." Antimicrob Agents Chemother **47**(12): 3831-3839.

Davies, J., L. Gorini and B. D. Davis (1965). "Misreading of RNA codewords induced by aminoglycoside antibiotics." Mol Pharmacol **1**(1): 93-106.

Davis, A. J., N. B. Sepuri, J. Holder, A. E. Johnson and R. E. Jensen (2000). "Two intermembrane space TIM complexes interact with different domains of Tim23p during its import into mitochondria." J Cell Biol **150**(6): 1271-1282.

Daviter, T., K. B. Gromadski and M. V. Rodnina (2006). "The ribosome's response to codon-anticodon mismatches." Biochimie **88**(8): 1001-1011.

Demirci, H., F. t. Murphy, E. Murphy, S. T. Gregory, A. E. Dahlberg and G. Jogl (2013). "A structural basis for streptomycin-induced misreading of the genetic code." Nat Commun **4**: 1355.

Dever, T. E. and R. Green (2012). "The elongation, termination, and recycling phases of translation in eukaryotes." Cold Spring Harb Perspect Biol **4**(7): a013706.

Doonan, S., E. Marra, S. Passarella, C. Saccone and E. Quagliariello (1984). "Transport of proteins into mitochondria." Int Rev Cytol **91**: 141-186.

Dudek, M., J. Romanowska, T. Witula and J. Trylska (2014). "Interactions of amikacin with the RNA model of the ribosomal A-site: Computational, spectroscopic and calorimetric studies." Biochimie.

Duff, P. (1992). "The aminoglycosides." Obstet Gynecol Clin North Am **19**(3): 511-517.

Dutnall, R. N., S. T. Tafrov, R. Sternglanz and V. Ramakrishnan (1998). "Structure of the histone acetyltransferase Hat1: a paradigm for the GCN5-related N-acetyltransferase superfamily." Cell **94**(4): 427-438.

Edelmann, P. and J. Gallant (1977). "Mistranslation in E. coli." Cell **10**(1): 131-137.

Edelmann, P. and J. Gallant (1977). "On the translational error theory of aging." Proc Natl Acad Sci U S A **74**(8): 3396-3398.

Eustice, D. C. and J. M. Wilhelm (1984). "Fidelity of the eukaryotic codon-anticodon interaction: interference by aminoglycoside antibiotics." Biochemistry **23**(7): 1462-1467.

Fan-Minogue, H. and D. M. Bedwell (2008). "Eukaryotic ribosomal RNA determinants of aminoglycoside resistance and their role in translational fidelity." RNA **14**(1): 148-157.

Feldman, M. B., D. S. Terry, R. B. Altman and S. C. Blanchard (2010). "Aminoglycoside activity observed on single pre-translocation ribosome complexes." Nat Chem Biol **6**(1): 54-62.

Felk, S., S. Ohrt, L. Kussmaul, A. Storch and F. Gillardon (2010). "Activation of the mitochondrial protein quality control system and actin cytoskeletal alterations in cells harbouring the MELAS mitochondrial DNA mutation." J Neurol Sci **295**(1-2): 46-52.

Fernandez, M. M., E. L. Malchiodi and I. D. Algranati (2011). "Differential effects of paromomycin on ribosomes of Leishmania mexicana and mammalian cells." Antimicrob Agents Chemother **55**(1): 86-93.

Francois, B., R. J. Russell, J. B. Murray, F. Aboul-ela, B. Masquida, Q. Vicens and E. Westhof (2005). "Crystal structures of complexes between aminoglycosides and decoding A site oligonucleotides: role of the number of rings and positive charges in the specific binding leading to miscoding." Nucleic Acids Res **33**(17): 5677-5690.

Gast, F. U., F. Peters and A. Pingoud (1987). "The role of translocation in ribosomal accuracy. Translocation rates for cognate and noncognate aminoacyl- and peptidyl-tRNAs on Escherichia coli ribosomes." J Biol Chem **262**(25): 11920-11926.

Gerard, M., A. Deleersnijder, J. Demeulemeester, Z. Debyser and V. Baekelandt (2011). "Unraveling the role of peptidyl-prolyl isomerases in neurodegeneration." Mol Neurobiol **44**(1): 13-27.

Ghosh, T., N. Pandey, A. Maitra, S. K. Brahmachari and B. Pillai (2007). "A role for voltage-dependent anion channel Vdac1 in polyglutamine-mediated neuronal cell death." PLoS One **2**(11): e1170.

Glick, B. S., E. M. Beasley and G. Schatz (1992). "Protein sorting in mitochondria." Trends Biochem Sci **17**(11): 453-459.

Gordon, D. M., A. Dancis and D. Pain (2000). "Mechanisms of mitochondrial protein import." Essays Biochem **36**: 61-73.

Gray, M. W., G. Burger and B. F. Lang (1999). "Mitochondrial evolution." Science **283**(5407): 1476-1481.

Gregersen, N., J. Hansen and J. Palmfeldt (2012). "Mitochondrial proteomics--a tool for the study of metabolic disorders." J Inherit Metab Dis **35**(4): 715-726.

Gupta, S., A. Deepti, S. Deegan, F. Lisbona, C. Hetz and A. Samali (2010). "HSP72 protects cells from ER stress-induced apoptosis via enhancement of IRE1alpha-XBP1 signaling through a physical interaction." PLoS Biol **8**(7): e1000410.

Hajek, P. and D. M. Bedwell (1994). "Characterization of the mitochondrial binding and import properties of purified yeast F1-ATPase beta subunit precursor. Import requires external ATP." J Biol Chem **269**(10): 7192-7200.

Haynes, C. M., C. J. Fiorese and Y. F. Lin (2013). "Evaluating and responding to mitochondrial dysfunction: the mitochondrial unfolded-protein response and beyond." Trends Cell Biol **23**(7): 311-318.

Haynes, C. M., K. Petrova, C. Benedetti, Y. Yang and D. Ron (2007). "ClpP mediates activation of a mitochondrial unfolded protein response in C. elegans." Dev Cell **13**(4): 467-480.

Haynes, C. M. and D. Ron (2010). "The mitochondrial UPR - protecting organelle protein homeostasis." J Cell Sci **123**(Pt 22): 3849-3855.

Haynes, C. M., Y. Yang, S. P. Blais, T. A. Neubert and D. Ron (2010). "The matrix peptide exporter HAF-1 signals a mitochondrial UPR by activating the transcription factor ZC376.7 in C. elegans." Mol Cell **37**(4): 529-540.

Hebert, D. N. and M. Molinari (2007). "In and out of the ER: protein folding, quality control, degradation, and related human diseases." Physiol Rev **87**(4): 1377-1408.

Hendrick, J. P. and F. U. Hartl (1995). "The role of molecular chaperones in protein folding." FASEB J **9**(15): 1559-1569.

Hershko, A., A. Ciechanover and A. Varshavsky (2000). "Basic Medical Research Award. The ubiquitin system." Nat Med **6**(10): 1073-1081.

Hetz, C. (2012). "The unfolded protein response: controlling cell fate decisions under ER stress and beyond." Nat Rev Mol Cell Biol **13**(2): 89-102.

Hinnebusch, A. G. (2014). "The scanning mechanism of eukaryotic translation initiation." Annu Rev Biochem **83**: 779-812.

Hobbie, S. N., C. Bruell, S. Kalapala, S. Akshay, S. Schmidt, P. Pfister and E. C. Bottger (2006). "A genetic model to investigate drug-target interactions at the ribosomal decoding site." Biochimie **88**(8): 1033-1043.

Hobbie, S. N., S. K. Kalapala, S. Akshay, C. Bruell, S. Schmidt, S. Dabow, A. Vasella, P. Sander and E. C. Bottger (2007). "Engineering the rRNA decoding site of eukaryotic cytosolic ribosomes in bacteria." Nucleic Acids Res **35**(18): 6086-6093.

Hobbie, S. N., P. Pfister, C. Bruell, P. Sander, B. Francois, E. Westhof and E. C. Bottger (2006). "Binding of neomycin-class aminoglycoside antibiotics to mutant ribosomes with alterations in the A site of 16S rRNA." Antimicrob Agents Chemother **50**(4): 1489-1496.

Hoogenraad, N. J. and M. T. Ryan (2001). "Translocation of proteins into mitochondria." IUBMB Life **51**(6): 345-350.

Horibe, T. and N. J. Hoogenraad (2007). "The chop gene contains an element for the positive regulation of the mitochondrial unfolded protein response." PLoS One **2**(9): e835.

Houtkooper, R. H., L. Mouchiroud, D. Ryu, N. Moullan, E. Katsyuba, G. Knott, R. W. Williams and J. Auwerx (2013). "Mitonuclear protein imbalance as a conserved longevity mechanism." Nature **497**(7450): 451-457.

Jackson, R. J., C. U. Hellen and T. V. Pestova (2012). "Termination and post-termination events in eukaryotic translation." Adv Protein Chem Struct Biol **86**: 45-93.

Jacobs, A. T. and L. J. Marnett (2010). "Systems analysis of protein modification and cellular responses induced by electrophile stress." Acc Chem Res **43**(5): 673-683.

Kaldi, K. and W. Neupert (1998). "Protein translocation into mitochondria." Biofactors **8**(3-4): 221-224.

Kampinga, H. H., J. Hageman, M. J. Vos, H. Kubota, R. M. Tanguay, E. A. Bruford, M. E. Cheetham, B. Chen and L. E. Hightower (2009). "Guidelines for the nomenclature of the human heat shock proteins." Cell Stress Chaperones **14**(1): 105-111.

Kato, H. and K. Mihara (2008). "Identification of Tom5 and Tom6 in the preprotein translocase complex of human mitochondrial outer membrane." Biochem Biophys Res Commun **369**(3): 958-963.

Kay, L., Z. Li, M. Mericskay, J. Olivares, L. Tranqui, E. Fontaine, T. Tiivel, P. Sikk, T. Kaambre, J. L. Samuel, L. Rappaport, Y. Usson, X. Leverve, D. Paulin and V. A. Saks (1997). "Study of regulation of mitochondrial respiration in vivo. An analysis of influence of ADP diffusion and possible role of cytoskeleton." Biochim Biophys Acta **1322**(1): 41-59.

Keeling, K. M., D. Wang, S. E. Conard and D. M. Bedwell (2012). "Suppression of premature termination codons as a therapeutic approach." Crit Rev Biochem Mol Biol **47**(5): 444-463.

Kondo, J., B. Francois, R. J. Russell, J. B. Murray and E. Westhof (2006). "Crystal structure of the bacterial ribosomal decoding site complexed with amikacin containing the gamma-amino-alpha-hydroxybutyryl (haba) group." Biochimie **88**(8): 1027-1031.

Konstantinidis, T. C., N. Patsoukis, C. D. Georgiou and D. Synetos (2006). "Translational fidelity mutations in 18S rRNA affect the catalytic activity of ribosomes and the oxidative balance of yeast cells." Biochemistry **45**(11): 3525-3533.

Kramer, E. B. and P. J. Farabaugh (2007). "The frequency of translational misreading errors in E. coli is largely determined by tRNA competition." RNA **13**(1): 87-96.

Kramer, E. B. and A. K. Hopper (2013). "Retrograde transfer RNA nuclear import provides a new level of tRNA quality control in Saccharomyces cerevisiae." Proc Natl Acad Sci U S A **110**(52): 21042-21047.

Kramer, E. B., H. Vallabhaneni, L. M. Mayer and P. J. Farabaugh (2010). "A comprehensive analysis of translational missense errors in the yeast Saccharomyces cerevisiae." RNA **16**(9): 1797-1808.

Kumar, A., J. R. Gibbs, A. Beilina, A. Dillman, R. Kumaran, D. Trabzuni, M. Ryten, R. Walker, C. Smith, B. J. Traynor, J. Hardy, A. B. Singleton and M. R. Cookson (2013). "Age-associated

changes in gene expression in human brain and isolated neurons." Neurobiol Aging **34**(4): 1199-1209.

Lang, B. F., M. W. Gray and G. Burger (1999). "Mitochondrial genome evolution and the origin of eukaryotes." Annu Rev Genet **33**: 351-397.

Lang, B. F., E. Seif, M. W. Gray, C. J. O'Kelly and G. Burger (1999). "A comparative genomics approach to the evolution of eukaryotes and their mitochondria." J Eukaryot Microbiol **46**(4): 320-326.

Laurberg, M., H. Asahara, A. Korostelev, J. Zhu, S. Trakhanov and H. F. Noller (2008). "Structural basis for translation termination on the 70S ribosome." Nature **454**(7206): 852-857.

Lecca, M. R., U. Wagner, A. Patrignani, E. G. Berger and T. Hennet (2005). "Genome-wide analysis of the unfolded protein response in fibroblasts from congenital disorders of glycosylation type-I patients." FASEB J **19**(2): 240-242.

Lee, J. C. and R. R. Gutell (2012). "A comparison of the crystal structures of eukaryotic and bacterial SSU ribosomal RNAs reveals common structural features in the hypervariable regions." PLoS One **7**(5): e38203.

Lee, Y. K., D. J. Liu, J. Lu, K. Y. Chen and A. Y. Liu (2009). "Aberrant regulation and modification of heat shock factor 1 in senescent human diploid fibroblasts." J Cell Biochem **106**(2): 267-278.

Lohse, M., O. Drechsel and R. Bock (2007). "OrganellarGenomeDRAW (OGDRAW): a tool for the easy generation of high-quality custom graphical maps of plastid and mitochondrial genomes." Curr Genet **52**(5-6): 267-274.

Lotz, C., A. J. Lin, C. M. Black, J. Zhang, E. Lau, N. Deng, Y. Wang, N. C. Zong, J. H. Choi, T. Xu, D. A. Liem, P. Korge, J. N. Weiss, H. Hermjakob, J. R. Yates, 3rd, R. Apweiler and P. Ping (2014). "Characterization, design, and function of the mitochondrial proteome: from organs to organisms." J Proteome Res **13**(2): 433-446.

Lynch, S. R. and J. D. Puglisi (2001). "Structural origins of aminoglycoside specificity for prokaryotic ribosomes." J Mol Biol **306**(5): 1037-1058.

Matt, T., C. L. Ng, K. Lang, S. H. Sha, R. Akbergenov, D. Shcherbakov, M. Meyer, S. Duscha, J. Xie, S. R. Dubbaka, D. Perez-Fernandez, A. Vasella, V. Ramakrishnan, J. Schacht and E. C. Bottger (2012). "Dissociation of antibacterial activity and aminoglycoside ototoxicity in the 4-

monosubstituted 2-deoxystreptamine apramycin." Proc Natl Acad Sci U S A **109**(27): 10984-10989.

Meisinger, C., A. Sickmann and N. Pfanner (2008). "The mitochondrial proteome: from inventory to function." Cell **134**(1): 22-24.

Melnikov, S., A. Ben-Shem, N. Garreau de Loubresse, L. Jenner, G. Yusupova and M. Yusupov (2012). "One core, two shells: bacterial and eukaryotic ribosomes." Nat Struct Mol Biol **19**(6): 560-567.

Meyer, E. H., N. L. Taylor and A. H. Millar (2008). "Resolving and identifying protein components of plant mitochondrial respiratory complexes using three dimensions of gel electrophoresis." J Proteome Res **7**(2): 786-794.

Milon, P. and M. V. Rodnina (2012). "Kinetic control of translation initiation in bacteria." Crit Rev Biochem Mol Biol **47**(4): 334-348.

Mironova, L. N., N. A. Provorov, M. D. Ter-Avanesyan, S. G. Inge-Vechtomov, V. N. Smirnov and A. P. Surguchov (1982). "The effect of paromomycin on the expression of ribosomal suppressors in yeast." Curr Genet **5**(2): 149-152.

Missiakas, D., F. Schwager, J. M. Betton, C. Georgopoulos and S. Raina (1996). "Identification and characterization of HslV HslU (ClpQ ClpY) proteins involved in overall proteolysis of misfolded proteins in Escherichia coli." EMBO J **15**(24): 6899-6909.

Moisoi, N., K. Klupsch, V. Fedele, P. East, S. Sharma, A. Renton, H. Plun-Favreau, R. E. Edwards, P. Teismann, M. D. Esposti, A. D. Morrison, N. W. Wood, J. Downward and L. M. Martins (2009). "Mitochondrial dysfunction triggered by loss of HtrA2 results in the activation of a brain-specific transcriptional stress response." Cell Death Differ **16**(3): 449-464.

Nargund, A. M., M. W. Pellegrino, C. J. Fiorese, B. M. Baker and C. M. Haynes (2012). "Mitochondrial import efficiency of ATFS-1 regulates mitochondrial UPR activation." Science **337**(6094): 587-590.

Nielsen, D. A., J. Chou, A. J. MacKrell, M. J. Casadaban and D. F. Steiner (1983). "Expression of a preproinsulin-beta-galactosidase gene fusion in mammalian cells." Proc Natl Acad Sci U S A **80**(17): 5198-5202.

Ochoa, S. (1967). "Translation of the genetic message." Bull Soc Chim Biol (Paris) **49**(7): 721-737.

Ogle, J. M. and V. Ramakrishnan (2005). "Structural insights into translational fidelity." Annu Rev Biochem **74**: 129-177.

Ortego, B. C., J. J. Whittenton, H. Li, S. C. Tu and R. C. Willson (2007). "In vivo translational inaccuracy in Escherichia coli: missense reporting using extremely low activity mutants of Vibrio harveyi luciferase." Biochemistry **46**(48): 13864-13873.

Ozawa, T., Y. Sako, M. Sato, T. Kitamura and Y. Umezawa (2003). "A genetic approach to identifying mitochondrial proteins." Nat Biotechnol **21**(3): 287-293.

Pagliarini, D. J., S. E. Calvo, B. Chang, S. A. Sheth, S. B. Vafai, S. E. Ong, G. A. Walford, C. Sugiana, A. Boneh, W. K. Chen, D. E. Hill, M. Vidal, J. G. Evans, D. R. Thorburn, S. A. Carr and V. K. Mootha (2008). "A mitochondrial protein compendium elucidates complex I disease biology." Cell **134**(1): 112-123.

Palmer, E. and J. M. Wilhelm (1978). "Mistranslation in a eucaryotic organism." Cell **13**(2): 329-334.

Pan, Y. (2011). "Mitochondria, reactive oxygen species, and chronological aging: a message from yeast." Exp Gerontol **46**(11): 847-852.

Parker, J. (1989). "Errors and alternatives in reading the universal genetic code." Microbiol Rev **53**(3): 273-298.

Paschen, W. (2003). "Endoplasmic reticulum: a primary target in various acute disorders and degenerative diseases of the brain." Cell Calcium **34**(4-5): 365-383.

Pellegrino, M. W., A. M. Nargund and C. M. Haynes (2013). "Signaling the mitochondrial unfolded protein response." Biochim Biophys Acta **1833**(2): 410-416.

Perez-Fernandez, D., D. Shcherbakov, T. Matt, N. C. Leong, I. Kudyba, S. Duscha, H. Boukari, R. Patak, S. R. Dubbaka, K. Lang, M. Meyer, R. Akbergenov, P. Freihofer, S. Vaddi, P. Thommes, V. Ramakrishnan, A. Vasella and E. C. Bottger (2014). "4'-O-substitutions determine selectivity of aminoglycoside antibiotics." Nat Commun **5**: 3112.

Pestova, T. V., V. G. Kolupaeva, I. B. Lomakin, E. V. Pilipenko, I. N. Shatsky, V. I. Agol and C. U. Hellen (2001). "Molecular mechanisms of translation initiation in eukaryotes." Proc Natl Acad Sci U S A **98**(13): 7029-7036.

Pfaller, R., H. F. Steger, J. Rassow, N. Pfanner and W. Neupert (1988). "Import pathways of precursor proteins into mitochondria: multiple receptor sites are followed by a common membrane insertion site." J Cell Biol **107**(6 Pt 2): 2483-2490.

Pfanner, N., J. Rassow, B. Guiard, T. Sollner, F. U. Hartl and W. Neupert (1990). "Energy requirements for unfolding and membrane translocation of precursor proteins during import into mitochondria." J Biol Chem **265**(27): 16324-16329.

Pfister, P., S. Hobbie, Q. Vicens, E. C. Bottger and E. Westhof (2003). "The molecular basis for A-site mutations conferring aminoglycoside resistance: relationship between ribosomal susceptibility and X-ray crystal structures." Chembiochem **4**(10): 1078-1088.

Preuten, T., E. Cincu, J. Fuchs, R. Zoschke, K. Liere and T. Borner (2010). "Fewer genes than organelles: extremely low and variable gene copy numbers in mitochondria of somatic plant cells." Plant J **64**(6): 948-959.

Qin, D., Q. Liu, A. Devaraj and K. Fredrick (2012). "Role of helix 44 of 16S rRNA in the fidelity of translation initiation." RNA **18**(3): 485-495.

Raja, V. and M. L. Greenberg (2014). "The functions of cardiolipin in cellular metabolism-potential modifiers of the Barth syndrome phenotype." Chem Phys Lipids **179**: 49-56.

Ramakrishnan, V. (1997). "Histone H1 and chromatin higher-order structure." Crit Rev Eukaryot Gene Expr **7**(3): 215-230.

Ramakrishnan, V., C. Davies, S. E. Gerchman, B. L. Golden, D. W. Hoffmann, T. N. Jaishree, J. H. Kyila, S. Porter and S. W. White (1995). "Structures of prokaryotic ribosomal proteins: implications for RNA binding and evolution." Biochem Cell Biol **73**(11-12): 979-986.

Ramakrishnan, V., S. Southern, N. B. Hart and K. Tzafetta (1998). "Endoscopically assisted gracilis harvest for use as a free and pedicled flap." Br J Plast Surg **51**(8): 580-583.

Raurell, A., S. Southern and V. Ramakrishnan (1997). "Pathological tissue expansion." Ann Plast Surg **39**(4): 435.

Rettig, J. (2011). Mitochondrial tRNA and protein import in Trypanosoma brucei. PhD Thesis. U. o. B. Faculty of Science.

Rocha, H., R. Ferreira, J. Carvalho, R. Vitorino, C. Santa, L. Lopes, N. Gregersen, L. Vilarinho and F. Amado (2011). "Characterization of mitochondrial proteome in a severe case of ETF-QO deficiency." J Proteomics **75**(1): 221-228.

Ryan, M. T., R. Wagner and N. Pfanner (2000). "The transport machinery for the import of preproteins across the outer mitochondrial membrane." Int J Biochem Cell Biol **32**(1): 13-21.

Salas-Marco, J. and D. M. Bedwell (2005). "Discrimination between defects in elongation fidelity and termination efficiency provides mechanistic insights into translational readthrough." J Mol Biol **348**(4): 801-815.

Schroder, M. and R. J. Kaufman (2005). "The mammalian unfolded protein response." Annu Rev Biochem **74**: 739-789.

Shao, M., B. Shan, Y. Liu, Y. Deng, C. Yan, Y. Wu, T. Mao, Y. Qiu, Y. Zhou, S. Jiang, W. Jia, J. Li, J. Li, L. Rui, L. Yang and Y. Liu (2014). "Hepatic IRE1alpha regulates fasting-induced metabolic adaptive programs through the XBP1s-PPARalpha axis signalling." Nat Commun **5**: 3528.

Sharma, R., H. Jiang, L. Zhong, J. Tseng and A. Gow (2007). "Minimal role for activating transcription factor 3 in the oligodendrocyte unfolded protein response in vivo." J Neurochem **102**(5): 1703-1712.

Sirrenberg, C., M. F. Bauer, B. Guiard, W. Neupert and M. Brunner (1996). "Import of carrier proteins into the mitochondrial inner membrane mediated by Tim22." Nature **384**(6609): 582-585.

Slezak, J. A., V. W. Persky, F. J. Kviz, V. Ramakrishnan and C. Byers (1998). "Asthma prevalence and risk factors in selected Head Start sites in Chicago." J Asthma **35**(2): 203-212.

Smakowska, E., M. Czarna and H. Janska (2014). "Mitochondrial ATP-dependent proteases in protection against accumulation of carbonylated proteins." Mitochondrion.

Smith, S. E., S. Granell, L. Salcedo-Sicilia, G. Baldini, G. Egea, J. H. Teckman and G. Baldini (2011). "Activating transcription factor 6 limits intracellular accumulation of mutant alpha(1)-antitrypsin Z and mitochondrial damage in hepatoma cells." J Biol Chem **286**(48): 41563-41577.

Soslau, G. and J. Parker (1989). "Modulation of platelet function by extracellular adenosine triphosphate." Blood **74**(3): 984-993.

St John, J. (2014). "The control of mtDNA replication during differentiation and development." Biochim Biophys Acta **1840**(4): 1345-1354.

Szaflarski, W., O. Vesper, Y. Teraoka, B. Plitta, D. N. Wilson and K. H. Nierhaus (2008). "New features of the ribosome and ribosomal inhibitors: non-enzymatic recycling, misreading and back-translocation." J Mol Biol **380**(1): 193-205.

Szychowski, J., J. Kondo, O. Zahr, K. Auclair, E. Westhof, S. Hanessian and J. W. Keillor (2011). "Inhibition of aminoglycoside-deactivating enzymes APH(3')-IIIa and AAC(6')-Ii by amphiphilic paromomycin O2''-ether analogues." ChemMedChem **6**(11): 1961-1966.

Taylor, S. W., E. Fahy, B. Zhang, G. M. Glenn, D. E. Warnock, S. Wiley, A. N. Murphy, S. P. Gaucher, R. A. Capaldi, B. W. Gibson and S. S. Ghosh (2003). "Characterization of the human heart mitochondrial proteome." Nat Biotechnol **21**(3): 281-286.

Trombetta, E. S. and A. J. Parodi (2003). "Quality control and protein folding in the secretory pathway." Annu Rev Cell Dev Biol **19**: 649-676.

Tsai, B., Y. Ye and T. A. Rapoport (2002). "Retro-translocation of proteins from the endoplasmic reticulum into the cytosol." Nat Rev Mol Cell Biol **3**(4): 246-255.

Tselika, S., T. C. Konstantinidis and D. Synetos (2008). "Two nucleotide substitutions in the A-site of yeast 18S rRNA affect translation and differentiate the interaction of ribosomes with aminoglycoside antibiotics." Biochimie **90**(6): 908-917.

Tuggle, K. L., S. E. Birket, X. Cui, J. Hong, J. Warren, L. Reid, A. Chambers, D. Ji, K. Gamber, K. K. Chu, G. Tearney, L. P. Tang, J. A. Fortenberry, M. Du, J. M. Cadillac, D. M. Bedwell, S. M. Rowe, E. J. Sorscher and M. V. Fanucchi (2014). "Characterization of defects in ion transport and tissue development in cystic fibrosis transmembrane conductance regulator (CFTR)-knockout rats." PLoS One **9**(3): e91253.

Tuite, M. F. and C. S. McLaughlin (1984). "The effects of paromomycin on the fidelity of translation in a yeast cell-free system." Biochim Biophys Acta **783**(2): 166-170.

Vabulas, R. M., S. Raychaudhuri, M. Hayer-Hartl and F. U. Hartl (2010). "Protein folding in the cytoplasm and the heat shock response." Cold Spring Harb Perspect Biol **2**(12): a004390.

Vallabhaneni, H. and P. J. Farabaugh (2009). "Accuracy modulating mutations of the ribosomal protein S4-S5 interface do not necessarily destabilize the rps4-rps5 protein-protein interaction." RNA **15**(6): 1100-1109.

Verfaillie, T., N. Rubio, A. D. Garg, G. Bultynck, R. Rizzuto, J. P. Decuypere, J. Piette, C. Linehan, S. Gupta, A. Samali and P. Agostinis (2012). "PERK is required at the ER-mitochondrial contact sites to convey apoptosis after ROS-based ER stress." Cell Death Differ **19**(11): 1880-1891.

Voellmy, R. and F. Boellmann (2007). "Chaperone regulation of the heat shock protein response." Adv Exp Med Biol **594**: 89-99.

Voigts-Hoffmann, F., S. Klinge and N. Ban (2012). "Structural insights into eukaryotic ribosomes and the initiation of translation." Curr Opin Struct Biol **22**(6): 768-777.

Vujanac, M., A. Fenaroli and V. Zimarino (2005). "Constitutive nuclear import and stress-regulated nucleocytoplasmic shuttling of mammalian heat-shock factor 1." Traffic **6**(3): 214-229.

Weddle, D. O., N. S. Tu, C. J. Guzik and V. Ramakrishnan (1995). "Positive association between dietetics recommendations and achievement of enteral nutrition outcomes of care." J Am Diet Assoc **95**(7): 753-758.

Wikipedia (2007). "Mitochondrial electron transport chain—Etc4." 2014.

Yonally, S. K. and R. A. Capaldi (2006). "The F(1)F(0) ATP synthase and mitochondrial respiratory chain complexes are present on the plasma membrane of an osteosarcoma cell line: An immunocytochemical study." Mitochondrion **6**(6): 305-314.

Yoneda, T., C. Benedetti, F. Urano, S. G. Clark, H. P. Harding and D. Ron (2004). "Compartment-specific perturbation of protein handling activates genes encoding mitochondrial chaperones." J Cell Sci **117**(Pt 18): 4055-4066.

Zaher, H. S. and R. Green (2009). "Fidelity at the molecular level: lessons from protein synthesis." Cell **136**(4): 746-762.

Zhao, Q., J. Wang, I. V. Levichkin, S. Stasinopoulos, M. T. Ryan and N. J. Hoogenraad (2002). "A mitochondrial specific stress response in mammalian cells." EMBO J **21**(17): 4411-4419.

8 XBP1 mitigates aminoglycoside-induced endoplasmic reticulum stress and neuronal cell death

Naoki Oishi, Stefan Duscha, Heithem Boukari, Martin Meyer, Jing Xie, Gao Wei, Thomas Schrepfer, Bernd Roschitzki, Erik C. Boettger, and Jochen Schacht

Abstract

Here we study links between aminoglycoside-induced mistranslation, protein misfolding, and neuropathy. We demonstrate that aminoglycosides induce misreading in mammalian cells and assess ER stress and unfolded protein response (UPR) pathways. Genome-wide transcriptome and proteome analyses revealed upregulation of genes related to protein folding and degradation. Quantitative PCR confirmed induction of UPR markers including CHOP, GRP94, BiP, and XBP1 mRNA splicing, which is crucial for UPR activation. We studied the effect of a compromised UPR on aminoglycoside ototoxicity in haploinsufficient XBP1 ($XBP1^{+/-}$) mice. Intra-tympanic aminoglycoside treatment caused high-frequency hearing loss in $XBP1^{+/-}$ mice but not in wild-type littermates. Densities of spiral ganglion cells and synaptic ribbons were decreased in gentamicin-treated $XBP1^{+/-}$ mice, while sensory cells were preserved. Co-injection of the chemical chaperone tauroursodeoxycholic acid attenuated hearing loss. These results suggest that aminoglycoside-induced ER stress and cell death in spiral ganglion neurons is mitigated by XBP1, masking aminoglycoside neurotoxicity at the organismal level.

Introduction

Translational fidelity is maintained throughout all three domains of life (archea, bacteria, eukaryota), suggesting a high selective pressure during evolution to minimize errors in protein synthesis.[1] In bacteria, erroneous protein synthesis induces protein misfolding.[2] In higher eukaryotes, protein misfolding results in

endoplasmatic reticulum (ER) stress and initiates the unfolded protein response (UPR), a cascade of integrated pathways regulating gene expression. The UPR^{ER} is mediated by three ubiquitously expressed transmembrane proteins in the ER: inositol-requiring enzyme 1 (IRE1), PKR–like ER kinase (PERK), and activating transcription factor 6 (ATF6).[3-7] Under normal conditions, the luminal domains of IRE1, PERK, and ATF6 are bound by the ER chaperone binding immunoglobulin protein (BiP) which inhibits self-dimerization and activation of the cytosolic domain.[8,9] Under ER stress, BiP is released resulting in dimerization of IRE1 and ATF6 and multimerization of PERK, initiating the UPR signaling cascades.[8,9] The initial UPR response is protective, increasing the expression of chaperone proteins promoting refolding and, if unsuccessful, the degradation of misfolded proteins.[10-13] Prolonged or severe stress triggers additional pathways that eventually lead to cellular apoptosis.[14-16]

Aminoglycoside antibiotics are well known to affect translational fidelity in bacteria and lower eukaryotes[17-20] but only few reports suggest that aminoglycoside antibiotics may also induce misreading in higher eukaryotes.[21-23] Aminoglycoside-mediated read-through activity has been exploited for therapy of human genetic diseases associated with premature stop codons.[24-27] In addition, aminoglycosides have been shown to induce apoptosis in human cell cultures accompanied by ER stress and mitochondrial cytochrome c release.[28,29] It was suggested that the observed ER stress may be the result of protein misfolding, reflecting aminoglycoside-induced mistranslation.[28] Despite this potential for misreading induced by aminoglycosides in eukaryotes, aminoglycoside treatment in animal models and in patients is well tolerated. Side effects are highly organ-specific, limited to the kidney and the inner ear,[30] while toxicity to the nervous system is not evident even in long-term aminoglycoside treatment.[31] In the case of ototoxicity, the primary drug target are the sensory hair cells, as convincingly demonstrated in various animal models, regardless of whether the drug is given systemically[32] or directly introduced into the cochlea.[33] Degeneration of spiral ganglion cells observed after ototoxic dosages of aminoglycosides are thought to occur only as a sequel to the loss of sensory hair cells in the vast majority of

cases. Surprisingly, however, a few analyses of human temporal bones have suggested that spiral ganglia can be affected by aminoglycosides without overt insult to the hair cells.[34,35] This rare pathology, unexplained by the treatment modus, suggests individual variability possibly based on genetic factors.

Prompted by the anecdotal reports of aminoglycoside-induced selective spiral ganglion damage, the objective of this study was to assess the contribution of ER stress to ototoxicity. We first investigated aminoglycoside-induced misreading and UPR responses in HEK293 cells *in vitro*. Next, we examined the role of ER stress in ototoxicity in cochlear organ cultures of CBA/J mice. Finally, we employed an *in-vivo* mouse model[36] with a compromised ER stress response due to XBP1 haploinsufficiency[37] in order to probe potential links between aminoglycoside neurotoxicity, translation fidelity and protein misfolding.

Results

Aminoglycosides alter translation fidelity. Drug-induced inhibition of translation was used to assess aminoglycoside activity on the eukaryotic ribosome. IC50 values were 0.3 μM for geneticin and 9.8 μM for gentamicin in the cell-free translation assays with rabbit reticulocyte lysate (RRL), and 4.4 μM for geneticin and 812 μM for gentamicin in assays with intact HEK293 cells (Supplementary Figure S1a and b). The ability of the drugs to induce mistranslation was analyzed using sensitive gain-of-function dual-luciferase assays to assess near-cognate misreading and stop-codon read-through. Near-cognate misreading was studied using constructs with substitution of amino acid 245 in the active site of mutated firefly luciferase (wild-type His CAC → near-cognate Arg CGC), which results in loss of enzymatic activity with enzymatic function restored by misreading; stopcodon read-through was determined using constructs with in-frame stop codons abolishing firefly luciferase activity. Both geneticin and gentamicin decreased ribosomal accuracy in cell free translation assays (RRL) and in HEK cells in a dose-dependent manner (Figure 1). Misreading

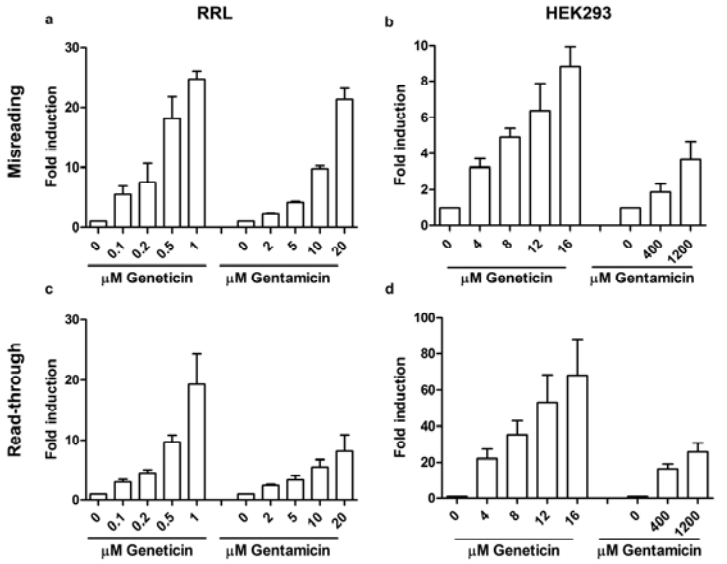

Figure 1 Aminoglycoside-induced mistranslation. (a–b) Misreading and (c–d) read-through measured in rabbit reticulocyte lysate (RRL; a,c) and HEK wild-type cells (b,d). Results are derived from the ratio hFluc/hRluc, given in -fold induction. Untreated samples are set as 1 (*n* = 3; ± SEM).

was induced up to 25-fold in RRL and up to 8.5-fold in HEK cells compared to untreated controls; read-through was induced up to 20-fold in RRL and up to 70-fold in HEK cells compared to untreated controls (Figure 1). In HEK cells transfected with the aminoglycoside phosphotransferase APH(3'), the geneticin-induced but not the gentamicin-induced translation inhibition and mistranslation were abrogated (Supplementary Figure S1c and d), consistent with the selectivity of the enzyme to inactivate geneticin but not gentamicin.[38,39] Aminoglycoside-treated and untreated HEK wild-type cells showed similar metabolic activities and viability (Supplementary Figure S1e and f).

Aminoglycosides induce genome-wide upregulation of cellular folding capacity. In order to study the cellular response to aminoglycoside-induced mistranslation, we used whole genome transcriptomic and proteomic analyses. A microarray analysis of geneticin-treated versus untreated cells revealed a broad transcriptional response totaling 705 genes (selected for a fold change >1.2, Benjamini-Hochberg corrected *p*-value <0.05; Supplementary Figure S2a). Protein folding and transcription were among the most enriched functional ontologies (Supplementary Figure S2b), including the induction of the ER-specific chaperones BiP (HSPA5), glucose-regulated protein 94 (GRP94; HSP90B1), calreticulin (CALR), GRP110 (HYOU1), ERdj3 (DNAJB11), and ERdj6

(DNAJC3), the ER foldases PDIA3 (ERp57), PDIA4 (ERp70), Erp44, and FKBP7, and the N-linked glycosylation factor SDF2L1. Likewise, ER-associated degradation (ERAD) components such as VCP (p97), Derlin2 (DERL2), and Herp (HERPUD1) were significantly upregulated (Supplementary Figure S2c). This transcriptional response indicates a general increased folding and degradation capacity in the ER. In addition, a large number of cytosolic chaperones[40] were upregulated, such as members of the Hsp40, Hsp70, Hsp90, and Hsp110 families and to a lesser extent foldases (peptidyl-prolyl cis/trans isomerases and protein disulfide isomerases; Supplementary Figure S2d and e), indicating an increased folding capacity in the cytosol. Table S1 lists the genes included in the analysis. The microarray data have been deposited in NCBI's Gene Expression Omnibus and are accessible through GEO Series accession number GSE57198 (http://www.ncbi.nlm.nih.gov/geo/query/acc.cgi?acc=GSE57198).

Proteome analysis found 77 proteins to be regulated by geneticin (Bonferroni-corrected *p*-value <0.05). When applying a minimum fold induction of 0.3 (log2 scale) we identified 35 proteins that were upregulated. Grouping according to function revealed a predominance of proteins involved in protein folding (Figure 2a). Proteins associated with the ER and cytoplasmic UPR, such as BiP, GRP94, calreticulin, foldases, and members of the Hsp70, Hsp90, Hsp110, and Hsp40 families, were also upregulated (Figure 2b). Comparison with corresponding mRNA levels showed an upregulation of the folding machinery both at the transcriptomic and the proteomic level (Figure 2c). The mass spectrometry proteomics data have been deposited to the ProteomeXchange Consortium via the PRIDE partner repository with the dataset identifier PXD000933 and DOI 10.6019/PXD000933.

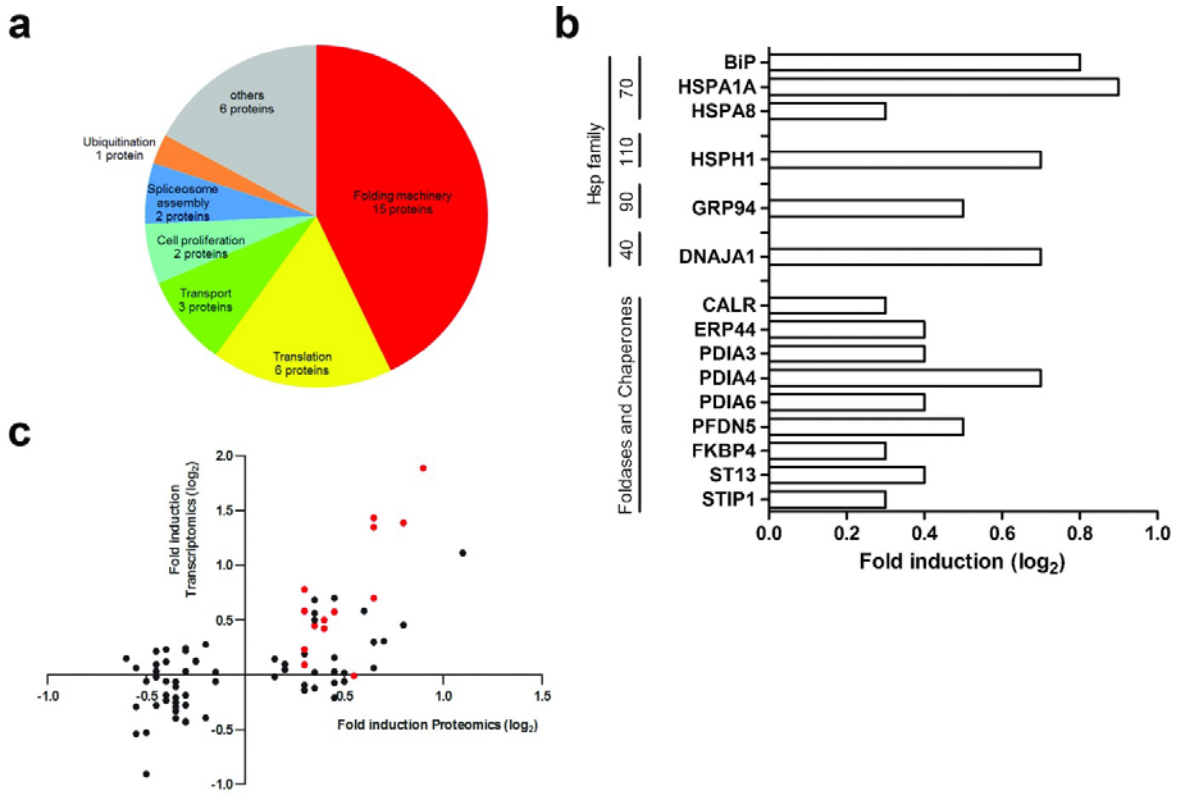

Figure 2 Proteomic analysis of geneticin-treated HEK wild-type cells. (a) Thirty-five upregulated proteins were grouped according to their biological function (Bonferroni corrected p-value < 0.05, $\log_2$ FC > 0.3). (b) Upregulation of the geneticin-induced heat-shock proteins, chaperones, and foldases (Bonferroni corrected p-value < 0.05, $\log_2$ FC > 0.3). (c) Comparison of the significantly regulated proteins (Bonferroni corrected p-value < 0.05) and their corresponding mRNA fold-induction. The upregulated proteins of the folding machinery are shown in red.

Aminoglycosides induce the UPR. To corroborate the results of the microarray analysis, mRNA levels of selected UPR genes were further analyzed by quantitative PCR and corresponding protein levels were assessed by Western blotting. Geneticin and gentamicin induced mRNA expression of C/EBP homologous protein (CHOP), GRP94, and BiP in a time-dependent manner (Figure 3a–c). Increased protein levels of the two ER chaperones BiP and GRP94 as well as the transcription factor ATF4, which is regulated at the translational level,[41] were observed in geneticin- and gentamicin-treated cells by Western blotting (Figure 3e). As a further element of the UPR, we studied

splicing of XBP1 mRNA, which is central for UPR activation[11]. Both geneticin and gentamicin induced XBP1 splicing (Figure 3d). In contrast, XBP1 splicing is induced neither by the non-misreading aminoglycoside hygromycin[42] nor by cycloheximide, an inhibitor of ribosomal translocation,[43] indicating that XBP1 splicing depends on misreading and not on inhibition of translation. Furthermore, the presence of APH(3‘) in HEK cells abrogated geneticin-induced but not gentamicin-induced XBP1 splicing.

The activity of transcription factors XBP1 and ATF6 was examined using reporter plasmids UPRE (p5xATF6-GL3-luc) and ERSE (pGL3-GRP78P(-132)-luc).[44,45] The UPRE reporter is specific for ATF6 activity, the ERSE reporter is regulated by both ATF6 and XBP1.[44,45] Both reporters showed a robust induction by geneticin and gentamicin (Figure 3f and g). Cycloheximide failed to induce any reporter activity consistent with the XBP1 splicing results (Figure 3d, 3f, 3e). The PERK signaling branch was investigated by assessing the formation of stress granules, cytosolic protein aggregates composed of 48S preinitiation complexes and other factors. Stress granules are induced upon activation of PERK and phosphorylation of eIF2α.[46] Treatment of HEK wild-type cells with geneticin for 24 h increased immunostaining of p-eIF2α in a dotted cytosolic distribution indicative of stress granules (Figure 3h). Arsenite treatment served as a positive control. A similar robust induction of UPR by aminoglycosides was observed in Hela cells (Figure S3).

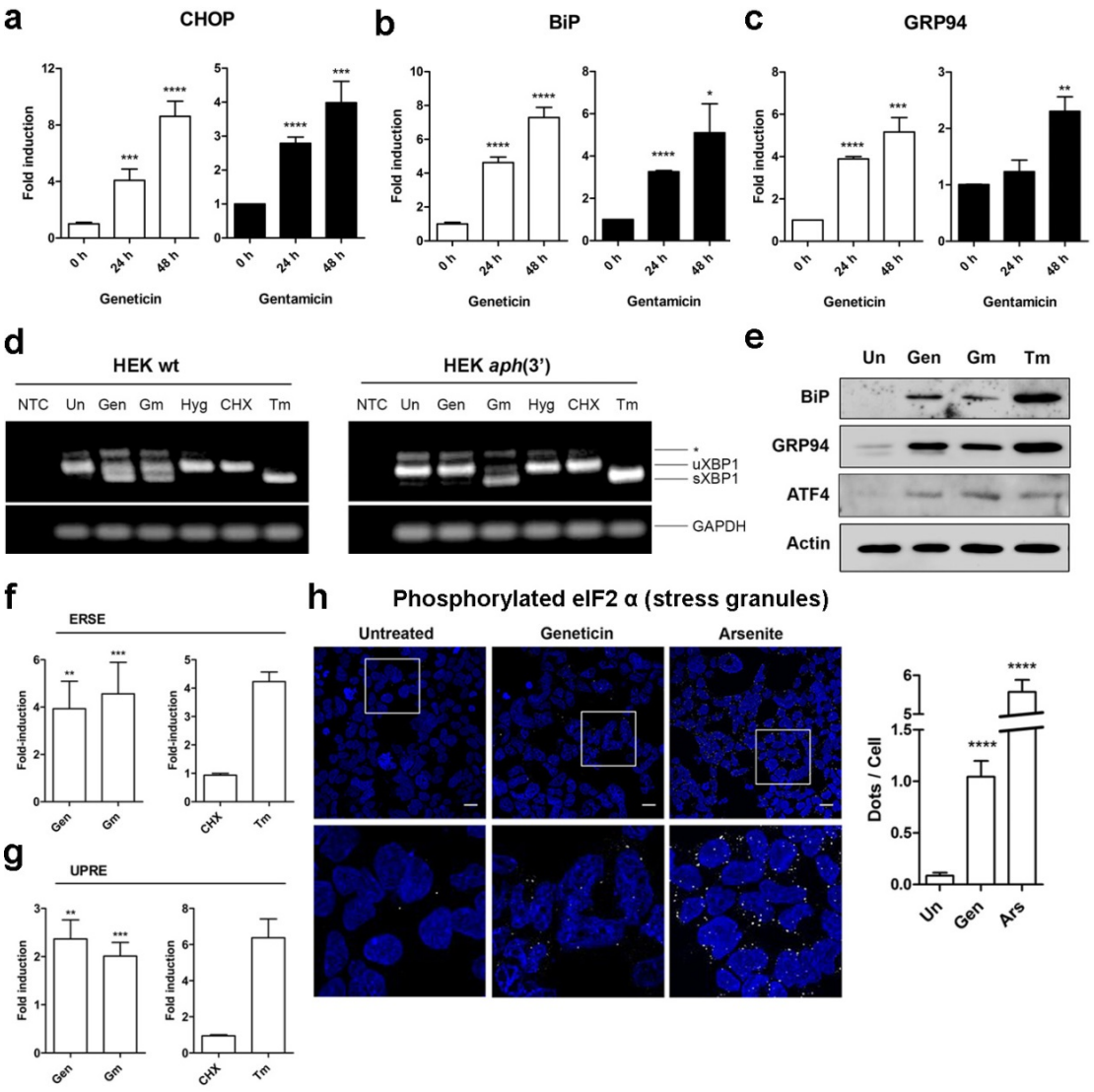
a
CHOP
Fold induction
0 h
24 h
48 h
Geneticin
Gentamicin
b
BiP
c
GRP94
d
HEK wt
HEK aph(3')
NTC Un Gen Gm Hyg CHX Tm
*
uXBP1
sXBP1
GAPDH
e
Un Gen Gm Tm
BiP
GRP94
ATF4
Actin
f
ERSE
Fold-induction
Gen
Gm
CHX
Tm
g
UPRE
h
Phosphorylated eIF2 α (stress granules)
Untreated
Geneticin
Arsenite
Dots / Cell
Un
Gen
Ars

Figure 3 Aminoglycosides induce the UPR. (**a–c**) qPCR analysis. HEK wild-type cells were treated with geneticin (16 µM) or gentamicin (400 µM) and incubated for the indicated times. Expression of CHOP (**a**), BiP (**b**), and GRP94 (**c**) mRNA is shown. Three biological replicates were each run in triplicate assays and means + SD of fold induction relative to 0 h (untreated) sample are presented; **P*<0.05; ***P*<0.01; ****P*< 0.005; *****P*<0.001. (**d**) XBP1 splicing assay. HEK wild-type or HEK *aph*(3') cells were treated with geneticin (16 µM), gentamicin (1250 µM), hygromycin (2 µM), cycloheximide (2 µM), tunicamycin (5 µg/mL) for 24 h or left untreated. NTC: no template control. Products of XBP1 PCR were analyzed by gel electrophoresis; unspliced and spliced versions of XBP1 are indicated. Tunicamycin was a positive control to induce ER stress; GAPDH was a loading control. The asterisk indicates the position of a hybrid amplicon (ref 15). (**e**) Western blot analysis. HEK wild-type cells were treated with geneticin (16 µM) or gentamicin (400 µM) and incubated for 24 h. 10 µg of total protein were loaded and BiP, GRP94 and ATF4 were detected by immunoblotting using specific antibodies. β-actin was used as a loading control. Tunicamycin (2.5 µg/mL) was used as a positive control. (**f-g**) Reporter assays. HEK cells were transfected with luciferase reporter plasmids (**f**) UPRE (reporter for ATF6 activity) or (**g**) ERSE (reporter for ATF6 and XBP1 activity). Cells were treated with geneticin (16 µM) or gentamicin (800 µM) for 24 h. Cycloheximide (16 µM) was used as a negative control, tunicamycin (2.5 µg/mL) was used as a positive control for UPR. Luciferase activities were determined and the Fluc/Rluc ratios were calculated. Untreated samples are set as 1 and fold inductions are given (n = 3-6, ± SEM). **P<0.01, ***P<0.005. (**h**) Stress granule formation. HEK wild-type cells were treated with geneticin (16 µM) for 24 h or arsenite (0.5 mM) for 1 h as a positive control. Phosphorylated eIF2α was detected by immunofluorescence. Scale bars: 40 µm. The lower panels show insets in higher magnification. Bar graph indicates quantification of peIF2α immunofluorescence (n number of cells; $n_{untreated}$ = 540; $n_{geneticin}$ = 249; $n_{arsenite}$ = 648); *****P*<0.001. Gen: Geneticin; Gm: Gentamicin; Hyg: Hygromycin; Tm: Tunicamycin; CHX: Cycloheximide; Ars: Arsenite; Un: Untreated.

preparations had established incubation with 0.07 µg/mL tunicamycin as a suitable treatment with hair cell death beginning at 48 h and progressing to 50% of cells by 72 h. The ER-stress-associated pro-apoptotic factor CHOP already appeared after 8 h of incubation with tunicamycin and was expressed in the nuclei of most hair cells by 24 h (Figure 4a and Supplementary Figure S4). Staining mostly had disappeared at 48 h (Supplementary Figure S4) when loss of hair cells became apparent, implicating CHOP in hair cell death. In the same explant model, treatment with gentamicin caused significant loss of hair cells with the pattern of loss showing the typical progression of aminoglycoside damage[47] with most destruction in the base (Supplementary Figure S5) while inner hair cells were mostly spared. Despite continuing and increasing cell death, CHOP was not observed throughout the entire time course up to 72 h (Figure 4a).

The response of ganglion neurons to ER stress was studied in spiral ganglion cells (SGCs) that were harvested from the base to the middle of the modiolus of cochlear explants and similarly treated with tunicamycin or gentamicin (Figure 4b). As expected from its activity as an ER stressor, tunicamycin induced CHOP in the nuclei of SGCs within 24 h. In contrast to its effect on hair cells, gentamicin increased the immunoreactivity to CHOP in SGCs, evident after 48 h of incubation.

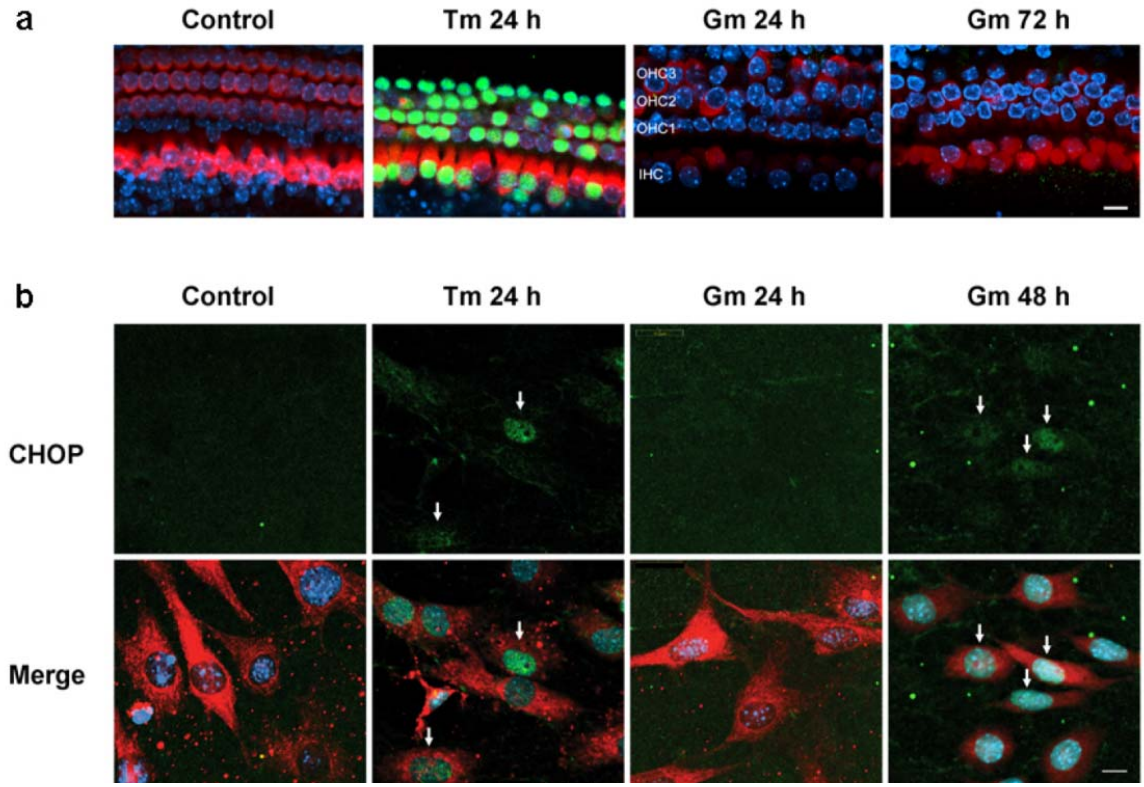

Figure 4 ER stress in cochlear tissues. (a) Tunicamycin but not gentamicin causes ER stress in hair cells. Tunicamycin (0.07 µg/mL) induced the specific ER stress-associated pro-apoptotic factor, CHOP (green), in the nuclei of hair cells in organ of Corti explants by 24 h but was not observed in any part of the organ of Corti throughout the entire time course of gentamicin treatment (3.5 µM) until hair cell death. Segments shown are from the basal turn. Green: CHOP, red: Myo 7a, blue: Hoechst 33342 staining for nuclei. The figure represents three different explants at each time point; focal plane is the nuclear level of outer hair cells. Scale bar (Gm): 10 µm. (b) Gentamicin induces ER stress in spiral ganglion cells (SGCs). Tunicamycin (0.07 µg/mL) treatment for 24 h induced CHOP in the nuclei of SGCs (arrows). With gentamicin (3.5 µM) treatment, CHOP appeared in the nuclei of SGCs by 48 h (arrows). Green: CHOP, red: neuronal class III β-tubulin staining for SGCs, blue: Hoechst 33342 staining for nuclei. The figure represents three different explants at each time point. Scale bar, 10 µm.

Gentamicin reduces spiral ganglion cells and synaptic ribbons but not hair cells in XBP1$^{+/-}$ mice *in vivo*. In wild-type strains such as the CBA/J mouse, the OHCs are the primary target of chronic aminoglycoside ototoxicity *in* and very little direct effect—if any—can be observed on SGCs. In view of the modest but significant gentamicin-induced CHOP expression in SGCs of cochlear explants, we investigated potential gentamicin-induced ER stress in a model of compromised UPR, an XBP1-haploinsufficient mouse. The local route of drug administration to the middle ear, chosen for this study, is able to isolate effects to the auditory periphery while avoiding adverse complications associated with systemic gentamicin treatment in the mouse.[30]

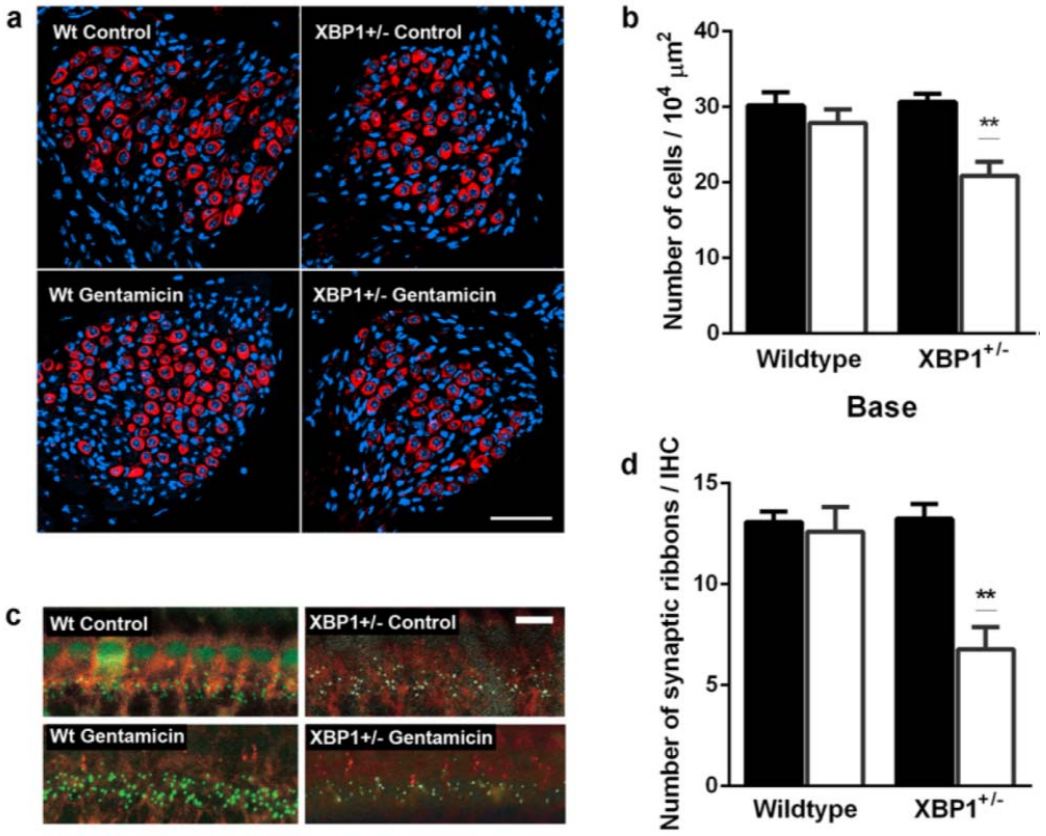

Figure 5 Gentamicin reduces the number of SGCs and IHC synapses in XBP1$^{+/-}$ mice. Gentamicin (0.56 M) was locally injected into the middle ear through the bulla as described in the Methods section "Drug administration *in vivo*." (a,b) Gentamicin reduces SGCs in XBP1$^{+/-}$ but not in wild-type (XBP1$^{+/+}$) littermates. (a) The number of SGCs was counted from high-magnification images of Rosenthal's canal of saline- and gentamicin-injected wild-type and XBP1$^{+/-}$ mice. Red: neuronal class III β-tubulin staining for neural cells, blue: Hoechst 33342 staining for nuclei. The figure represents five different animals at each condition. Scale bar: 50 μm. (b) Quantitative evaluation revealed that SGC density in the basal turn of XBP1$^{+/-}$ mice but not in wildtype mice was significantly decreased by gentamicin. Filled bars, controls; open bars, gentamicin treatment. n = 5 in each group; $^{**}P<0.01$. Middle and apical turns were not affected. (c,d) Gentamicin reduces synaptic ribbons in XBP1$^{+/-}$ but not in wild-type mice. (c) Hair cells were stained with anti-Myo7 antibodies (red) and synaptic ribbons with antibodies to CtBP2 (green). The number of synaptic ribbons per IHC in the basal turn was quantified from 3-D images created by using Imaris software. Staining of some nuclei is consistent with a partial nuclear localization of this protein,[66] which has also been confirmed for IHCs.[67] The figure represents three different animals at each condition. Scale bar: 20 μm. (d) Quantitative evaluation demonstrated that synaptic ribbon density of XBP1$^{+/-}$ mice but not of wildtype littermates was diminished by local injection of gentamicin. Filled bars, controls; open bars, gentamicin treatment. n = 3 in each group; $^{**}P<0.01$

Surface preparations from XBP1$^{+/-}$ and wild-type littermates treated with gentamicin *in vivo* were examined from base to apex three weeks after drug injection. OHCs were present in all parts of the cochlea in both wild-type and XBP1$^{+/-}$ mice except for scattered loss at the very end of the basal turn (Supplementary Figure S5c). Quantitation of hair cell loss along the entire cochlea confirmed only minor damage at the extreme the basal turn with no difference between wild-type and XBP1$^{+/-}$ mice.

In the absence of any discernible defects on hair cell integrity and prompted by the in-vitro results, we then analyzed spiral ganglion density and synaptic connections. Three weeks after gentamicin injection, the SGCs were counted on mid-modiolar cryosections stained for β-tubulin and nuclei. There was a significant reduction in spiral ganglion density in the basal turn of the cochlea in XBP1$^{+/-}$ mice but not in wild-type littermates (Figures 5a and 5b). The innervation of hair cells by the spiral ganglion was assessed by staining synaptic ribbons with antibody to CtBP2, a constituent of the ribbon protein RIBEYE. The number of synaptic ribbons per IHC was reduced by approximately 50% in the basal turn of

the cochlea of the XBP1$^{+/-}$ mice but not of corresponding wild-type littermates (Figures 5c and 5d).

Auditory physiology corroborates auditory pathology and ER stress. In order to assess the impact of the observed pathology on auditory function, we measured auditory brain stem responses (ABR) and distortion product otoacoustic emissions (DPOAE). ABR provides information on the ascending auditory pathway reflecting synaptic and neuronal activity, while DPOAE probes the functional integrity of outer hair cells. Deterioration of auditory thresholds was apparent one week after the injection of gentamicin and remained stable for up to three weeks, the latest time point studied (Figure 6a). Large threshold shifts were observed at 32 kHz in XBP1$^{+/-}$ mice but not in wild-type littermates, which were little affected. Consistent with the morphological observations of intact outer hair cells, DPOAE remained unaffected by gentamicin treatment (Supplementary Figure S6).

Finally, in order to validate the potential contribution of protein misfolding to the changes in auditory thresholds, we treated animals with TUDCA, a clinically used chemical chaperone. Systemic TUDCA co-administration significantly attenuated gentamicin-induced ototoxicity in the XBP1$^{+/-}$ mice (Figure 6b) as measured by ABR three weeks after the drug treatment.

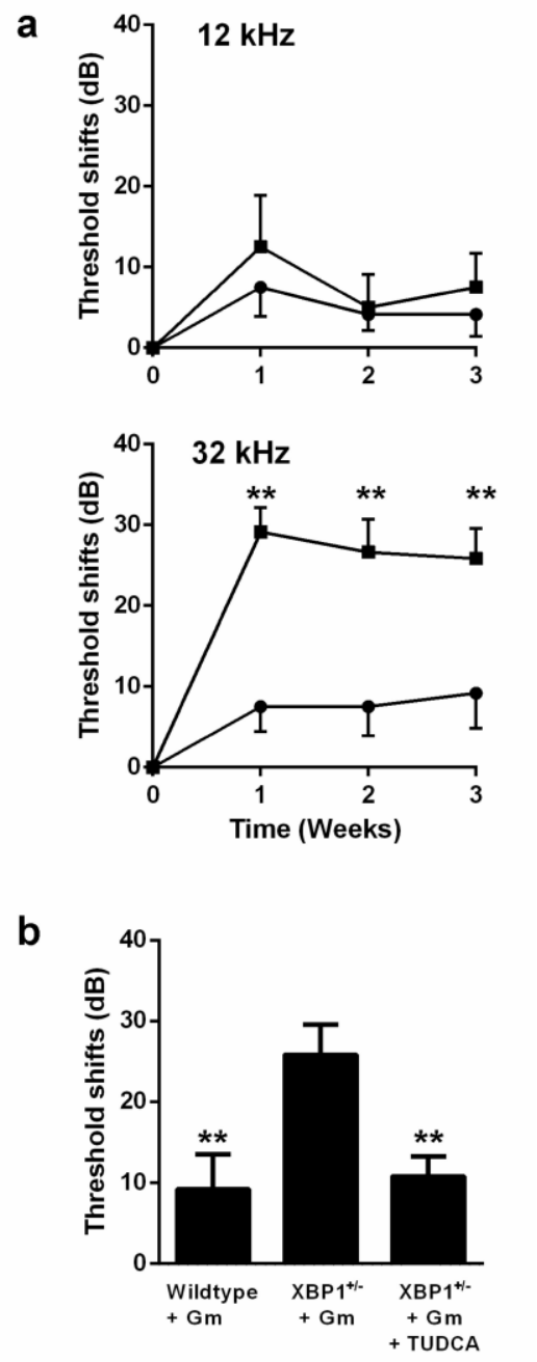

Figure 6 Auditory threshold shifts induced by gentamicin. (a) Gentamicin (0.56 M) was locally injected into the middle ear through the bulla as described in 'Methods'. Three weeks after treatment, large threshold shifts had developed at 32 kHz in XBP1$^{+/-}$ mice (square symbols) but not in wild-type littermates (circles). Data are presented as mean + SD for XBP1$^{+/-}$ mice and mean - SD for wild-types. *n* = 6 in each group; ***P*<0.01. (b) TUDCA attenuates gentamicin ototoxicity in XBP1$^{+/-}$ mice. Animals in all three groups received the local injection of gentamicin and, as indicated, TUDCA co-treatment (500 mg/kg i.p. at 6 d, 3 d, and 3 h before gentamicin injection). Data are presented as means + SD of threshold shifts at 32 kHz, determined three weeks after treatment. *n* = 6 in each; ***P*<0.01

Discussion

Aminoglycoside-induced loss of translational fidelity in eukaryotes is evident from our experiments on HEK293 cells and, moreover, is clearly linked to the ribosomal activity of the drugs. We have primarily chosen HEK293 cells for study as these cells are readily transfected, facilitating the use of reporter constructs to study drug-induced misreading.[49] However, we have obtained similar results in human Hela cells. The known misreading-inducers geneticin and gentamicin, but not hygromycin or cycloheximide, elicit a UPR. Gentamicin was selected as a classical clinical aminoglycoside to bridge the findings from our *in-vitro* studies to the animal model. Geneticin was included because its inactivation by the APH(3‘) enzyme allowed to control for the specificity of drug action.[39] Modification of geneticin by APH(3‘) (which abrogates its anti-ribosomal activity by phosphorylation of the 3‘ OH group) eliminates the ability of geneticin to cause both misreading and ER stress. In contrast, APH(3‘) did not affect the misreading activity of gentamicin, which lacks the 3‘ OH group and thus is not a target for APH(3‘). The finding that the cell viability and the metabolic activity of HEK wild-type cells remain intact despite drug-induced mistranslation attests to the protective efficacy of cellular homeostatic responses such as the UPR and allows us to extrapolate that the UPR, at least in part, mitigates mistranslation induced by aminoglycosides in eukaryotic organisms.

Consistent with this notion, $XBP1^{+/-}$ haploinsufficient mice but not wild-type mice sustain gentamicin-induced loss of SGCs. XBP1 is one of the central components in the three main pathways of the UPR, regulating molecular chaperones and promoting ER-associated degradation.[50] The crucial function of XBP1 for cell survival is indicated by embryonic lethality of homozygous XBP1 knock-out mice.[37] Haploinsufficient mice are viable but are less capable of inducing chaperones and promoting ERAD under ER stress conditions.[51] Consequently, ER stress is prone to damage cells in $XBP1^{+/-}$ but not in wild-type mice.

Oxidative stress is a major factor in the pathomechanism of aminoglycoside ototoxicity,[48] but evidence for an involvement of ER stress has been only indirect or lacking. Upregulation of heat shock proteins protects the mouse cochlea in part from aminoglycoside-induced ototoxicity *in vivo*.[52] However, the ER stress marker m-calpain is unaffected by aminoglycoside treatment in the mouse cochlea *in vivo*.[53] Despite the extensive loss of hair cells that gentamicin can cause in cochlear explants, no ER stress marker develops there. This is in contrast to their induction with the ER stressor tunicamycin, a finding consistent with previous observations of tunicamycin-induced hearing loss in the rat.[54] Further distinguishing the pathological effects of the two drugs, the damage caused by tunicamycin broadly encompasses all regions of the cochlea while the pattern of gentamicin-induced damage in the explants follows the base-to-apex gradient characteristic of aminoglycosides.[48]

Our results clarify that aminoglycoside-induced ER stress in the cochlea is limited to neurons of the spiral ganglion. In the *in-vivo* model, the local application of a single low dose of gentamicin does not lead to hair cell death. However, spiral ganglion cells were significantly reduced in the base of the cochlea, corroborating the *in-vitro* results on ER stress in the nerve but not in hair cells. Gentamicin-induced ER stress has also been observed in rat kidneys *in vivo* as part of its nephrotoxic actions,[55] a result in agreement with our findings that aminoglycosides are capable of inducing ER stress in mammalian tissues. In accord with a gentamicin-reduced density of spiral ganglion cells, synaptic connections to hair cells are lost, providing an explanation for the observed high-frequency hearing loss.

The selective actions of gentamicin on spiral ganglion cells and synapses suggest a heightened sensitivity to neurodegeneration in the XBP1$^{+/-}$ haploinsufficient mice in contrast to the more common pathology of hair cell loss. It is interesting in this context that a loss of afferent nerve terminals and subsequent degeneration of the cochlear nerve has also been observed after moderate noise exposure that leaves the sensory cells intact.[56]

On a mechanistic level, disruption of translational fidelity causes protein misfolding and aggregation. The ability of XBP1 to maintain cell integrity upon drug-induced mistranslation appears to be mediated by induction of ER chaperones such as BiP, which we also find to be upregulated in response to aminoglycoside challenge. On an organismal level, protein misfolding has been associated with a variety of disorders collectively termed conformational diseases.[57] Presumably, cell-type specific differences in the buffering capacity of the proteostasis network account for the cell- or organ-selectivity in some of these diseases.[58] Aminoglycoside-induced death of hair cells has previously been associated with inhibition of host-cell protein synthesis[47,59] and oxidative stress.[48] The hypothesis presented here that aminoglycoside-induced loss of SGCs in XBP1$^{+/-}$ haploinsufficient mice is conferred by the drug's misreading activity is supported by the observation that administration of a chemical chaperone significantly alleviated the hearing loss. Specifically, we postulate that the UPR is normally able to maintain a protein folding equilibrium in the presence of aminoglycoside-induced mistranslation in SGCs. However, when the UPR system is compromised, e.g. by genetic haploinsufficiency of XBP1, aminoglycoside-induced mistranslation can manifest as neuropathology.

EXPERIMENTAL PROCEDURES

Materials and sources. Monoclonal anti-GADD 153 antibody, Santa Cruz Biotechnology (Dallas, TX, USA); polyclonal antibody against neuronal class III β-Tubulin, Covance (Princeton, NJ, USA); monoclonal anti-CtBP2 antibody, BD Biosciences (San Jose, CA, USA); polyclonal antibody against p-eIF2α, Cell Signaling (Danvers, MA, USA); polyclonal anti-myosin7a antibody (Proteus Biosciences, Ramona, CA, USA); secondary goat anti-rabbit antibody conjugated with Texas Red, Abcam (Cambridge, MA, USA); rhodamine phalloidin, Invitrogen (Life Technologies, Carlsbad, CA, USA); HEK293 cells, Innoprot (Biscay, Spain); geneticin, gentamicin, tunicamycin, cycloheximide, arsenite, saponin, and HEK *aph*(3') cells, Sigma Aldrich (St. Louis, MO, USA); hygromycin, PAA Laboratories

(Cansera, Canada); nucleotide primers, Microsynth (Balgach, Switzerland); cell culture media and trypsin, Life Technologies (Carlsbad, CA, USA).

Assessment of mistranslation. Misreading and stop-codon read-through were assessed in gain-of-function dual luciferase assays.[60,61] For translation in rabbit reticulocyte lysates (RRL, Promega, Madison, WI, USA), luciferase mRNA was produced *in vitro* using T7 RNA polymerase (Thermo Scientific, Waltham, MA, USA) and plasmids pGL4.14 (firefly luciferase, hFluc) and pGL4.75 (renilla luciferase, hRluc; both from Promega), where the mammalian promoter was replaced by the T7 bacteriophage promoter. For misreading, we replaced residue His245 (CAC codon) with Arg245 (CGC near-cognate) in the hFluc protein by site-directed mutagenesis. Read-through was assessed with a fusion construct in which hRluc and hFluc were fused by a 27-nucleotide linker encoding the polypeptide STCDQPFGF, using overlap PCR mutagenesis to result in the pT7 hRluc-hFluc vector; a UGA nonsense-codon was introduced at the glutamine residue (wild-type CAA) of the linker sequence by site-directed PCR mutagenesis. A cell-free luciferase translation assay was performed as described.[51] Mistranslation in HEK cells was determined using the pRM hRluc-hFluc H245R vector, where His245 (CAC codon) was replaced by Arg245 (CGC codon) in the pRM hRluc-hFluc vector. Read-through was determined by pRM hRluc-hFluc D357X, where Asp357 (GAC codon) was replaced by a UGA nonsense-codon in the firefly luciferase transcript. Both constructs were designed by site-directed PCR mutagenesis. HEK wild-type cells were transfected with reporter plasmid using TurboFect (Fermentas) according to the manufacturer‘s protocol. After a 24-h incubation, medium was replaced by F10 with 15 µg/mL saponin. Aminoglycoside antibiotics were added and cells were incubated for another 24 h. Cells were lysed and luciferase activities determined; hRluc mRNA was used as an internal control and misreading and read-through were quantified by calculating mutant firefly/renilla activities. The basal error frequency of the eukaryotic ribosome is 4 x 10^{-4} to 10^{-5}.[62] For each set of replicates, the hFluc/hRluc ratio of the untreated samples were set as 1, which reflects this

basal error frequency. Luminescence was measured in a luminometer FLx800 (Bio-Tek Instruments, Winooski, VT).

Viability assay. HEK cells were grown to 70% confluence and treated with 16 µM geneticin or 400 µM gentamicin in F10 medium with 15 µg/mL saponin for the indicated time. Ten-percent Alamar Blue solution was added (v/v) for 3 h and fluorescence was monitored at 530 nm for excitation and 590 nm for emission. The fluorescence level of the control sample (untreated) was set as 100% after subtraction of background fluorescence, measured in cell-free wells.

Sytox dead cell stain. HEK cells were grown to 60% confluence in DMEM with 10% FBS. Medium was changed to F10 with 15 µg/mL saponin and aminoglycoside antibiotics were added and cells were incubated for 24 h or 48 h. Cells were detached by adding 100 µL accutase (Life Technologies) and were resuspended in 400 µL FACS buffer (1x PBS, 2% FBS) and transferred to FACS tubes. Sytox Red (Life Technologies) was added to the cell suspension. The nucleic acid stain penetrates cells with compromised plasma membranes but will not cross uncompromised cell membranes. The samples were then analyzed with a BD FACS Canto II and the FlowJo data analysis software.

Microarray analysis. See legend to Supplemental Figure S2.

Proteome analysis. Cell samples were incubated with lysis buffer (150 mM NaCl, 0.1% SDS, 0.5% Na-deoxycholate, 50 mM Tris pH 7.5, and 1× complete protease inhibitor (Roche)) for 10 min at RT on a shaking mixer. The lysate was ultrasonicated for 10 min and centrifuged for 20 min at 16,000 × *g* at 4 °C. Eighty micrograms of protein of each sample were used for iTRAQ labeling (AB SCIEX). Each iTRAQ 4-plex experiment was carried out with two biological replicates of untreated HEK wild-type cells (114 and 116 label) and two biological replicates of cells treated with 16 µM geneticin for 32 h (115 and 117 label) following the manufacturer's protocol. iTRAQ samples were pooled, dried, reconstituted in solvent A (5% ACN, 8 mM KH_2PO_4, pH 4.5), and fractionated by HILIC-HPLC (Pack Polyamine II, 250 × 4 mm, 120 Å S-5 µm, YMC). The column was equilibrated with solvent A. Peptides were eluted using solvent B (5% ACN, 100

mM KH_2PO_4, pH 4.5) by a gradient of: 0–7.5 min, 0% B; 7.5–37.5 min, 0–50% B; 37.5–42.5 min, 50–100% B; 42.5–47.5 min, 100% B at a flow rate of 0.4 mL/min. The resulting 13 fractions were desalted using ZipTips (Millipore) according to the manufacturer's protocol and reconstituted in solvent C (3% ACN and 0.1% formic acid) for LC-MS/MS analysis. Samples were auto-injected into an Eksigent-nano-HPLC system and separated on a custom reverse phase tip column (75 µm × 150 mm) packed with C_{18} material (3 µm, 200 Å, AQ, Bischoff GmbH). The column was equilibrated with solvent C and 5% solvent D (0.2% FA in ACN). For elution, a flow rate of 300 nL/min was used and a gradient of 0–70 min, 5–25% D; 70–85 min, 25–50% D; 85–88 min, 50–98% D. High accuracy mass spectra were acquired with an AB SCIEX 5600 mass spectrometer (AB SCIEX) in the range of 385–1250 m/z. Up to 36 data-dependent MS/MS were recorded in high sensitivity mode of the most intense ions with charge states 2+, 3+, and 4+ using collision-induced dissociation. Target ions already selected for MS/MS were dynamically excluded for 90 s after three occurrences. MS/MS data were analyzed using Mascot 2.4 (Matrix Science) and searched against a decoyed human database from Swissprot (release December 2012) concatenated with an in-house build contaminant database. The search parameters were: precursor ion mass tolerance of 20 ppm, fragment ion mass tolerance of 0.05 Da, trypsin digestion, fixed modifications of MMTS-labeled cysteine, 4-plex iTRAQ modifications of free amines at the N-termini and of lysine, and variable modification 4-plex iTRAQ of tyrosine. Peptides without 4-plex iTRAQ labelling at the N-terminus or at a lysine were excluded from the analysis. Scaffold_4.1 (Proteome Software Inc., Portland, OR) was used to validate MS/MS-based peptide and protein identifications. We identified and quantified 1,785 proteins (protein prophet probability 95%, minimum two peptides for identification of a protein, and minimum Mascot Ionscore of 40). After the permutation test and further amendment of the *p*-value with the Bonferroni correction, 77 proteins were found to be regulated (p-value < 0.05). Thirty-five proteins were upregulated based on a threshold of 0.3 (log_2-scale).

XBP1-splicing assay and qPCR. RNA samples from HEK cells were prepared using Trizol extraction (Life Technologies) and were reverse transcribed using a ThermoScript RT-PCR System (Life Technologies) according to the manufacturer‘s instructions. The XBP1 splicing assay employed XBP1-specific primers that amplify spliced (-26 nt) and unspliced XBP1 mRNA (forward 5‘-TTACGAGAGAAAACTCATGGCC-3’, reverse 5’-GGGTCCAAGTTGTCCAGAATGC-3’). PCR products were analyzed on a 2.7% agarose gel. Amplification of GAPDH cDNA served as loading control. For qPCR the Quantitect SYBR Green PCR Kit (Qiagen) was used together with the 7500 Fast Real-Time PCR System (Applied Biosystems). The primers were CHOP: forward 5‘-GCGCATGAAGGAGAAAGAAC-3‘, reverse 5‘-CCAATTGTTCATGCTTGGTG-3‘; BiP: forward 5‘-TTTCTGCCATGGTTCTCACTAAAA-3‘, reverse 5‘-AACATTTAGGCCAGCAATAGTTCC-3‘; GAPDH: forward 5‘-ACCCACTCCTCCACCTTTGA-3‘, reverse 5‘-CTGTTGCTGTAGCCAAATTCGT-3‘; GRP94 forward 5‘-TGGGAAGAGGTTCCAGAATG-3‘, reverse 5‘-GTTGCCAGACCATCCGTACT-3‘. For relative quantification, GAPDH mRNA served as a reference. Measured quantification cycles were analyzed according to Pfaffl[63], comparing treated with untreated samples. Three biological replicates were run in triplicates each and means and standard deviations were calculated.

Western Blot. HEK cells were grown to 60% confluence in DMEM with 10% FBS. Medium was changed to F10 with 15 µg/mL saponin and aminoglycoside antibiotics were added and cells were incubated for 24 h. Cells were lysed in hypotonic buffer (20 mM HEPES pH 7.5, 10 mM KCl, 3 mM Mg Acetate, 1 mM DTT and 10 µg/ml DNase I) and ultrasonicated. Lysates were centrifuged (13.000 rpm, 10 min) and protein concentration in the supernatant was measured by the Micro BCA Protein Assay Kit (Thermo). Ten µg of total protein were resolved on 10% SDS-polyacrylamide gels and blotted on nitrocellulose membranes, which were probed with specific antibodies. Amersham ECL Prime Western Blotting Detection Reagent (GE Healthcare, RPN2232) was used as a substrate for the horseradish peroxidase (HRP). The specific antibodies used in

this study were: anti-BiP antibody (Abcam, ab21685); anti-GRP94 antibody (Abcam, ab87886); anti-ATF4 antibody (Abcam, ab23760); anti-β-actin antibody (Sigma, A1978-200UL); HRP-conjugated goat anti-rabbit (Invitrogen, G-21234) and goat anti-mouse antibodies (Invitrogen, A10551).

UPR reporter assay. Reporter plasmids UPRE (p5xATF6-GL3) and ERSE (pGL3-GRP78P(-132)-luc) carrying luciferase under the control of UPR-specific cis-acting elements were kind gifts from Kazutoshi Mori (Kyoto University, Japan). HEK cells were grown to 60% confluence and co-transfected with reporter constructs and pGL4.75 (Rluc) using TurboFect reagent (Fermentas) according to the manufacturer's protocol. After a 24-h incubation medium was replaced by F10 with 15 μg/mL saponin. Aminoglycosides were added and cells were incubated for another 24 h. Cells were lysed and luciferase activities determined. Normalization of luciferase activities was performed as described above. Cycloheximide was used as a mistranslation negative control and tunicamycin was used as a positive control for UPR.

P-eIF2α immunofluorescence assay. HEK cells grown on poly-D-lysine (Sigma)-coated cover slips (Thermo Scientific) were treated for 24 h with geneticin in F10 medium with 15 μg/mL saponin, or with arsenite for 1 h (positive control). Cells were then fixed with 4% paraformaldehyde and methanol and incubated with blocking solution (1× PBS with 1% BSA and 0.5% saponin) for 1 h at RT. Immunostaining used a rabbit polyclonal antibody against p-eIF2α (1:250) and a secondary goat anti-rabbit antibody conjugated with Texas Red (1:250) diluted in blocking solution. Cover slips were mounted on glass slides (VWR) using Dapi fluoromount (Southern Biotech), and cells were imaged using a Lyca Sp2 confocal microscope and a 63× objective. p-eIF2α and nuclear signals were quantified using Imaris software (Bitplane) and the dots-per-cell ratio was calculated.

Animals. Male and female CBA/J mice were purchased from Harlan Sprague-Dawley Co. (http://www.harlan.com/products_and_services/research_models_and_services/r

esearch_models/cbaj_inbred_mice.hl) at an age of 6–8 weeks and bred in-house in order to obtain pups for organotypic cultures of the post-natal organ of Corti and SGCs (see next section). $XBP1^{+/-}$ mice, originally derived from D3 embryonic stem cells, were from a stock kindly provided by Dr. Laurie H. Glimcher[31] and received via Dr. Randal J. Kaufman, University of Michigan. Littermates served as wild-type ($XBP1^{+/+}$) controls. Animals were kept on a 12-h light/12-h dark cycle with free access to water and diet (Purina 5001) and used in the *in-vivo* studies at an age of 3–4 months. Experimental protocols were approved by the University of Michigan Committee on the Use and Care of Animals and animal care was under the supervision of the University of Michigan's Unit for Laboratory Animal Medicine.

Organotypic cultures of post-natal organ of Corti and spiral ganglion cells. The procedures were as described previously.[64] Mice at post-natal day 2–3 (p2–3) were euthanized and cochleae dissected in cold Hank's Balanced Salt Solution to isolate the organ of Corti; spiral ganglion cells (SGCs) were dissected from the base to the middle of the modiolus. Explants were placed onto a culture dish in 2 mL of medium consisting of Basal Medium Eagle, 1% serum-free supplement (Gibco #51500-056, Life Technologies), 1% bovine serum albumin, 5 mg/mL glucose and 10 U/mL penicillin G, allowed to settle for 4 h (37 °C, 5% CO_2) and incubated for 2 d to mitigate dissection stress. Medium was then exchanged for new media with or without drugs and incubation continued. For immunofluorescent labeling, explants were fixed with 4% paraformaldehyde overnight at 4 °C and permeabilized for 30 min with 3% Triton X-100 in phosphate buffered saline (PBS) at room temperature. After three washes with PBS and blocking with 10% goat serum for 30 min at RT, incubation with the primary antibodies followed at 4 °C for 72 h. After three washes with PBS, secondary antibodies were applied (Alexa Fluor 488-conjugated goat anti-mouse and Alexa Fluor 546-conjugated goat anti-rabbit antibody; 1:200 in PBS) at 4 °C overnight in darkness. After several rinses, specimens were mounted on a slide with Prolong Gold anti-fade reagent (Life Technologies) and imaged with an Olympus Fluoview Confocal Laser Scanning Microscope-FV500 (Olympus

America, Center Valley, PA). For staining of hair cells, specimens were incubated at RT with rhodamine phalloidin (1:100) for 1 h; or for staining of nuclei with Hoechst 33342 (2 µg/mL in PBS) for 40 min. Presence or absence of OHCs and IHCs was determined on a Leitz Orthoplan microscope (Leica, Wetzlar, Germany) whose right objective had a 0.19-mm scale imposed on the field. Successive 0.19-mm fields were evaluated beginning at the apex by observers blinded to the experimental conditions. Cell counts were compared to a normative database (KHRI Cytocochleogram, version 3.0.6, Kresge Hearing Research Institute, University of Michigan, Ann Arbor, MI, USA).

Drug administration *in vivo*. Gentamicin was locally delivered as previously described.[65] Mice were anesthetized with an intra-peritoneal injection of xylazine (7 mg/kg) and ketamine (90 mg/kg) and body temperature was maintained. The temporal bone was approached via a retro-auricular incision and a small hole was made in the thin part of the bulla with a 30-G needle. Surgical tubing was inserted through the hole, and 10 µL of 0.56 M gentamicin dissolved in saline was slowly injected. The skin incision was closed with tissue adhesive. TUDCA (Calbiochem, EMD Millipore, Billerica, MA, USA) was dissolved in 0.15 M $NaHCO_3$ (adjusted to pH 7.4) and injected subcutaneously at 500 mg/kg body weight 6 d, 3 d, and 3 h before gentamicin administration. Injections of 0.15 M $NaHCO_3$ served as vehicle controls. Injection of TUDCA did not cause any apparent side effects.

Hair cell counts in adult mice. Three weeks after injections, cochleae were fixed as described above. The apical bony capsule was removed and the cochlea decalcified in 4% sodium EDTA (adjusted to pH 7.4) for 7 d at 4 °C. Subsequently, cochleae were dissected into apical, middle, and basal segments. Segments were permeabilized in 3% Triton X-100 for 30 min at room temperature, washed three times with PBS, and incubated with rhodamine phalloidin (1:100) at room temperature for 1 h. The procedures for cell counting were the same as for explants.

Quantification of spiral ganglion cells and synaptic ribbons. Following decalcification with 4% EDTA, cochleae were cryo-sectioned. Sections of 8 µm thickness were incubated in 0.3% Triton X-100 in PBS for 30 min at room temperature, blocked with 10% goat serum for 30 min, followed by incubation with anti-neuronal class III β-Tubulin antibody (1:2,000) for 48 h at 4 °C. After three rinses in PBS, sections were incubated with a secondary antibody (Alexa Fluor 546-conjugated; 1:500) at 4 °C overnight in darkness. After three washes with PBS, sections were stained with Hoechst 33342 (2 µg/mL in PBS) for 40 min at room temperature. After a final wash, the slides were mounted with Prolong Gold anti-fade reagent. Controls were processed without primary antibody. The number of SGCs in Rosenthal's canal was quantified using ImageJ software (National Institutes of Health, Bethesda, MD) by counting the β-tubulin- and Hoechst-positive cells on images taken with an Olympus laser confocal microscope. Two mid-modiolar sections, separated by 40 to 50 µm, were used to obtain the average for each animal. For synaptic ribbon counts, cryo-sections were incubated for 30 min at room temperature with 5% donkey serum in PBS with 0.3% Triton X-100 and overnight in darkness at 4 °C with antibodies against CtBP2 (1:200) and Myo7a (1:200). After three washes in PBS (15 min each), tissues were incubated with secondary antibodies (Alexa Fluor 488- and Alexa Fluor 546-conjugated; 1:1,000) at room temperature for 1 h. After three washes, the epithelia were mounted and images taken on an Olympus laser confocal microscope. Images were reconstructed 3-dimensionally using Imaris software (Bitplane). The number of synaptic ribbons was quantified per IHC based on an average of 14 IHCs per sample.

Auditory function measurements. For auditory brainstem responses (ABR), animals were anesthetized with an intra-peritoneal injection of xylazine (7 mg/kg), ketamine (65 mg/kg), and acepromazine (2 mg/kg), and placed in a sound-isolated and electrically shielded booth (Acoustic Systems, Austin, TX, USA). Body temperature was maintained near 37 °C with a heating pad. Acoustic stimuli were delivered monaurally to a Beyer earphone attached to a speculum inserted into the left ear canal. Sub-dermal electrodes were inserted at the vertex

of the skull, under the left ear, and under the right ear (ground). ABRs were measured at 12 kHz and 32 kHz using Tucker Davis Technology (TDT) System III hardware and SigGen/Biosig software to present the stimuli (15 ms tone bursts, 1 ms rise-fall time) and record up to 1024 responses for each stimulus level. Thresholds were determined by reducing the intensity in 10-dB increments and then in 5-dB steps until no organized responses were detected. Threshold shifts were calculated for individual animals as the difference in auditory thresholds between ABR measurements before and at the end of the studies. For the DPOAE procedure, see the legend to Supplementary Figure S6.

Statistical analysis. Data were evaluated by one-way ANOVA followed by Tukey's Honestly Significant Difference tests using JMP version 8.0.1 (SAS Institute Inc.) or Student's t-test. All tests were two-sided with significance set at $P<0.05$.

Conflict of Interest. The authors declare no conflicts of interest.

Acknowledgements. The data discussed in this publication have been deposited in NCBI's Gene Expression Omnibus and are accessible through GEO Series accession number GSE57198 (http://www.ncbi.nlm.nih.gov/geo/query/acc.cgi?acc=GSE57198).

The mass spectrometry proteomics data have been deposited to the ProteomeXchange Consortium via the PRIDE partner repository with the dataset identifier PXD000933 and DOI 10.6019/PXD000933.

We thank Ariane Kanicki and the Histology Core at KHRI for valuable help with cochlear histology. We thank Christian Trachsel, Jonas Grossman and Claudia Fortes from the FGCZ proteomics team for technical help and advice, and Christele Thibault and Doulaye Dembele from the Microarray and Sequencing Platform of the IGBMC, Illkirch, France, for help with the microarray analysis.

The project was supported by grant R01 DC-003685 and core grant P30 DC-05188 from the National Institute on Deafness and Other Communication Disorders, National Institutes of Health to JS.

Author contributions: JS, NO, and ECB designed the study. All authors discussed the data. NO, SD, HB, JS, and ECB wrote the paper with input from all authors.

Personal contributions: MM performed the misreading assays *in-vitro* and *in-vivo* as well as the readthrough assays *in-vitro* and *in-vivo*.

References

1. Drummond DA, Wilke CO. Mistranslation-induced protein misfolding as a dominant constraint on coding-sequence evolution. *Cell* 2008; **134:** 341-352.

2. Goltermann L, Good L, Bentin T. Chaperonins fight aminoglycoside-induced protein misfolding and promote short-term tolerance in Escherichia coli. *J Biol Chem* 2013; **288**:10483-10489.

3. Prostko CR, Brostrom MA, Malara EM, Brostrom CO. Phosphorylation of eukaryotic initiation factor (eIF) 2 alpha and inhibition of eIF-2B in GH3 pituitary cells by perturbants of early protein processing that induce GRP78. *J Biol Chem* 1992; **267:** 16751-16754.

4. Shi Y, Vattem KM, Sood R, An J, Liang J, Stramm L*, et al.* Identification and characterization of pancreatic eukaryotic initiation factor 2 alpha-subunit kinase, PEK, involved in translational control. *Mol Cell Biol* 1998; **18:** 7499-7509.

5. Tirasophon W, Welihinda AA, Kaufman RJ. A stress response pathway from the endoplasmic reticulum to the nucleus requires a novel bifunctional protein kinase/endoribonuclease (Ire1p) in mammalian cells. *Genes Dev* 1998; **12:** 1812-1824.

6. Haze K, Yoshida H, Yanagi H, Yura T, Mori K. Mammalian transcription factor ATF6 is synthesized as a transmembrane protein and activated by proteolysis in response to endoplasmic reticulum stress. *Mol Biol Cell*. 1999; **10**: 3787-3799.

7. Yoshida H, Okada T, Haze K, Yanagi H, Yura T, Negishi M*, et al.* ATF6 activated by proteolysis binds in the presence of NF-Y (CBF) directly to the cis-acting element responsible for the mammalian unfolded protein response. *Mol Cell Biol* 2000; **20:** 6755-6767.

8. Shen J, Chen X, Hendershot L, Prywes R. ER stress regulation of ATF6 localization by dissociation of BiP/GRP78 binding and unmasking of Golgi localization signals. *Dev Cell.* 2002; **3**: 99-111.

9. Bertolotti A1, Zhang Y, Hendershot LM, Harding HP, Ron D. Dynamic interaction of BiP and ER stress transducers in the unfolded-protein response. *Nat Cell Biol*. 2000; **2**: 326-32.

10. Schroder M, Kaufman RJ. The mammalian unfolded protein response. *Annu Rev Biochem* 2005; **74:** 739-789.

11. Zhang K, Kaufman RJ. The unfolded protein response: a stress signaling pathway critical for health and disease. *Neurology* 2006; **66:** S102-109.

12. Hetz C. The unfolded protein response: controlling cell fate decisions under ER stress and beyond. *Nat Rev Mol Cell Biol* 2012; **13:** 89-102.

13. Travers KJ, Patil CK, Wodicka L, Lockhart DJ, Weissman JS, Walter P. Functional and genomic analyses reveal an essential coordination between the unfolded protein response and ER-associated degradation. *Cell* 2000; **101:** 249-258.

14. Yoshida H, Matsui T, Hosokawa N, Kaufman RJ, Nagata K, Mori K. A time-dependent phase shift in the mammalian unfolded protein response. *Dev Cell.* 2003; **4**: 265-271.

15. Lin JH, Li H, Yasumura D, Cohen HR, Zhang C, Panning B*, et al.* IRE1 signaling affects cell fate during the unfolded protein response. *Science* 2007; **318:** 944-949.

16. Haynes CM, Titus EA, Cooper AA. Degradation of misfolded proteins prevents ER derived oxidative stress and cell death. *Mol Cell* 2004; **15:** 767-776.

17. Edelmann P, Gallant J. Mistranslation in E. coli. *Cell* 1977; **10:** 131-137.

18. Palmer E, Wilhelm JM. Mistranslation in a eucaryotic organism. *Cell* 1978; **13:** 329-334.

19. Palmer E, Wilhelm JM, Sherman F. Phenotypic suppression of nonsense mutants in yeast by aminoglycoside antibiotics. *Nature* 1979; **277:** 148-150.

20. Stansfield I, Jones KM, Herbert P, Lewendon A, Shaw WV, Tuite MF. Missense translation errors in Saccharomyces cerevisiae. *J Mol Biol* 1998; **282:** 13-24.

21. Wilhelm JM, Pettitt SE, Jessop JJ. Aminoglycoside antibiotics and eukaryotic protein synthesis: structure--function relationships in the stimulation of misreading with a wheat embryo system. *Biochem* 1978; **17:** 1143-1149.

22. Buchanan JH, Stevens A, Sidhu J. Aminoglycoside antibiotic treatment of human fibroblasts: intracellular accumulation, molecular changes and the loss of ribosomal accuracy. *Eur J Cell Biol* 1987; **43:** 141-147.

23. Abraham AK, Pihl A. Effect of protein synthesis inhibitors on the fidelity of translation in eukaryotic systems. *Biochim Biophys Acta* 1983; **741:** 197-203.

24. Burke JF, Mogg AE. Suppression of a nonsense mutation in mammalian cells in vivo by the aminoglycoside antibiotics G-418 and paromomycin. *Nucleic Acids Res* 1985; **13:** 6265-6272.

25. Howard M, Frizzell RA, Bedwell DM. Aminoglycoside antibiotics restore CFTR function by overcoming premature stop mutations. *Nat Med* 1996; **2:** 467-469.

26. Bedwell DM, Kaenjak A, Benos DJ, Bebok Z, Bubien JK, Hong J, et al. Suppression of a CFTR premature stop mutation in a bronchial epithelial cell line. *Nat Med* 1997; **3**: 1280-1284.

27. Nudelman I, Rebibo-Sabbah A, Shallom-Shezifi D, Hainrichson M, Stahl I, Ben-Yosef T, *et al.* Redesign of aminoglycosides for treatment of human genetic diseases caused by premature stop mutations. *Bioorg Med Chem Lett* 2006; **16:** 6310-6315.

28. Jin QH, Zhao B, Zhang XJ. Cytochrome c release and endoplasmic reticulum stress are involved in caspase-dependent apoptosis induced by G418. *Cell Mol Life Sci*. 2004; **61**:1816-1825.

29. Quiros Y, Vicente-Vicente L, Morales AI, López-Novoa JM, López-Hernández FJ. An integrative overview on the mechanisms underlying the renal tubular cytotoxicity of gentamicin. *Toxicol Sci*. 2011; **119**: 245-256.

30. Forge A, Schacht J. Aminoglycoside antibiotics. *Audiol Neurootol* 2000; **5:** 3-22. 25.

31. Kass JS, Shandera WX. Nervous system effects of antituberculosis therapy. *CNS drugs* 2010; **24:** 655-667.

32. Tan J, Shepherd RK. Aminoglycoside-induced degeneration of adult spiral ganglion neurons involves differential modulation of tyrosine kinase B and p75 neurotrophin receptor signaling. *Am J Pathol* 2006; **169:** 528-543.

33. Jeong SW, Kim LS, Hur D, Bae WY, Kim JR, Lee JH. Gentamicin-induced spiral ganglion cell death: apoptosis mediated by ROS and the JNK signaling pathway. *Acta Otolaryngol* 2010; **130:** 670-678.

34. Hinojosa R, Lerner SA. Cochlear neural degeneration without hair cell loss in two patients with aminoglycoside ototoxicity. *J Infect Dis* 1987; **156:** 449-455.

35. Sone M, Schachern PA, Paparella MM. Loss of spiral ganglion cells as primary manifestation of aminoglycoside ototoxicity. *Hear Res* 1998, **115:** 217-223.

36. Wu WJ, Sha SH, McLaren JD, Kawamoto K, Raphael Y, Schacht J. Aminoglycoside ototoxicity in adult CBA, C57BL and BALB mice and the Sprague-Dawley rat. *Hear Res* 2001; **158:** 165-178.

37. Reimold AM, Etkin A, Clauss I, Perkins A, Friend DS, Zhang J*, et al.* An essential role in liver development for transcription factor XBP-1. *Genes Dev* 2000; **14:** 152-157.

38. Southern PJ, Berg P. Transformation of mammalian cells to antibiotic resistance with a bacterial gene under control of the SV40 early region promoter. *J Mol Appl Genet* 1982; **1:** 327-341.

39. Takano M, Okuda M, Yasuhara M, Hori R. Cellular toxicity of aminoglycoside antibiotics in G418-sensitive and -resistant LLC-PK1 cells. *Pharm Res* 1994; **11:** 609-615.

40. Kampinga HH, Hageman J, Vos MJ, Kubota H, Tanguay RM, Bruford EA*, et al.*Guidelines for the nomenclature of the human heat shock proteins. *Cell Stress Chaperones* 2009; **14:** 105-111.

41. Harding HP, Novoa I, Zhang Y, Zeng H, Wek R, Schapira M, Ron D. Regulated translation initiation controls stress-induced gene expression in mammalian cells. *Mol Cell.* 2000; **6**: 1099-1108.

42. Manuvakhova M, Keeling K, Bedwell DM. Aminoglycoside antibiotics mediate contextdependent suppression of termination codons in a mammalian translation system. *Rna* 2000; **6:** 1044-1055.

43. Schneider-Poetsch T, Ju J, Eyler DE, Dang Y, Bhat S, Merrick WC*, et al.* Inhibition of eukaryotic translation elongation by cycloheximide and lactimidomycin. *Nat Chem Biol* 2010; **6:** 209-217.

44. Wang, Y., Shen, J., Arenzana, N., Tirasophon, W., Kaufman, R. J., and Prywes. Activation of ATF6 and an ATF6 DNA Binding Site by the Endoplasmic Reticulum Stress Response. R. *J Biol Chem.* 2000; **275**: 27013-27020.

45. H. Yoshida, K. Haze, H. Yanagi, T. Yura, and K. Mori. Identification of the *cis*-acting endoplasmic reticulum stress response element responsible for transcriptional induction of mammalian glucose-regulated proteins; involvement of basic leucine zipper transcription factors. *J Biol Chem*. 1998; **273**: 33741-33749.

46. Anderson P, Kedersha N. Stressful initiations. *J Cell Sci* 2002; **115:** 3227-3234.

47. Shulman E, Belakhov V, Wei G, Kendall A, Meyron-Holtz EG, Ben-Shachar D*, et al.* Designer aminoglycosides that selectively inhibit cytoplasmic rather than mitochondrial ribosomes show decreased ototoxicity: a strategy for the treatment of genetic diseases. *J Biol Chem* 2014; **289:** 2318-2330.

48. Xie J, Talaska AE, Schacht J. New developments in aminoglycoside therapy and ototoxicity. *Hear Res* 2011; **281:** 28-37.

49. Geisse S, Voedisch B. Transient expression technologies: past, present, and future. *Methods Mol Biol* 2012; **899:** 203-219.

50. Walter P, Ron D. The unfolded protein response: from stress pathway to homeostatic regulation. *Science* 2011; **334:** 1081-1086.

51. Ozcan U, Cao Q, Yilmaz E, Lee AH, Iwakoshi NN, Ozdelen E*, et al.* Endoplasmic reticulum stress links obesity, insulin action, and type 2 diabetes. *Science* 2004; **306:** 457-461.

52. Taleb M, Brandon CS, Lee FS, Harris KC, Dillmann WH, Cunningham LL. Hsp70 inhibits aminoglycoside-induced hearing loss and cochlear hair cell death. *Cell Stress Chaperones* 2009; **14:** 427-437.

53. Jiang H, Sha SH, Forge A, Schacht J. Caspase-independent pathways of hair cell death induced by kanamycin in vivo. *Cell Death Differ* 2006; **13:** 20-30.

54. Fujinami Y, Mutai H, Mizutari K, Nakagawa S, Matsunaga T. A novel animal model of hearing loss caused by acute endoplasmic reticulum stress in the cochlea. *J Pharmacol Sci* 2012; **118**: 363-372.

55. Peyrou M, Hanna PE, Cribb AE. Cisplatin, gentamicin, and p-aminophenol induce markers of endoplasmic reticulum stress in the rat kidneys. *Toxicol Sci* 2007; **99**: 346-353.

56. Kujawa SG, Liberman MC. Adding insult to injury: cochlear nerve degeneration after—temporary‖ noise-induced hearing loss. *J Neurosci* 2009; **29**: 14077-14085.

57. Carrell RW, Lomas DA. Conformational disease. *Lancet* 1997; **350:** 134-138.

58. Gidalevitz T, Kikis EA, Morimoto RI. A cellular perspective on conformational disease: the role of genetic background and proteostasis networks. *Curr Opin Struct Biol* 2010; **20:** 23-32.

59. Francis SP, Katz J, Fanning KD, Harris KA, Nicholas BD, Lacy M, Pagana J, Agris PF, Shin JB. A novel role of cytosolic protein synthesis inhibition in aminoglycoside ototoxicity. *J Neurosci* 2013; **33**: 3079-3093.

60. Matt T, Ng CL, Lang K, Sha SH, Akbergenov R, Shcherbakov D*, et al.* Dissociation of antibacterial activity and aminoglycoside ototoxicity in the 4-monosubstituted 2-deoxystreptamine apramycin. *Proc Natl Acad Sci* 2012; **109:** 10984-10989.

61. Salas-Marco J, Bedwell DM. Discrimination between defects in elongation fidelity and termination efficiency provides mechanistic insights into translational readthrough. *J Mol Biol* 2005; **348:** 801-815.

62. Kramer EB, Vallabhaneni H, Mayer LM, Farabaugh PJ. A comprehensive analysis of translational missense errors in the yeast Saccharomyces cerevisiae. *Rna* 2010; **16:** 1797-1808.

63. Pfaffl MW. A new mathematical model for relative quantification in real-time RT-PCR. *Nucleic Acids Res* 2001; **29:** e45.

64. Oishi N, Kendall A, Schacht J. Metformin protects against gentamicin-induced hair cell death in vitro but not ototoxicity in vivo. *Neurosci Lett* 2014; **583**: 65-69.

65. Oishi N, Chen FQ, Zheng HW, Sha SH. Intra-tympanic delivery of short interfering RNA into the adult mouse cochlea. *Hear Res* 2013; **296:** 36-41.

66. Zhao LJ, Subramanian T, Zhou Y, Chinnadurai G. Acetylation by p300 regulates nuclear localization and function of the transcriptional corepressor CtBP2. *J Biol Chem* 2006; **281:** 4183-4189.

67. Tong M, Brugeaud A, Edge AS. Regenerated synapses between postnatal hair cells and auditory neurons. *J Assoc Res Otolaryngol* 2013; **14:** 321-329.

Supplementary Information

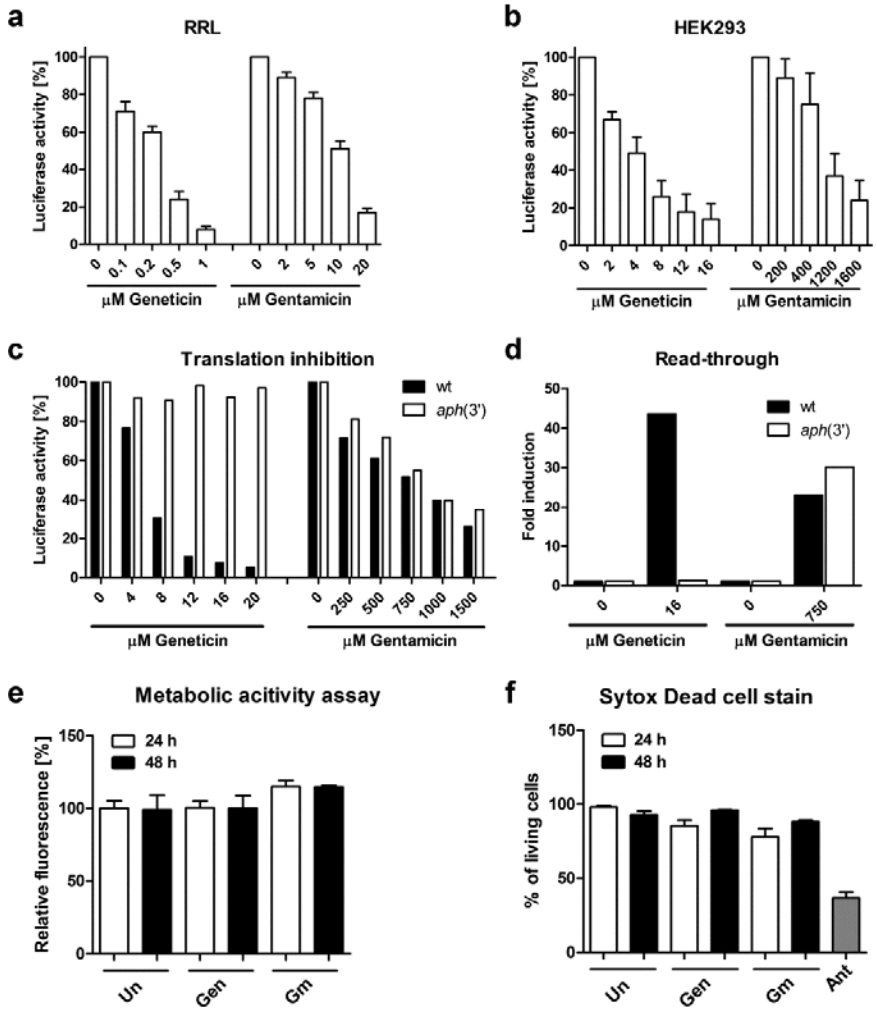

Figure S1 Translation and viability assays. (**a–c**) Aminoglycoside-induced translation inhibition in (**a**) Rabbit reticulocyte lysate (RRL), (**b**) HEK wild-type cells, (**c**) HEK wild-type versus HEK *aph*(3') cells. Translation inhibition is measured by hRluc activity; hRluc signals of untreated samples are set as 100% luciferase activity. (**d**) Read-through, measured in HEK wild-type versus HEK *aph*(3') cells, indicated by the ratio hFluc/hRluc and given as fold induction. Untreated samples are set as 1. (**e**) Metabolic activity assay. HEK wild-type cells were treated with geneticin (16 µM) or gentamicin (400 µM). The Alamar Blue fluorescence level of the untreated samples average was set as 100%. No statistical difference was observed between treated and untreated controls. (**f**) Sytox Dead cell stain. HEK wild-type cells were treated with geneticin (16 µM) or gentamicin (400 µM), stained with Sytox Red and analyzed by FACS. Antimycin (20 µg/mL for 8 h) was used as positive control for cell death. The fluorescence level of the untreated samples average was set as 100% and percentage of living cells are presented. Treatment with geneticin

and gentamicin slightly decreased cell viability by 5-15% ($p<0.05$) (**a,b,e,f**) Data are presented as means + SEM (n = 3). Gen: Genteicin; Gm: Gentamicin; Ant: Antimycin; Un: Untreated.

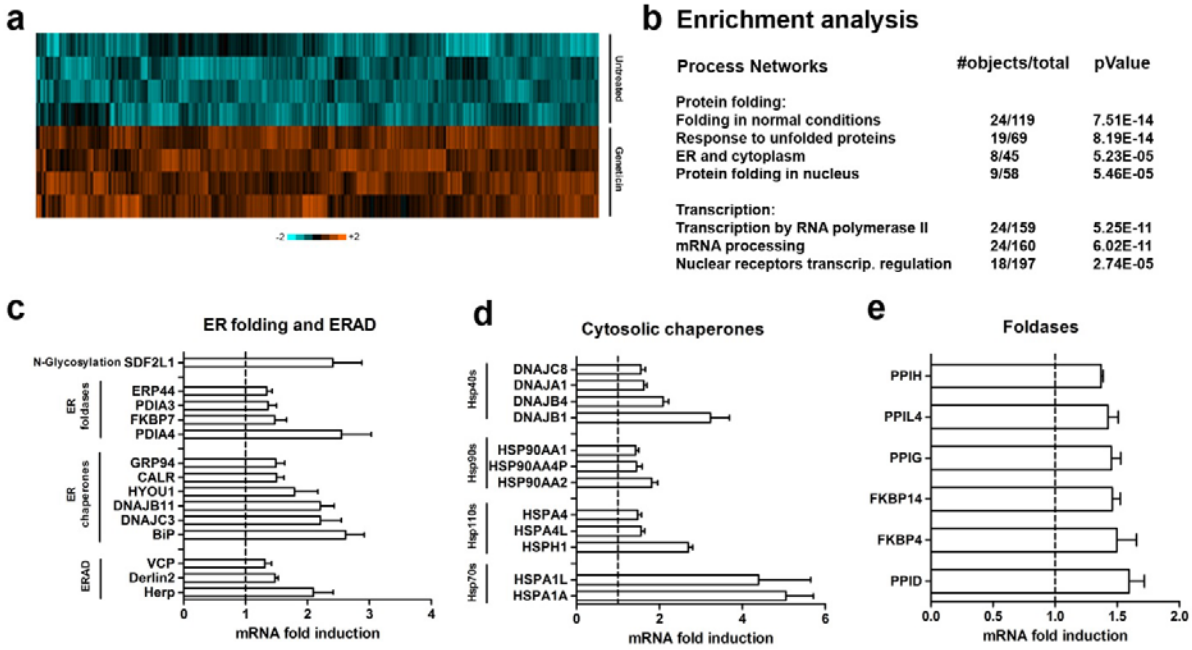

Figure S2 Transcriptome analysis of geneticin-treated HEK wild-type cells (**a**) A comparison of microarray analyses of four geneticin-treated biological replicates against four untreated biological replicates revealed 705 genes induced by geneticin (*Benjamini-Hochberg* corrected p-value < 0.05, FC > 1.2). The figure represents a heat map of the genes. (**b**) Functional ontology enrichment analysis indicating the most significantly enriched networks (p-value < 0.0001) of the 705 up-regulated genes. (**c, d, e**) mRNA fold induction of individual ER folding machinery and ERAD components(**c**), chaperones of the Hsp70, Hsp90, Hsp110, and Hsp40 protein families (**d**), and foldases (**e**) (*Benjamini-Hochberg* corrected p-value < 0.05).

Methods HEK cells were treated with 16 µM geneticin in F10 medium with 15 ug/mL saponin at 37 °C for 32 h. RNA was extracted from four independent samples for each condition (geneticin-treated, untreated). Biotinylated single-strand cDNA targets were prepared from 200 ng of total RNA, using the Ambion WT Expression Kit and the Affymetrix GeneChip WT Terminal Labeling Kit according to the manufacturer's protocols. Following fragmentation and end-labeling, 1.9 µg of cDNAs were hybridized for 16 h at 45 °C on GeneChip Human Gene 1.0 ST arrays (Affymetrix) interrogating 28,869 genes represented by approximately 27 probes spread across the full length of the gene. The chips were washed and stained in the GeneChip Fluidics Station 450 (Affymetrix) and scanned with the GeneChip® Scanner 3000 7G (Affymetrix) at a resolution of 0.7 µm. Raw data (.CEL intensity files) were extracted from the scanned images using the Affymetrix GeneChip Command Console, version 3.2. CEL files were further processed with Affymetrix Expression Console software version 1.1 to calculate probe set signal intensities using Robust Multi-array Average algorithms with default settings. Hierarchical clustering was performed using Cluster and TreeView software (http://www-microarrays.u-strasbg.fr). Functional ontology enrichment of process networks was analysed with the MetaCore software (GeneGo, Thomson Reuters). Significance of the difference in expression of each gene between treated and untreated samples was tested using the

TREAT method and the correction of Benjamini-Hochberg for multiple testing was applied in order to take into account the number of tests performed. Corrected p-values < 0.05 were considered as significant.

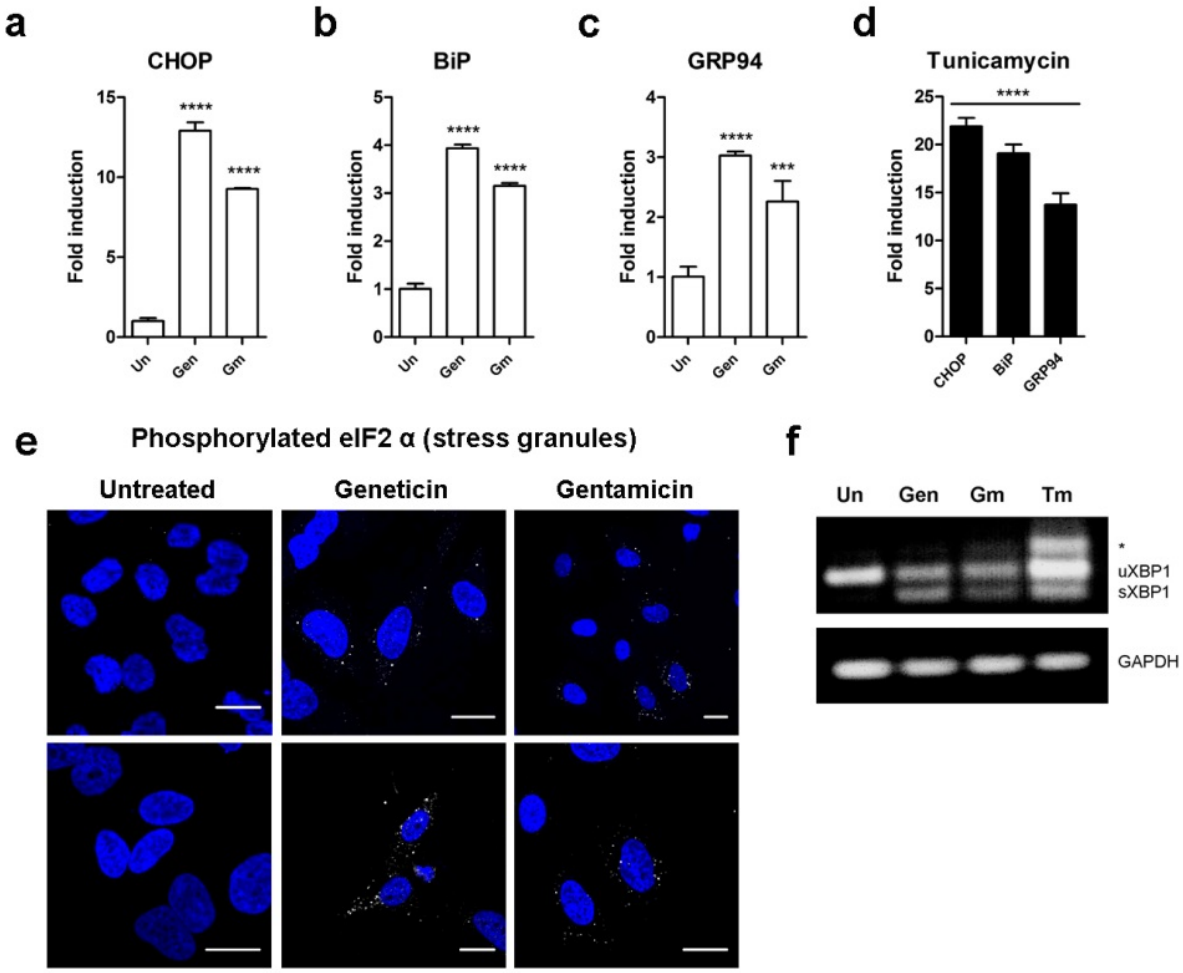

Figure S3 Aminoglycoside-induced UPR in Hela cells. (**a–d**) qPCR analysis. Hela wild-type cells were treated with geneticin (16 µM) or gentamicin (400 µM) and incubated for 24 h. Expression of CHOP (**a**), BiP (**b**), and GRP94 (**c**) mRNA is shown. (**d**) Tunicamycin was use as positive control. Experiments were run in triplicates and means + SD of fold induction relative to untreated samples are presented; ***P< 0.005; ****P<0.001. (**e**) Stress granule formation. Hela wild-type cells were treated with geneticin (16 µM) or gentamicin (400 µ M) for 24 h. Phosphorylated eIF2α was detected by immunofluorescence. Scale bars: 20 µm. Two representative pictures shown for each sample. (**f**) XBP1 splicing assay. Hela wild-type cells were treated with geneticin (16 µM) or gentamicin (400 µM) for 24 h, or left untreated. Products of XBP1 PCR were analyzed by gel electrophoresis; unspliced (uXBP1) and spliced (sXBP1) versions of XBP1 are indicated. Tunicamycin (2.5 µg/mL) was a positive control to induce ER stress; GAPDH was a loading control. The asterisk indicates the position of a hybrid amplicon (ref 15). Gen: Geneticin; Gm: Gentamicin; Tm: Tunicamycin; UN: Untreated.

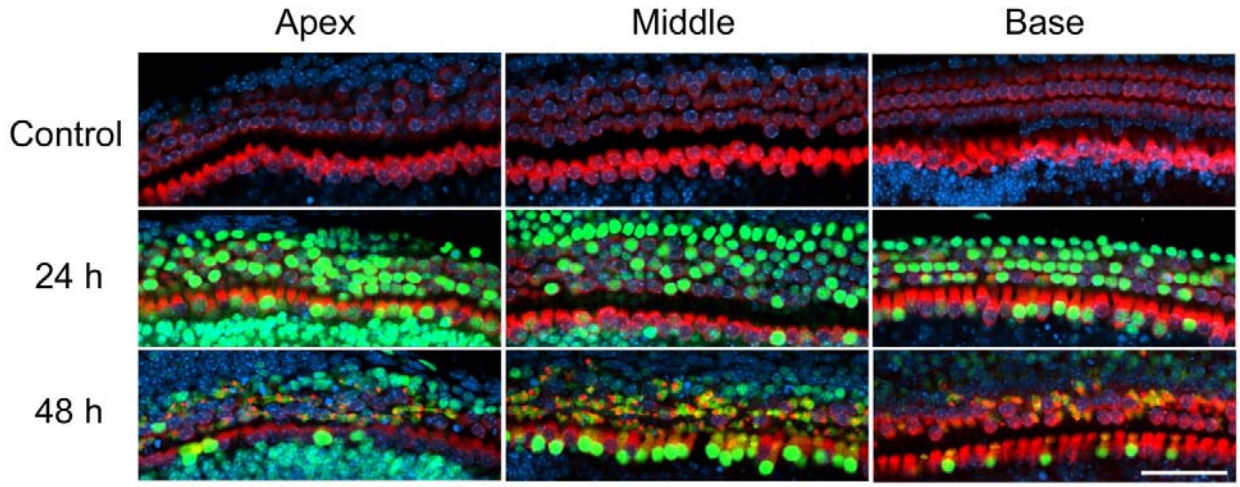

Figure S4 Effect of tunicamycin on cochlear explants: Control: The specific ER stress-associated pro-apoptotic factor, CHOP (green) is absent from untreated organ of Corti explants of CBA/J mice (P2–3). **24 h:** After a 24-h incubation, tunicamycin (0.07 µg/mL) induced CHOP in the nuclei of most hair cells from base to apex of the organ of Corti. **48 h:** Loss of staining consistent with beginning hair cell death. Green: CHOP, red: Myo 7a stain for hair cells, blue: Hoechst 33342 staining for nuclei. The figure represents three different explants at each time point. Scale bar: 50 µm.

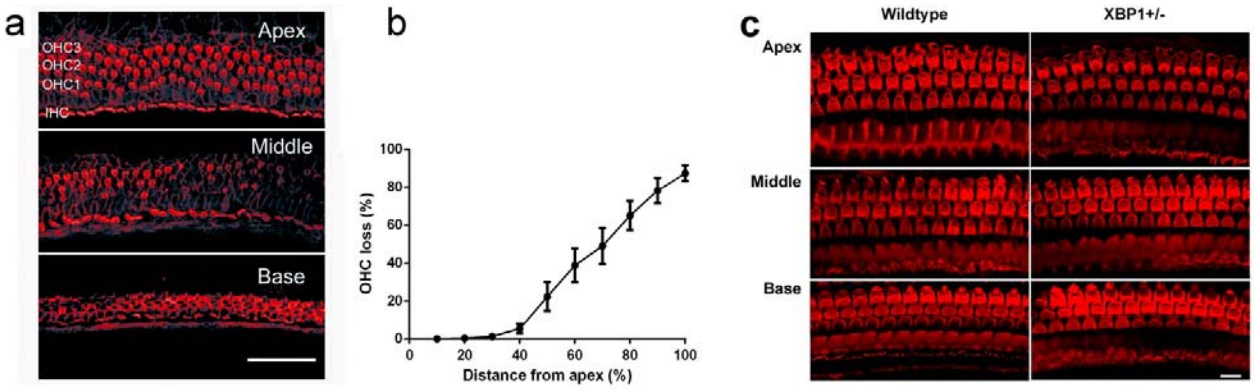

Figure S5 Effect of gentamicin on hair cells *in vitro* and *in vivo:* a, b: Effect of gentamicin on hair cells in cochlear explants. (**a**) Loss of OHCs due to gentamicin treatment (3.5 µM for 72 h) showed the typical base-to-apex gradient with most destruction in the base. The figure represents six different explants from CBA/J mice. (**b**) Complete quantification of hair cell loss from apex to base of the explant. Data are mean ± SD. Red: rhodamine phalloidin to outline hair cell structure. Scale bar: 50 µm.

c: Effect of intratympanic application of gentamicin. Surface preparations from adult wild-type and $XBP1^{+/-}$ mice previously treated with intratympanically applied gentamicin were examined from base to apex. Actin staining (red) showed the presence of OHC cuticular plates and stereocilia in all parts of the cochlea, except for minor scattered loss at the base. Five wildtype and five $XBP1^{+/-}$ mice were treated with gentamicin; the images are representative samples. Scale bar: 10 µm.

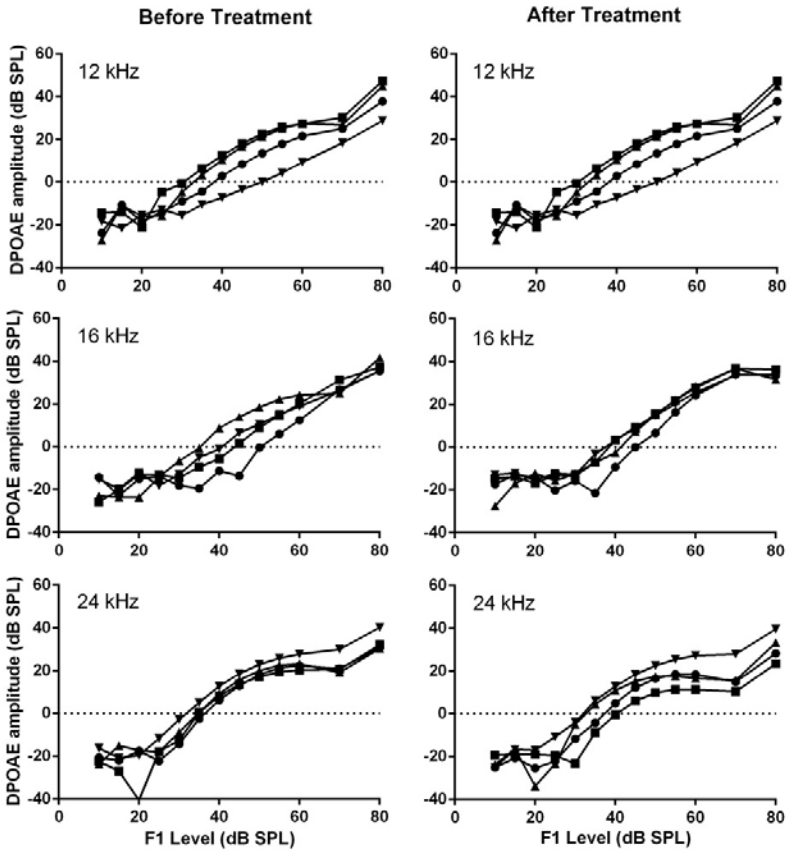

Figure S6 Distortion product otoacoustic emissions (DPOAE) remain unaltered by intratympanic gentamicin treatment. Animals were anesthetized with ketamine 65 mg/kg, xylazine 3.5 mg/kg, and acepromazine 2 mg/kg and body temperature was maintained. The primary tones, F1 and F2, were set at a F2/F1 ratio of 1.2. The intensity of F1 (L1) was varied in 5- or 10-dB steps (with the intensity of F1 ranging from 10–80 dB SPL), and the intensity of F2 (L2) was maintained 10 dB lower than L1. DPOAE were measured at 2F1 - F2. Tones were presented via two EC1 drivers (TDT) connected through an electret condenser microphone (Knowles Acoustics, type FG-23329-P07). TDT System III hardware and SigGen/BioSig software were used to present the stimuli and record responses. DPOAE responses in four adult XBP1$^{+/-}$ mice were measured before and after gentamicin treatment. Lines for the four animals are distinguished by different symbols.

Supplementary Table 1.

List of analyzed UPR and ER folding machinery genes and human chaperones and foldases.

* Genes considered significantly regulated (p-value ≤ BH correction)

Gene symbol	Other symbols	Fold change	P-value	BH correction
UPR(Lecca, Wagner et al. 2005, Sharma, Jiang et al. 2007, Hetz 2012)				
UPR sensors				
ERN1	IRE1	0.88	0.193	0.013
EIF2AK3	PERK	1.26	0.033	0.006
ATF6		1.03	0.778	0.034
ATF6B		0.68	0.001*	0.001
UPR Transcription factors				
ATF3		0.99	0.898	0.041
ATF4		0.82	0.013	0.004
ATF6		1.03	0.778	0.034
ATF6B		0.68	0.001*	0.001
XBP1		1.30	0.012	0.004
DDIT3	CHOP	1.51	0.020	0.005
ERAD(Araki and Nagata 2011)				
Processing and targeting				
EDEM1		0.97	0.913	0.042
EDEM2		1.04	0.806	0.036
EDEM3		1.12	0.182	0.012
PDIA2	PDI, PDIP, PDIR	0.91	0.458	0.022
HSPA5	BiP, GRP78	2.62	<0.001*	<0.001
HSP90B1	GRP94	1.49	<0.001*	<0.001
DNAJB9	ERdj4, MDG1	1.78	0.003	0.002
DNAJC10	ERdj5, JPD1	0.82	0.015	0.004
FOXRED2	ERFAD	0.74	<0.001*	<0.001
PPIB	CyclophilinB, CYPB	1.00	0.987	0.049
OS9	ERLEC2	0.96	0.724	0.032
ERLEC1	XTP3-B	1.21	0.037	0.006
SEL1L		1.25	0.061	0.007

Possible retrotranslocation channel				
SEC61A1	SEC61	1.03	0.845	0.038
SEC61A2		1.13	0.300	0.017
SEC61B		1.14	0.141	0.011
SEC61G		1.57	0.001*	0.001
DERL1	Derlin 1	1.08	0.458	0.022
DERL2	Derlin 2	1.48	<0.001*	<0.001
DERL3	Derlin 3	1.43	0.008	0.003
Other possible component or regulator				
HERPUD1	HERP, Mif1, SUP	2.10	<0.001*	<0.001
VIMP	SELS	1.43	0.004	0.002
BCAP31	BAP31	1.09	0.442	0.021
JKAMP	HSPC213, JAMP	1.20	0.011	0.004
DNAJB12	DJ10	0.99	0.961	0.046
HM13	SPP	0.99	0.949	0.045
SSR1	TRAP alpha	0.87	0.114	0.010
SSR2	TRAP beta	1.00	0.984	0.049
SSR3	TRAP gamma	0.97	0.828	0.037
SSR4	TRAP delta	0.88	0.176	0.012
TICAM2	TRAM	1.17	0.082	0.008
AUP1		1.22	0.002	0.002
SVIP		1.15	0.212	0.013
E2 ubiquitin-conjugating enzyme				
UBE2K	UBC1, HIP2	1.20	0.008	0.003
UBE2D1	UBCH5	1.42	<0.001*	<0.001
UBE2J1	UBC6	0.96	0.725	0.032
UBE2J2		1.14	0.154	0.011
UBE2G1	UBC7	1.04	0.788	0.035
UBE2G2		1.17	0.090	0.009
UBE2N	UBC13	1.11	0.233	0.014
E3 ubiquitin-ligase				
NEDD4L	NEDD4-2	1.15	0.135	0.011

PARK2	PDJ	0.67	0.001*	0.001
RNF5	RMA1	1.34	0.001*	0.001
AMFR	RNF45, GP78	0.95	0.638	0.028
SYVN1	HRD1, DER3	1.28	0.007	0.003
MARCH6	TEB4, DOA10	0.96	0.772	0.034
RNF139	HRCA1, TRC8	1.27	0.006	0.003
TRIM13	CAR, RNF77	1.01	0.971	0.047
RNF103	KF1	1.09	0.343	0.018
RNF19A	RNF19	1.12	0.212	0.013
RNF121		1.36	0.003	0.002
STUB1	CHIP	0.95	0.679	0.030
SKP1-CUL1-F-box (SCF) E3				
SKP1	OCP	1.36	0.006	0.003
CUL1	cullin-1	1.23	0.004	0.002
FBXO2	FBG1	0.88	0.160	0.011
FBXO6	FBG2	0.91	0.247	0.015
RBX1	RNF75, ROC1	1.09	0.357	0.018
E4 ubiquitin-conjugating enzyme				
UBE4B	UFD2	0.90	0.240	0.014
Substrate extraction and recruiting				
VCP	p97, ALS14	1.31	0.001*	0.002
UFD1L	UFD1	1.30	0.003	0.002
NPLOC4	NPL4	1.13	0.187	0.012
UBXD family protein				
UBXN6	UBXD1	1.02	0.905	0.042
UBXN4	UBXD2	1.12	0.226	0.014
UBXN7	UBXD7	1.31	0.010	0.003
FAF2	UBXD8	1.47	<0.001*	0.001
UBXN1	UBXD10	1.02	0.844	0.038
Deglycosylating enzyme				
NGLY1	PNGase	1.11	0.270	0.015

DUB (deubiquitination)				
VCPIP1	DUBA3, VCIP135	1.21	0.011	0.004
YOD1	DUBA8, YOD1	1.57	<0.001*	<0.001
ATXN3	Ataxin-3	1.12	0.259	0.015
USP19		1.19	0.071	0.008
Shuttle protein				
UBQLN1	Ubiquilin1	1.18	0.017	0.004
RAD23A	HR23A	0.78	0.004	0.003
RAD23B	HR23B	0.91	0.382	0.019
Ubiquitin receptor				
PSMD4	Rpn10	0.86	0.159	0.011
PSMC3	Rpt5	0.95	0.686	0.030
ADRM1	Rpn13	1.13	0.247	0.015
ER Chaperones(Lecca, Wagner et al. 2005, Hebert and Molinari 2007, Araki and Nagata 2011)				
DNAJC1	ERdj1, MTJ1	0.97	0.834	0.037
SEC63	ERdj2, DNAJC23	0.91	0.343	0.018
DNAJB11	ERdj3, HEDJ, ERj3	2.21	<0.001*	<0.001
DNAJB9	ERdj4, MDG1	1.78	0.003	0.002
DNAJC10	ERdj5, JPD1	0.82	0.015	0.004
TOR1A	Torsin A	1.05	0.636	0.028
SIL1	BAP, ULG5	1.02	0.886	0.040
HYOU1	GRP170	1.79	<0.001*	0.001
HSP90B1	GRP94	1.49	<0.001*	<0.001
HSPA5	BiP	2.62	<0.001*	<0.001
CALR	Calreticulin	1.50	<0.001*	0.001
CANX	Calnexin	1.10	0.310	0.017
SERPINH1	HSP47	1.24	0.024	0.005
LRPAP1	RAP	1.07	0.558	0.025
LEPRE1	P3H1	0.95	0.641	0.028
P4HB	P4H, ERP59, PDIA1	0.95	0.668	0.029

DNAJC3	ERdj6	2.21	<0.001*	<0.001
ER foldases(Lecca, Wagner et al. 2005, Schroder and Kaufman 2005, Hebert and Molinari 2007, Bernasconi and Molinari 2011)				
PDIA3	ERP57, ERP61, ERP60	1.36	0.001*	0.002
PDIA4	ERP70, ERP72	2.55	<0.001*	<0.001
DNAJC10	ERdj5	0.82	0.015	0.004
PDIA5	PDIR	0.97	0.832	0.037
MUTED	ERP46, PDIA15	0.98	0.903	0.042
PDIA2	PDI, PDIp, PDIr	0.91	0.458	0.022
PDILT	PDIA7	0.93	0.507	0.024
ERP44	PDIA10, TXNDC4	1.34	0.001*	0.001
TXNDC12	ERP18, PDIA16, ERP19	1.17	0.035	0.006
TMX1	TMX, PDIA11	1.06	0.589	0.026
TMX2	PDIA12	1.26	0.021	0.005
TMX3	PDIA13	0.96	0.755	0.033
TMX4	PDIA14	0.90	0.297	0.016
PDIA6	P5, ERP5, TXNDC7	1.42	0.002	0.002
ERO1LB	ERO1B	1.60	0.003	0.002
ERO1L	ERO1A	0.79	0.004	0.002
P4HB	PDIA1, ERP59	0.95	0.668	0.029
ERP29	PDIA9, ERP28, ERP31	0.67	<0.001*	0.001
PPIB	CyclophilinB, CYPB	1.00	0.987	0.049
FKBP2	FKBP13	1.05	0.717	0.032
FKBP7	FKBP23	1.47	<0.001*	0.001
FKBP10	FKBP65	0.74	0.002	0.002
FKBP11	FKBP19	1.14	0.370	0.019
N-linked Glycosylation(Lecca, Wagner et al. 2005, Schroder and Kaufman 2005)				
UGGT1	UGT1	1.00	0.973	0.047
UGGT2	UGT2	1.09	0.478	0.023
SDF2		1.50	0.003	0.002
SDF2L1		2.41	<0.001*	<0.001
MOGS	alpha glucosidase I	1.11	0.366	0.019
GANAB	alpha glucosidase II	0.80	0.006	0.003

MAN1A1	alpha mannosidase I	0.99	0.953	0.046
MAN2A1	alpha mannosidase II	0.81	0.023	0.005
ALG12		1.29	0.008	0.003
ALG5		1.30	0.006	0.003
PIGA	GPI3	1.35	0.012	0.004
PIGB		0.87	0.169	0.012
RPN1	OST1	1.01	0.942	0.045
STT3A	STT3, ITM1	0.90	0.226	0.014
DDOST	WBP1	0.95	0.653	0.029
Human Chaperones(Kampinga, Hageman et al. 2009) HSPA (Hsp70 chaperones)				
HSPA1A		5.05	<0.001*	<0.001
HSPA1L		4.40	<0.001*	<0.001
HSPA2		1.37	0.005	0.003
HSPA5	BiP, GRP78	2.62	<0.001*	<0.001
HSPA6		1.65	0.004	0.002
HSPA7		1.65	0.004	0.002
HSPA8		1.17	0.021	0.005
HSPA9		1.00	0.977	0.048
HSPA12A		0.92	0.381	0.019
HSPA12B		0.96	0.680	0.030
HSPA13		1.05	0.715	0.031
HSPA14		1.26	0.007	0.003
HSPH (Hsp110 chaperones)				
HYOU1	GRP170	1.79	<0.001*	0.001
HSPH1		2.70	<0.001*	<0.001
HSPA4		1.48	<0.001*	<0.001
HSPA4L		1.56	<0.001*	<0.001
HSPC (Hsp 90 chaperones)				
HSP90AA1		1.43	<0.001*	<0.001
HSP90AA2		1.81	<0.001*	<0.001
HSP90AB1		1.06	0.651	0.029
HSP90B1	GRP94	1.49	<0.001*	<0.001

TRAP1		0.82	0.016	0.004
DnaJA (Hsp40 co-chaperones)				
DNAJA1		1.62	<0.001*	<0.001
DNAJA2		1.14	0.121	0.010
DNAJA3		1.12	0.169	0.012
DNAJA4		0.99	0.938	0.044
DnaJB (Hsp40 co-chaperones)				
DNAJB1		3.23	<0.001*	<0.001
DNAJB2		0.90	0.376	0.019
DNAJB3		0.93	0.517	0.024
DNAJB4		2.09	<0.001*	<0.001
DNAJB5		1.10	0.321	0.017
DNAJB6		1.22	0.018	0.004
DNAJB7		0.99	0.921	0.043
DNAJB8		0.90	0.217	0.014
DNAJB9		1.78	0.003	0.002
DNAJB11		2.21	<0.001*	<0.001
DNAJB12		0.99	0.961	0.046
DNAJB13		1.00	0.963	0.047
DNAJB14		1.04	0.721	0.032
DnaJC (Hsp40 co-chaperones)				
DNAJC1		0.97	0.834	0.037
DNAJC2	MPP11	1.19	0.021	0.005
DNAJC3	ERdj6	2.21	<0.001*	<0.001
DNAJC4		0.82	0.020	0.005
DNAJC5		1.05	0.693	0.030
DNAJC5B		0.99	0.946	0.045
DNAJC5G		1.00	0.984	0.049
DNAJC6		1.31	0.006	0.003
DNAJC7		1.10	0.223	0.014
DNAJC8		1.55	0.001*	0.001
DNAJC9		1.22	0.028	0.005
DNAJC10	ERdj5	0.82	0.015	0.004

DNAJC11		1.38	0.008	0.003
DNAJC12		1.11	0.372	0.019
DNAJC13		0.96	0.781	0.035
DNAJC14		1.01	0.924	0.043
DNAJC15		0.98	0.874	0.040
DNAJC16		0.80	0.015	0.004
DNAJC17		#N/A	#N/A	#N/A
DNAJC18		0.75	0.001*	0.001
DNAJC19	TIMM14	0.98	0.897	0.041
DNAJC21		1.03	0.769	0.034
DNAJC22		0.98	0.868	0.039
DNAJC24	DPH4	1.15	0.112	0.010
DNAJC25		1.19	0.023	0.005
DNAJC27		1.12	0.349	0.018
DNAJC28		0.96	0.703	0.031
DNAJC30		0.99	0.972	0.047
HSCB		1.04	0.776	0.034
SEC63	ERdj2	0.91	0.343	0.018
GAK	DNAJC26	1.06	0.638	0.028
SACS	DNAJC29	1.10	0.328	0.017
HspB (small heat shock proteins)				
HSPB1	HSP25	1.90	0.001*	0.001
HSPB2	HSP27	0.93	0.532	0.024
HSPB3	HSPL27	1.07	0.611	0.027
HSPB6	HSP20	#N/A	#N/A	#N/A
HSPB7		0.92	0.466	0.022
HSPB8		1.42	0.121	0.010
HSPB9		0.91	0.356	0.018
HSPB11		1.11	0.290	0.016
HSPBAP1		1.18	0.049	0.007
CRYAA		0.88	0.224	0.014
CRYAB		1.03	0.811	0.036
Chaperonin (Hsp10 and 60)				
HSPD1	HSP60, GROEL	1.15	0.036	0.006

HSPD1P1		1.36	0.010	0.003
HSPE1	HSP10, GROES	1.58	<0.001*	<0.001
MKKS		0.99	0.940	0.045
BBS10		1.30	0.012	0.004
BBS12		1.15	0.260	0.015
Chaperone regulator				
STIP1		1.72	<0.001*	<0.001
CLIPs (ribosome-associated chaperones)				
TCPA1		1.19	0.005	0.003
CCT2		1.07	0.525	0.024
CCT3		1.13	0.133	0.010
CCT4		1.10	0.264	0.015
CCT5		1.14	0.047	0.007
CCT6A		1.26	<0.001*	0.001
CCT6B		0.97	0.855	0.039
CCT7		1.13	0.089	0.009
CCT8		1.10	0.292	0.016
PFDN1		1.22	0.007	0.003
PFDN2		1.15	0.088	0.009
VBP1		1.29	0.009	0.003
PFDN4		1.21	0.048	0.007
PFDN5		0.99	0.963	0.047
PFDN6		1.48	<0.001*	0.001
DNAJC2		1.19	0.021	0.005
HSPA14		1.26	0.007	0.003
BTF3		1.01	0.956	0.046
NACA		1.01	0.955	0.046
Peptidylprolyl cis-trans Isomerases (PPI)(Gerard, Deleersnijder et al. 2011, Benham 2012)				
FKBP1A		1.04	0.056	0.007
FKBP1B		1.14	0.197	0.013
FKBP2		1.05	0.717	0.032
FKBP3		1.04	0.723	0.032
FKBP4		1.50	<0.001*	0.001

FKBP5		1.27	0.003	0.002
FKBP6		0.88	0.206	0.013
FKBP7		1.47	<0.001*	0.001
FKBP8		0.97	0.817	0.036
FKBP9		0.83	0.060	0.007
FKBP9L		0.81	0.023	0.005
FKBP10		0.74	0.002	0.002
FKBP11		1.14	0.370	0.019
FKBP14		1.46	0.001*	0.001
FKBPL		1.02	0.843	0.038
PIN1		1.15	0.073	0.008
PIN1P1		#N/A	#N/A	#N/A
PIN4		1.18	0.154	0.011
PPIA		1.08	0.418	0.020
PPIAL4A		1.02	0.927	0.044
PPIAL4B		1.00	0.927	0.044
PPIAL4C		1.00	0.927	0.044
PPIAL4D		#N/A	#N/A	#N/A
PPIAL4E		1.00	0.927	0.044
PPIAL4F		1.00	0.927	0.044
PPIAL4G		0.97	0.908	0.042
PPIB	CyclophilinB, CYPB	1.00	0.987	0.049
PPIC		0.92	0.432	0.021
PPID		1.59	<0.001*	0.001
PPIE		1.19	0.077	0.008
PPIEL		1.04	0.949	0.045
PPIF		1.00	0.992	0.049
PPIG		1.45	<0.001*	0.001
PPIH		1.37	<0.001*	<0.001
PPIL1		1.17	0.045	0.007
PPIL2		0.82	0.010	0.003
PPIL3		0.91	0.304	0.017
PPIL4		1.42	0.001*	0.001
PPIL6		0.85	0.095	0.009
PPWD1		1.10	0.325	0.017

Protein Disulfide Isomerases (PDI)[11]				
PDIA2		0.91	0.458	0.022
PDIA3		1.36	0.001*	0.002
PDIA4		2.55	<0.001*	<0.001
PDIA5		0.97	0.832	0.037
PDIA6		1.42	0.002	0.002
PDILT		0.93	0.507	0.024
PDIK1L		0.93	0.502	0.023
P4HB		0.95	0.668	0.029
ERP27		0.97	0.880	0.040
ERP29		0.67	<0.001*	0.001
ERP44		1.34	0.001*	0.001
TMX1		1.06	0.589	0.026
TMX2		1.26	0.021	0.005
TMX3		0.96	0.755	0.033
TMX4		0.90	0.297	0.016
TXNDC5		1.21	0.274	0.016
TXNDC12		1.17	0.035	0.006
AGR2		1.07	0.528	0.024
AGR3		0.97	0.898	0.041
DNAJC10		0.82	0.015	0.004
CASQ1		0.98	0.930	0.044
CASQ2		0.92	0.397	0.020

References

Araki, K. and K. Nagata (2011). "Protein folding and quality control in the ER." Cold Spring Harb Perspect Biol **3**(11): a007526.

Benham, A. M. (2012). "The protein disulfide isomerase family: key players in health and disease." Antioxid Redox Signal **16**(8): 781-789.

10 LIST OF PUBLICATIONS

1. **Decoding and deafness: two sides of a coin.** Akbergenov R, Scherbakov D, Matt T, Duscha S, **Meyer M**, Perez Fernandez D, Pathak R, Harish S, Kudyba I, Dubbaka SR, Silva S, Ruiz Ruiz MC, Salian S, Vasella A, Böttger EC (2011). In: Ribosomes. Eds: Rodnina MV, Wintermeyer W, Green R. Springer Verlag Vienna, Austria, p. 249-261
2. **Molecular basis for the selectivity of antituberculosis compounds capreomycin and viomycin.** Akbergenov R, Shcherbakov D, Matt T, Duscha S, **Meyer M**, Wilson DN,Böttger EC (2011). Antimicrob. Agents Chemother. 55:4712-4717
3. **Structure-activity relationships among the kanamycin aminoglycosides: role of ring I hydroxy and amino groups.** Salian S, Matt T, Akbergenov R, Harish S, **Meyer M**, Duscha S, Shcherbakov D, Bernet BB, Vasella A, Westhof E, Böttger EC (2012). Antimicrob. Agents Chemother. 56:6104-6108
4. **Dissociation of antibacterial activity and aminoglycoside ototoxicity in the 4-monosubstituted 2-deoxystreptamine apramycin.** Matt T, Ng CL, Lang K, Sha SH, Akbergenov R, Shcherbakov D, **Meyer M**,Duscha S, Xie J, Dubbaka SR, Perez-Fernandez D, Vasella A, Ramakrishnan V, Schacht J, Böttger EC (2012). Proc. Natl. Acad. Sci. USA 109:10984-10989
5. **4'-O-substitutions determine selectivity of aminoglycoside antibiotics.** Perez-Fernandez D, Shcherbakov D, Matt T, Leong NC, Kudyba I, Duscha S,Boukari H, Patak R, Dubbaka SR, Lang K, **Meyer M**, Akbergenov R, Freihofer P, Vaddi S, Thommes P, Ramakrishnan V, Vasella A, Böttger EC (2014). Nature Communications 5:3112
6. **In vivo efficacy of apramycin in murine infection models. Meyer M**, Freihofer P, Scherman M, Teague J, Lenaerts A, Böttger EC (2014) Antimicrob Agents Chemother. 58(11):6938-41

7. **XBP1 mitigates aminoglycoside-induced endoplasmic reticulum stress and neuronal cell death.** Schacht J, Oishi N, Duscha S, Boukari H, **Meyer M**, Xie J, Gao W, Roschitzki B, and Boettger EC (2015). Cell Death and Disease. 6:e1763. doi: 10.1038/cddis.2015.108

11 CONFERENCE PRESENTATIONS

2010 **5th International Conference on the Ribosome, Orvieto, Italy**

Aminoglycosides, Ototoxicity and Malfunction of the Mitoribosome: Towards Synthesis of New Compounds with Altered Drug-Target Interaction. E.C. Böttger, T. Matt, R. Akbergenov, D. Sherbakov, S. Duscha, **M. Meyer**, D. Perez-Fernandez, S.R. Dubbaka, A. Vasella

2011 **EMBO Protein synthesis and translational control, Heidelberg, Germany**

Genetic reconstructions combined with chemical compound-mediated manipulation of function to investigate phylogenetic principles and mechanisms in A-site decoding. H. Boukari, P. Freihofer, D. Sherbakov, T. Matt, S. Duscha, **M. Meyer**, E.C. Böttger

Dissociation of antibacterial activity and aminoglycoside ototoxicity in the 4-monosubstituted 2-deoxystreptamine apramycin. S. Duscha, T. Matt, **M. Meyer**, N.C. Leong, K. Lang, S. Sha, R. Akbergenov, D. Sherbakov, S.R. Dubbaka, J. Xie, A. Vasella, V. Ramakrishnan, J. Schacht, E.C. Böttger

Molecular basis for the selectivity of antituberculosis compounds capreomycin and viomycin. **M. Meyer**, R. Akbergenov, S. Duscha, D. Wilson, E.C. Böttger

2012 **EMBO Quality Control – From Molecules to Organelles, Heidelberg, Germany**

Mitochondrial DNA positions 1555 and 1494 control quality of mitoribosomal protein biogenesis. D. Shcherbakov, H. Boukari, R. Akbergenov, T. Matt, S. Duscha, **M. Meyer**, P. Freihofer, E.C. Böttger

12 SEMINARS AND COLLOQUIA

2010 **Seminar, Institute of Medical Microbiology, UZH**

Project presentation

Life Science Graduate School Zurich MLS Retreat, Chandolin, Switzerland

Poster: Stress induced misreading: Measuring ribosomal translation fidelity in vivo in higher eukaryotic cells

2011 **Seminar, Institute of Medical Microbiology, UZH**

Progress report I

Life Science Graduate School Zurich
Committee Meeting I

2012 **Seminar, Institute of Medical Microbiology, UZH**

Progress report II

Life Science Graduate School Zurich
Committee Meeting II

2013 **Seminar, Institute of Medical Microbiology, UZH**

Progress report III

Life Science Graduate School Zurich
Committee Meeting III

2014 **Seminar, Institute of Medical Microbiology, UZH**

Progress report IV